

THE WATER PERMEABILITY OF THE HUMAN ERYTHROCYTE  
IN THE TEMPERATURE RANGE +25°C to -10°C

by

THOMAS H. PAPANEK

B.S., COLUMBIA UNIVERSITY (1972)

S.M., Massachusetts Institute of Technology (1975)

SUBMITTED IN PARTIAL FULFILLMENT  
OF THE REQUIREMENTS FOR THE  
DEGREE OF

DOCTOR OF PHILOSOPHY

at the

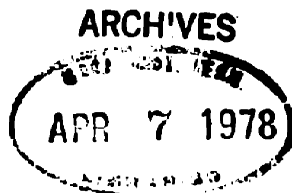
MASSACHUSETTS INSTITUTE OF TECHNOLOGY

JANUARY 1978

Signature of Author.....  
Department of Mechanical Engineering, January 18, 1978

Certified by.....  
Thesis Supervisor

Accepted by.....  
Chairman, Department Committee on Graduate Students



THE WATER PERMEABILITY OF THE HUMAN ERYTHROCYTE  
IN THE TEMPERATURE RANGE  $+25^{\circ}\text{C}$  to  $-10^{\circ}\text{C}$

by

THOMAS H. PAPANEK

Submitted to the Department of Mechanical Engineering on January 18, 1978 in partial fulfillment of the requirements for the Degree of Doctor of Philosophy.

ABSTRACT

As part of the effort to quantify thermodynamic events occurring in a cell during freezing, an experimental method has been developed and applied to measure human red cell membrane permeabilities at low temperature. The stop flow technique is used to impose a step change in extracellular solute concentration, and the resulting changes in cell volume are monitored by photometrically measuring the light scattering characteristics of the cell suspension. A high speed digital data acquisition system and dedicated microprocessor provide high resolution storage and manipulation of experimental results. An electronically controlled thermal system maintains the apparatus at the desired temperature. High concentrations of ethylene glycol are used to depress the freezing points of the experimental solutions. Coupled transport equations, solution models and cell volume models have been derived to describe the resulting non-dilute, non-ideal conditions. A computer program has been developed which uses a statistical criterion to converge on those values of the membrane parameters which yield the best fit between the experimental data and the theoretical modelling equations. The apparent activation energy for water transport is found to be between 3.4 and 4.7 Kcal/mol; in addition, the water permeability is found to be a strong function of concentration, diminishing by a factor of ten as the total mean solute concentration is increased from isotonic to 5.6 osmol/Kg.

Thesis Supervisor: Ernest G. Cravalho  
Associate Director for Medical Engineering and  
Medical Physics, Harvard-MIT Division of Health  
Sciences and Technology and Matsushita Professor  
of Mechanical Engineering in Medicine, MIT

## TABLE OF CONTENTS

	Page
TABLE OF CONTENTS	3
LIST OF TABLES	5
LIST OF FIGURES	6
NOMENCLATURE	9
CHAPTER 1: INTRODUCTION	12
CHAPTER 2: MEMBRANE TRANSPORT MODELS	16
2.1 IRREVERSIBLE THERMODYNAMICS, THE LINEAR FLUX EQUATIONS, AND THE KEDEM-KATCHALSKY TRANS- FORMATION	17
2.2 CRITICAL EXAMINATION OF MODEL ASSUMPTIONS	29
CHAPTER 3: GENERAL SOLUTION MODELS	36
3.1 CHEMICAL POTENTIAL, ACTIVITY, AND OSMOLALITY	37
3.2 DILUTE APPROXIMATIONS	42
3.3 A METHOD OF COMPUTING SOLUTE ACTIVITY	45
CHAPTER 4: THE PSEUDO-BINARY INTRACELLULAR MODEL	50
4.1 THE PSEUDO-BINARY SOLUTION MODEL	51
4.2 RED CELL VOLUME	60
CHAPTER 5: NON-DIMENSIONAL FORMS OF THE MODELLING EQUATIONS	69
CHAPTER 6: THE EXPERIMENTAL APPARATUS	78
6.1 INTRODUCTION TO STOP FLOW: THE FLUID HANDLING SYSTEM	79
6.2 OPTICAL SYSTEM	90
6.3 DATA ACQUISITION	107
6.4 THERMAL CONTROL SYSTEM	112

CHAPTER 7: EXPERIMENTAL TECHNIQUE AND TYPICAL RESULTS	117
CHAPTER 8: DATA REDUCTION	139
8.1 THE GENERAL ALGORITHM	140
8.2 COMPUTER PROGRAM DESCRIPTION	144
8.3 PROGRAM TESTS	154
CHAPTER 9: RESULTS AND DISCUSSION	160
APPENDICES	
A. MUTUAL DIFFUSION COEFFICIENT OF A PSEUDO-BINARY SOLUTION	180
B. COUPLED HEAT AND MASS TRANSFER	183
C. THE VAN LARR COMPUTATIONAL SCHEME	186
D. PERM2 PROGRAM LISTING (DATA REDUCTION)	189
E. DEAD TIME EXPERIMENT	213
F. POLYNOMIAL CURVE FITS OF SOLUTION DATA	218
G. VOLSIM2 PROGRAM LISTING (CELL VOLUME SIMULATION)	223
H. RED CELL AND BLOOD PHYSICAL PROPERTIES	230
I. CONCENTRATION CONVERSIONS	234
J. CONFIDENCE LIMITS OF THE VOLUME/VOLTAGE CALIBRATION DATA	237
K. LIST OF MANUFACTURERS	239
L. THERMOCOUPLE TABLE FOR LIQUID NITROGEN REFERENCE	241
REFERENCES	242
BIBLIOGRAPHY OF STOP FLOW TECHNIQUES	247
BIOGRAPHY	248



## LIST OF TABLES

1. Summary of pseudo-binary constants	59
2. Results of data reduction program tests	157
3. Experimental conditions (solution composition)	162
4. Water permeability temperature dependence at $\bar{C} = .475$ Osm	175
5. Permeability temperature dependence at $\bar{C} = 5.58$ Osm	176
6. Kedem-Katchalsky membrane parameters as a function of concentration at 25°C	177
7. Linear membrane parameters as a function of concentration at 25°C	178
H1. Properties of normal human whole blood	230
H2. Human erythrocyte dimensions	231
H3. Water content of human red cells as measured by drying	231
H4. Principal contents of human erythrocyte	232

## LIST OF FIGURES

	Page
1. Flow through a homogeneous permeable membrane	19
2. Solute polarization	33
3. Water activity in a binary NaCl solution	41
4. Molal osmotic coefficient of ethylene glycol in an aqueous solution	48
5. Ethylene glycol activity in an aqueous solution	49
6. Hemoglobin osmotic coefficient	55
7. Potassium chloride osmotic coefficient	56
8. The computed osmotic coefficient of the pseudo-binary solute	58
9. Equilibrium red cell volume as a function of extracellular NaCl concentration	63
10. Equilibrium cell volume as a function of ethylene glycol concentration	66
11. Equilibrium cell volume as a function of NaCl concentration, in the presence of 4 M ethylene glycol	68
12. Overall schematic of the experimental apparatus	80
13. The experimental apparatus (photo)	81
14. The stop flow drive system	83
15. The experimental apparatus, showing the source lamp and photomultiplier, drive system and thermostat block, supporting frame and thermal enclosure, thermal system heat exchanger, gas heater and pre-cooler (photo)	84
16. Typical drive ram velocity history	85
17. The stop flow thermostat block and fluid system	87
18. The mixer-optical assembly	88
19. Lamp power regulation circuit	92
20. Spectra of hemoglobin and optical system components	94

	Page
21. Photomultiplier output as a function of cell volume	97
22. Photomultiplier output as a function of cell number density	101
23. Photomultiplier output as a function of percentage of cells hemolyzed	104
24. Photomultiplier output as a function of suspending medium solute concentration	106
25. Microprocessor average of a repeated sine wave with superimposed noise	111
26. Temperature controller circuit	113
27. Schematic of calibration and experimental protocols	120
28. Precision hematocrit reader (photo)	122
29. Typical calibration results, strip chart records of photomultiplier output	126
30. System reproducibility, five superimposed repeat runs of a typical experiment (data acquisition system hard copy)	127
31. Strip chart record of a typical "shrink-swell" experiment	128
32. Hardcopy of microprocessor average of eight repeat runs of a typical experiment	129
33. Two superimposed runs from a typical experiment set, showing consistency of initial values (data acquisition hard copy)	130
34. Microprocessor average of four repeat runs of experimental type shown in Figure 33	131
35. System resolution, data acquisition record of a typical experiment with very small volume changes	132
36. The short time optical transient, effect of cell storage age	134
37. The long time optical transient	135
38. Flow chart of data reduction program	146
39. Results of a typical data reduction run, experimental data points and computer generated best fit line	148

	Page
40. Data points and best fit line, typical permeable solute "shrink-swell" experiment	149
41. Data points and computer best fit, typical "hypertonic shrink" experiment	150
42. Program test - simulated noisy data	156
43. Program test - simulated optical transient	159
44. Water permeability $L_p$ as a function of temperature, for mean concentrations .475 Osm (S 3 conditions) and 5.58 Osm (EG 9 conditions)	164
45. Ethylene glycol permeability $\omega$ as a function of temperature, under EG 9 conditions (see Table 3 for details of experimental conditions)	166
46. Water permeability as a function of mean concentration $\bar{C}$ at 25°C	168
47. Water permeability as a function of mean concentration at 25°C, expanded scale	169
C1. Pseudo-binary data and van Laar correlation best fit line	188
E1. Experimental determination of stop flow dead time	216
I1. Ethylene glycol molar - molal conversions	236

## NOMENCLATURE

$A_C$	cell surface area ( $135 \times 10^{-8} \text{cm}^2$ )
a	chemical activity
a	general constant
a	general parameter, Chapter 8
C	concentration, molal or molar
D	diffusion coefficient ( $\text{cm}^2/\text{sec}$ )
h	hydration number (mol water/mol)
Hct	hematocrit (ml cells/100 ml suspension)
%H	percent hemolysis (cells destroyed/total number of cells)
J	mass flux ( $\text{mol}/\text{cm}^2 \text{ sec}$ ) except Appendix A
L	phenomenological coefficient, see Chapter 2
$L_p$	water permeability, see equation 2.25
$\ell$	length
MW	molecular weight (gm/mol)
m	molal concentration, also as 0.5 m ( $\text{mol}/\text{Kg H}_2\text{O}$ )
M	molar concentration (mol/liter solution)
Osm	concentration (osmol/Kg) see section 3.1
P	pressure
R	universal gas constant (8.313 joule/mol °K)
T	temperature (°C or °K)
t	time
v	partial molar volume ( $\text{cm}^3/\text{mol}$ )
V	volume
X	generalized driving force

$x$	mol fraction, see equation 3.4
$x,y,z$	generalized coordinates or variables

### Greek Symbols

$\bar{\alpha}, \bar{\beta}$	matrices of Marquardt algorithm, Chapter 8
$\gamma$	activity coefficient, see equation 3.3
$\delta$	small variation
$\Delta$	finite difference
$\theta$	volume fraction, see equation 2.16
$\lambda$	interpolation factor, Chapter 8
$\mu$	chemical potential (joule/mol)
$\mu^*$	chemical potential reference
$\nu$	dissociation number (ions/molecule)
$\rho$	density (gm/cm <sup>3</sup> )
$\sigma$	reflection coefficient, see equations 2.23, 2.24
$\sigma_i$	standard deviation of $i^{\text{th}}$ data point, Chapter 8
$\tau$	time constant
$\Phi$	dissipation function, see equation 2.12
$\phi$	molal osmotic coefficient, see equation 3.6
$\chi^2$	chi-square, see equation 8.1
$\omega$	solute permeability, see equation 2.20 and 2.22

Subscripts

b	bulk solution
c	cell, as in $V_c$ , $A_c$
c	characteristic, as in $C_c$ or $\ell_c$
Hb	hemoglobin
i	$i^{\text{th}}$ component in solution
i,j,k	general indices
iso	isotonic, .290 osmol/Kg, normal physiological state
m	membrane
pb	pseudo-binary solute
s	solute
si	solute, impermeable
sp	solute, permeable
w	water or solvent in general

Superscripts

b	bound	
f	free (unbound)	see especially Chapter 4
h	hydrated	
i	inside, intracellular	
m	mean	
o	outside, extracellular	
^	non-dimensional	
—	mean	

**CHAPTER 1**  
**INTRODUCTION**



Whole organ transplantation shows great promise as a surgical technique, but is seriously hampered by the short ex-vivo lifetime of donor organs. Though donor organs may be available, they are not always available at the time and place of need. Banks of organs preserved by freezing offer a solution to this problem, but at present only a limited number of biomaterials, principally blood, spermatozoa and cornea can be frozen successfully.

Experiments with individual cells indicate that different cell types require highly specific freezing protocols for maximum viability. As part of the effort to understand the behavior of single cells and extend that knowledge to complex organs, a mathematical model was developed by Mazur [1] describing thermodynamic processes in the cell during freezing. Work in this laboratory has continued that effort, with particular emphasis on the human erythrocyte [2] [3] [4] in the belief that thorough understanding of the red cell will provide the theoretical basis for development of successful freezing protocols for other cell types and whole organs without extensive experimentation. In order to do this, it is necessary to specify the physio-chemical parameters of each cell type.

The most significant cell parameter contained in the analytical models has been found to be the membrane resistance to water flow. The water permeability has been extensively studied at room temperature (e.g. [5] [6] [7] [8] and in the range 37°C to 7°C [9], but prior to this work no measurements have been made at sub-zero temperatures. Theoretical simulations of freezing, utilizing extrapolations of existing membrane data, have not correlated

well with experimental freezing work [3] [4].

The original intent of this work, then, was to measure the red cell membrane permeability in the sub-zero regime and so supply the absent data. However, as a consequence of the high concentrations of permeable solute used to depress the freezing point of the experimental solutions, it became evident that the water permeability is also strongly concentration dependent. This is a significant result, since as a cell suspension is cooled below its equilibrium freezing point the remaining liquid solution becomes increasingly concentrated as water is removed in the form of ice. The membrane conductivity will then be affected by both the temperature and concentration of the suspending medium.

The data presented here will include the erythrocyte water permeability as a function of temperature at two different concentration levels, the concentration dependence of the water permeability at 25°C, and the membrane parameters characterizing transport of two common cryoprotective additives, ethylene glycol and glycerol.

The experimental concept is simple. A cell initially at equilibrium in one solution is suddenly exposed to another solution with different solute concentration. The transmembrane difference in concentration acts as a driving force for flows of water and permeable solute, which cause changes in the volume of the cell. By measuring the cell volume time history and applying appropriate thermodynamic and transport models, one may then obtain the membrane resistance to flow.

To successfully implement this scheme, we will develop the following tools:

- 1) Coupled transport models which relate mass flows through the membrane to thermodynamic driving forces, as a function of membrane parameters.
- 2) Solution models which express the driving force, chemical potential, as a function of known concentrations.
- 3) A model for cell volume as a function of water and solute content.
- 4) An experimental technique for rapidly mixing a cell suspension with a solution of different composition and measuring the subsequent volume changes.
- 5) A data reduction scheme which, given the experimental data and non-linear theoretical modelling equations, computes the best-fit values of the membrane parameters.

**CHAPTER 2**  
**MEMBRANE TRANSPORT MODELS**

## 2.1 Irreversible Thermodynamics, The Linear Flux Equations And The Kedem-Katchalsky Transformation

There are two possible analytical approaches to passive membrane transport: microscopic models which postulate specific transport mechanisms, or macroscopic schemes in which the membrane is regarded as a lumped resistance with unknown internal characteristics. The author strongly feels that at the present time there are insufficient transport data for the erythrocyte membrane to justify any choice among the many intuitively plausible microscopic models. Therefore the emphasis in this work will be on the development of well defined lumped models which adequately describe the experimental data with a minimum of analytical complexity and successfully predict membrane behavior in new circumstances.

The theory of irreversible thermodynamics provides a suitable framework in which to formulate such a model. While classical equilibrium thermodynamics yields information about end states independent of time, the theory of irreversible processes allows one to draw general conclusions about rates without specifying mechanisms. The following development closely parallels that of the texts of de Groot and Mazur [10], Prigogine [11], and Katchalsky and Curran [12].

We begin by considering one-dimensional diffusion in an isothermal, isobaric, continuous medium. The local rate of entropy generation due to irreversible mass transfer is given by

$$\frac{ds^*}{dt} = \frac{1}{T} \sum_i J_i \frac{d\mu_i}{dz} \quad (2.1)$$

where  $J_i$  is the mass flux (mol/area-time) in the  $z$  direction and  $\mu_i$  the chemical potential (energy/mol) of the  $i^{\text{th}}$  component. The rate of internal entropy production per unit volume  $\frac{ds^*}{dt}$  is not equal to the total change in entropy  $\frac{ds}{dt}$ , since there may also be an entropy flux across the boundaries of the local volume element.

Equation 2.1 holds only if the system is in a stationary state, that is, if all the system state variables are time invariant, even though the system is not at equilibrium. Such stationary states are difficult to achieve experimentally, but it is often the case that boundary conditions change slowly with respect to changes in the internal state and the system may be considered to be quasi-stationary. It is also crucial to recognize that in the steady state conservation of mass requires that the fluxes  $J_i$  are not functions of position  $z$ .

We next apply equation 2.1 to the isothermal discontinuous case shown in Figure 1, a permeable membrane separating two bulk solutions. We consider only membranes which are homogeneous from point to point on the surface, but whose properties may vary through the membrane. That is, we model the membrane as a uniform lipid bilayer without imbedded proteins or pores. The chemical potential profile shown in the figure represents a situation in which transport is rate limited primarily by intra-membrane diffusion rather than by the solution/membrane interfaces, but the actual profile is, of course, unknown.

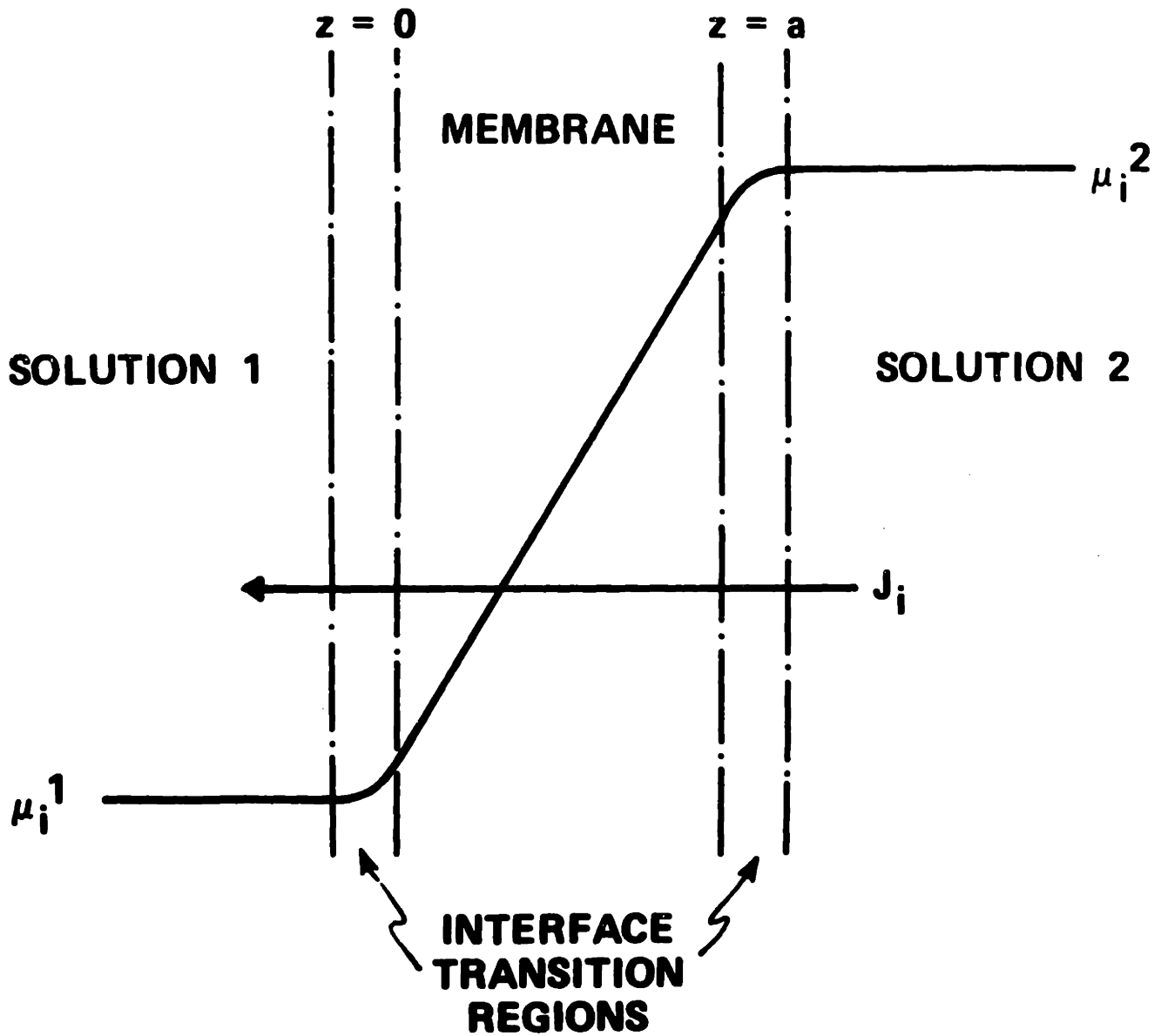


FIGURE 1 Flow through a homogeneous permeable membrane

In order to integrate equation 2.1 it is now only necessary to assume that at some point very near the interface the chemical potential is equal to that in the bulk solution. Then the internal entropy generation per unit area of membrane is given by

$$\frac{dS^*}{dt} = \int_0^a \frac{ds^*}{dt} dz = \frac{1}{T} \int_0^a \sum_i J_i d\mu_i = \frac{1}{T} \sum_i J_i \Delta\mu_i \quad (2.2)$$

where  $\Delta\mu_i = \mu_i^2 - \mu_i^1$ .

If a system is near equilibrium it is usually considered reasonable to assume that each flux  $J_i$  is a linear function of driving potential. Fourier's law of heat conduction is a well known example of such a linearization. While it is difficult to justify a linear formulation a priori, it may be validated by the final results. Another basic concept of irreversible thermodynamics is that if the conjugate potentials and flows are such that the sum of their products is equal to the entropy generation, as in equation 2.2, then each flux will depend linearly on all the driving potentials, viz,

$$J_i = \sum_j L_{ij}^* \Delta\mu_j \quad (2.3)$$

The  $L_{ij}^*$  are termed the phenomenological coefficients and are not considered to be functions of driving potential  $\Delta\mu$ , but may be functions of system state. In fact, the non-linear chemical potential profile shown in Figure 1 is possible only if we accept local coefficients  $L_{ij}^*(z)$  which



vary with position within the membrane. The electrical analog is a series resistor combination to which we apply an overall DC potential. If we measure the current through the resistor string we can compute the total resistance, but the voltage drops and individual resistances within the string are unknown to us.

The general results of equation 2.3 may be applied to a membrane which is permeable only to water  $w$  and a solute  $sp$  to yield the relations

$$J_w = L_{11}^* \Delta\mu_w + L_{12}^* \Delta\mu_{sp} \quad (2.4)$$

$$J_{sp} = L_{21}^* \Delta\mu_w + L_{22}^* \Delta\mu_{sp} \quad (2.5)$$

For the cellular membrane let us define  $\Delta\mu = \mu^i - \mu^o$  where superscript  $i$  denotes the intracellular and  $o$  the extracellular condition. A flux  $J$  is then defined as positive if that component is exiting the cell.

According to the Onsager reciprocal relation, well established on theoretical and experimental grounds, the matrix of coefficients is symmetric, so that

$$L_{12}^* = L_{21}^* \quad (2.6)$$

Thus, for the present case of two coupled flows, only three parameters are required to completely characterize the membrane: a water permeability  $L_{11}^*$ , a solute permeability  $L_{22}^*$ , and a coupling coefficient  $L_{12}^*$ . Another relation between the coefficients may be obtained by combining equations 2.2, 2.4 and 2.5 in the form

$$T \frac{dS^*}{dt} = L_{11}^* \Delta\mu_w^2 + (L_{12}^* + L_{21}^*) \Delta\mu_w \Delta\mu_{sp} + L_{22}^* \Delta\mu_{sp}^2 \quad (2.7)$$

The second law of thermodynamics requires that the entropy production be positive for arbitrary  $\Delta\mu_j$ , which is true only if the phenomenological coefficients satisfy the following inequalities

$$\begin{aligned} L_{11}^* &\geq 0 \\ L_{22}^* &\geq 0 \\ L_{12}^* &\leq \sqrt{L_{11}^* L_{22}^*} \end{aligned} \quad (2.8)$$

The linear flux equations 2.4 and 2.5, simplified by the Onsager relation and subject to the above constraints, provide a simple picture of coupled passive membrane transport which adequately fits the physical data. However, they are written in terms of chemical potential, a variable which is not directly measurable. Therefore, Kedem and Katchalsky [13] in 1958 developed an alternate set of transport equations in terms of simple concentration driving forces by a transformation of the linear set above. In performing this transformation they also derived new membrane parameters which have been widely used ever since. Unfortunately, these equations are valid only for membranes exposed to dilute solutions, and are considerably more complex than the linear set. To remove the dilute

restriction, the transformation scheme of Kedem and Katchalsky will be used in the following section to derive new transport equations based on the Kedem-Katchalsky (K-K) parameters and non-dilute chemical potential driving forces.

We begin by defining a volume flux  $J_V$  and a relative solute flux  $J_D$  in terms of the absolute fluxes  $J_w$  and  $J_{sp}$

$$J_V = J_w v_w + J_{sp} v_{sp} \quad (2.9)$$

$$J_D = \frac{J_{sp}}{C_{sp}^m} - J_w v_w \quad (2.10)$$

where  $v$  is the partial molar volume. The mean permeable solute concentration  $C_{sp}^m$  is defined in terms of the bulk solution concentrations (mol/liter)

$$C_{sp}^m = \frac{C_{sp}^i - C_{sp}^o}{\ln\left(\frac{C_{sp}^i}{C_{sp}^o}\right)} \approx \frac{C_{sp}^o + C_{sp}^i}{2} \quad (2.11)$$

In the original K-K derivation the logarithmic definition was motivated by the concentration approximation for chemical potential. In the present case the definition is arbitrary and the arithmetic mean will be used.

The product of system temperature and internal entropy generation is often termed the dissipation function  $\phi = T \frac{dS^*}{dt}$ , so we may write equation 2.2 as

$$\phi_1 = J_w \Delta\mu_w + J_{sp} \Delta\mu_{sp} \quad (2.12)$$

We now introduce a second dissipation function

$$\phi_2 = J_v \chi_v + J_D \chi_D \quad (2.13)$$

where the conjugate driving forces  $\chi_v$  and  $\chi_D$  are undetermined. By imposing the requirement that the entropy generation be invariant under the transformation so  $\phi_1 = \phi_2$  and by recognizing that the fluxes  $J_w$  and  $J_{sp}$  are independent we may use equations 2.9, 2.10, 2.12 and 2.13 to obtain

$$\chi_v = \frac{\Delta\mu_w}{u_w(1+\theta)} + \frac{C_{sp}^m}{1+\theta} \Delta\mu_{sp} \quad (2.14)$$

and

$$\chi_D = \frac{C_{sp}^m}{1+\theta} \left[ \Delta\mu_{sp} - \frac{u_{sp}}{u_w} \Delta\mu_w \right] \quad (2.15)$$

where the mean permeable solute volume fraction  $\theta$  is defined by

$$\theta = u_{sp} C_{sp}^m \quad (2.16)$$

As before, each flux is assumed to be linearly coupled to both driving forces

$$J_V = L_{11}' X_V + L_{12}' X_D \quad (2.17)$$

$$J_D = L_{12}' X_V + L_{22}' X_D \quad (2.18)$$

Using equations 2.9 and 2.10, equation 2.18 may now be rewritten in terms of the solute flux

$$J_{sp} = \frac{C_{sp}^m}{(1+\theta)^2} \left\{ L_{11}' \left[ \frac{\Delta\mu_w}{u_w} + C_{sp}^m \Delta\mu_{sp} \right] + L_{12}' \left[ \frac{1-\theta}{u_w} \Delta\mu_w + 2C_{sp}^m \Delta\mu_{sp} \right] \right. \\ \left. + L_{22}' \left[ \frac{-\theta}{u_w} \Delta\mu_w + C_{sp}^m \Delta\mu_{sp} \right] \right\} \quad (2.19)$$

A new parameter  $\omega$ , the solute permeability under conditions of zero volume flow is then defined by

$$J_{sp} = \omega C_{sp}^m \Delta\mu_{sp} \quad \left| \quad J_V = 0 \right. \quad (2.20)$$

To obtain  $\omega$  in terms of the phenomenological coefficients, equations 2.14, 2.15, and 2.17 are solved for  $\Delta\mu_w$  and the results substituted into equation 2.19 with the result

$$J_{sp} = \frac{(c_{sp}^m)^2}{1+\theta} \left( \frac{L_{11}^i L_{22}^i - (L_{12}^i)^2}{L_{11}^i - \theta L_{12}^i} \right) \Delta\mu_{sp} \Big|_{J_V = 0} \quad (2.21)$$

Thus, the solute permeability is a combination of the coefficients and mean concentration

$$\omega = \frac{c_{sp}^m}{1+\theta} \left[ \frac{L_{11}^i L_{22}^i - (L_{12}^i)^2}{L_{11}^i - \theta L_{12}^i} \right] \quad (2.22)$$

Another new parameter, the solute reflection coefficient  $\sigma$ , is defined by

$$\sigma = 1 + \frac{1}{v_w c_{sp}^m} \frac{\Delta\mu_w}{\Delta\mu_{sp}} \Big|_{J_V = 0} \quad (2.23)$$

We set the volume flux  $J_V$  to zero and apply equations 2.14, 2.15 and 2.17 to obtain

$$\sigma = \frac{-L_{12}^i (1+\theta)}{L_{11}^i - \theta L_{12}^i} \quad (2.24)$$

The reflection coefficient is usually taken to be a measure of membrane selectivity: if  $\sigma = 1$  the solute is completely excluded and the membrane behaves as an ideal semipermeable barrier; for  $\sigma < 1$  the solute is only partially excluded (reflected).

It is now possible, through a series of algebraic manipulations, to write flux equations based on the parameters  $L_{11}$  (usually denoted  $L_p$ ),  $\omega$  and  $\sigma$  as follows

$$J_w = \frac{1}{v_w(1+\theta-\theta\sigma)} \left\{ \left[ \frac{L_p}{1+\theta-\theta\sigma} + \theta v_{sp}\omega \right] \frac{\Delta\mu_w}{v_w} + \left[ \frac{L_p(1-\sigma)}{1+\theta-\theta\sigma} - v_{sp}\omega \right] C_{sp}^m \Delta\mu_{sp} \right\} \quad (2.25)$$

$$J_{sp} = \frac{1}{1+\theta-\theta\sigma} \left\{ \left[ \frac{L_p(1-\sigma)}{1+\theta-\theta\sigma} - v_{sp}\omega \right] C_{sp}^m \frac{\Delta\mu_w}{v_w} + \left[ \frac{L_p(1-\sigma)^2}{1+\theta-\theta\sigma} C_{sp}^m - \omega \right] C_{sp}^m \Delta\mu_{sp} \right\} \quad (2.26)$$

where  $L_p$  has units  $\text{cm}^3/\text{dyne sec}$  and  $\omega$  is in  $\text{mol}/\text{dyne sec}$ .

In the dilute limit  $\theta \rightarrow 0$  and the dilute approximation for solute chemical potential, equation 3.19, may be used. It is also true for most biological membrane - solute combinations that  $L_p \gg \omega$  so the above flux equations reduce to the usual K-K formulations

$$J_w = \frac{-RT}{v_w} \left\{ L_p \Delta C_{si} + (L_p\sigma + v_{sp}\omega) \Delta C_{sp} \right\} \quad (2.27)$$

$$J_{sp} = -RT C_{sp}^m \left\{ L_p(1-\sigma) \Delta C_{si} + \left[ L_p\sigma(1-\sigma) - \frac{\omega}{C_{sp}^m} \right] \Delta C_{sp} \right\} \quad (2.28)$$

where  $\Delta C_{si}$  is the trans-membrane difference in impermeable solute concentration (osmol/Kg). We have not explicitly included the conversion factors  $10^3 \text{ cm}^3/\text{liter}$  and  $\rho_w = 1 \text{ gm}/\text{cm}^3$ .

It should also be noted that the dilute approximations may be applied at any point in the above development and the definition or expression of interest will collapse to the forms originally presented by Kedem and Katchalsky and Katchalsky and Curran.

To gain some physical insight into these parameters, let us consider the following experiment: a cell initially at equilibrium in a solution of impermeable solute is suddenly exposed to a permeable solute. The cell will rapidly lose water and shrink because of the decreased extracellular water chemical potential, then slowly swell as solute and water enter the cell, driven by the solute concentration gradient. The rate of the rapid initial shrinkage will be determined almost wholly by the water permeability  $L_p$ , as  $L_p \gg \omega$  and there is initially very little solute transport. As solute begins to enter, and water continues to exit the cell, the interaction term  $\sigma$  becomes important. The shape of the volume minimum seen, for instance, in Figure 35, will be fixed primarily by  $\sigma$ . As solute slowly enters, the rate of swelling is almost entirely a function of solute permeability  $\omega$ . During this phase, intracellular concentration is increasing and water re-enters the cell, but the change in cell volume is rate limited by permeable solute entry.

Any of the above flux equations may be transformed into rate expressions for intracellular water and solute by applying the following mass conservation relations



$$\frac{dn_w}{dt} = -A_c J_w \quad [\text{mol/sec}] = [\text{cm}^2][\text{mol/cm}^2\text{sec}] \quad (2.29)$$

and

$$\frac{dn_{sp}}{dt} = -A_c J_{sp} \quad (2.30)$$

where  $A_c$  is the cell surface area and effluxes are considered positive.

## 2.2 Critical Examination of Transport Model Assumptions

The preceding transport models were derived for isothermal, isobaric, stationary membrane systems. How valid are these assumptions in the present case?

Although the experimental solutions and cells are initially in thermal equilibrium, the membrane is not an adiabatic barrier, and coupling between mass and heat transfer could exist. However, based on the analysis of Appendix B we may conclude that the maximum trans-membrane temperature difference induced by mass flow would be on the order of .01°C. In addition, thermal equilibrium within the cell would be reached very quickly - the lumped thermal time constant of the red cell is roughly

$$\tau_T = \frac{\ell_c^2}{a_T} = \frac{(.7 \times 10^{-4} \text{ cm})^2}{1.34 \times 10^{-3} \text{ cm}^2/\text{sec}} = 4 \times 10^{-6} \text{ sec}$$

where we have used the thermal diffusivity  $a_T$  of water and taken the characteristic length  $\ell_c$  to be the ratio of cell volume to area.

The maximum pressure difference which the membrane can withstand is about  $2 \times 10^{-4}$  atm [14]. Such a  $\Delta P$  alters the chemical potential of water by an amount equivalent to a  $10^{-5}$  osmol/Kg concentration difference and can be neglected.

The assumption that intramembrane conditions are quasi-steady is critical to the irreversible thermodynamics development. Let us first examine the simple case of water transport only. If the water chemical potential at a boundary is suddenly changed and then held fixed, conditions within the membrane will approach a new steady state within a characteristic time

$$(\tau_m)_w = \frac{\ell_m}{L_p} = \frac{100 \times 10^{-8} \text{ cm}}{10^{-2} \text{ cm/sec}} = 10^{-4} \text{ sec}$$

where  $\ell_m$  is the membrane thickness and we have used a mean experimental value of the conductivity  $L_p$ . By inspecting typical experimental records it may be seen that the time constant for changes in cell volume and hence cell water content and water chemical potential following a step change

in extracellular concentration is of the order  $10^{-2}$  second. The intracellular boundary condition thus changes slowly with respect to intramembrane rates, and the quasi-stationary assumption is reasonable.

The time required for a solute flux to reach steady state is much longer. For example, the measured ethylene glycol permeability is about  $10^{-6}$  cm/sec, so  $(\tau_m)_{sp}$  will be of the order of 1 second. Now, in the typical permeable solute experiment discussed earlier we see there are two distinct time scales - an initial rapid phase dominated by water transport and a later slow phase rate limited by solute flow. The time constant of this slow phase is of the order  $10^2$  seconds, so again the quasi-steady assumption is not unreasonable. However, during the rapid changes of the first few hundred milliseconds the solute flux will clearly be unsteady. At this point the theory falls apart, since equation 2.1 does not apply, nor is the integration in equation 2.2 possible. Is this important, though, in the context of our present objectives? We are really interested in measuring macroscopic membrane properties under varied conditions, and then using this data to predict cell response to freezing protocols. Now, we note that our computed permeability parameter values are quite insensitive to the magnitude of solute flow during the initial rapid phase. Therefore, even though the theory does not hold rigorously, we may still use the theoretical framework to arrive at a self consistent set of operational permeability parameters.

The final question we address is whether the membrane boundary conditions  $C$  are equal to the bulk solution concentrations  $C_b$ . When water flows through the membrane, the competing effects of convective transport and diffusion in the bulk solutions will alter the concentration in fluid boundary layers adjacent to the membrane, as shown in Figure 2. This is the unstirred layer or solute polarization effect discussed by Dick [15], Dainty [16], Sha'afi [17], Levin [4], and others.

To estimate the importance of this, we formulate the following simple model: (1) transport is one-dimensional and the membrane is an infinite plane; (2) we examine only short times, before any permeable solute transport is significant, and thus treat solutions as pseudo-binary and the membrane as ideal semi-permeable; (3) we neglect motion of the membrane boundary; (4) we neglect solution non-ideality. The resulting governing equation for diffusion in the intracellular solution is

$$\frac{\partial C^i}{\partial t} = D^v \frac{\partial^2 C^i}{\partial x^2} \quad 0 < x < \ell_c$$

At the cell center, symmetry requires that

$$\frac{\partial C^i}{\partial x} = 0 \quad x = 0$$

The boundary condition at the membrane states that the quantity of solute swept to the membrane surface by the water flux  $J_w$  must equal the amount removed by back diffusion

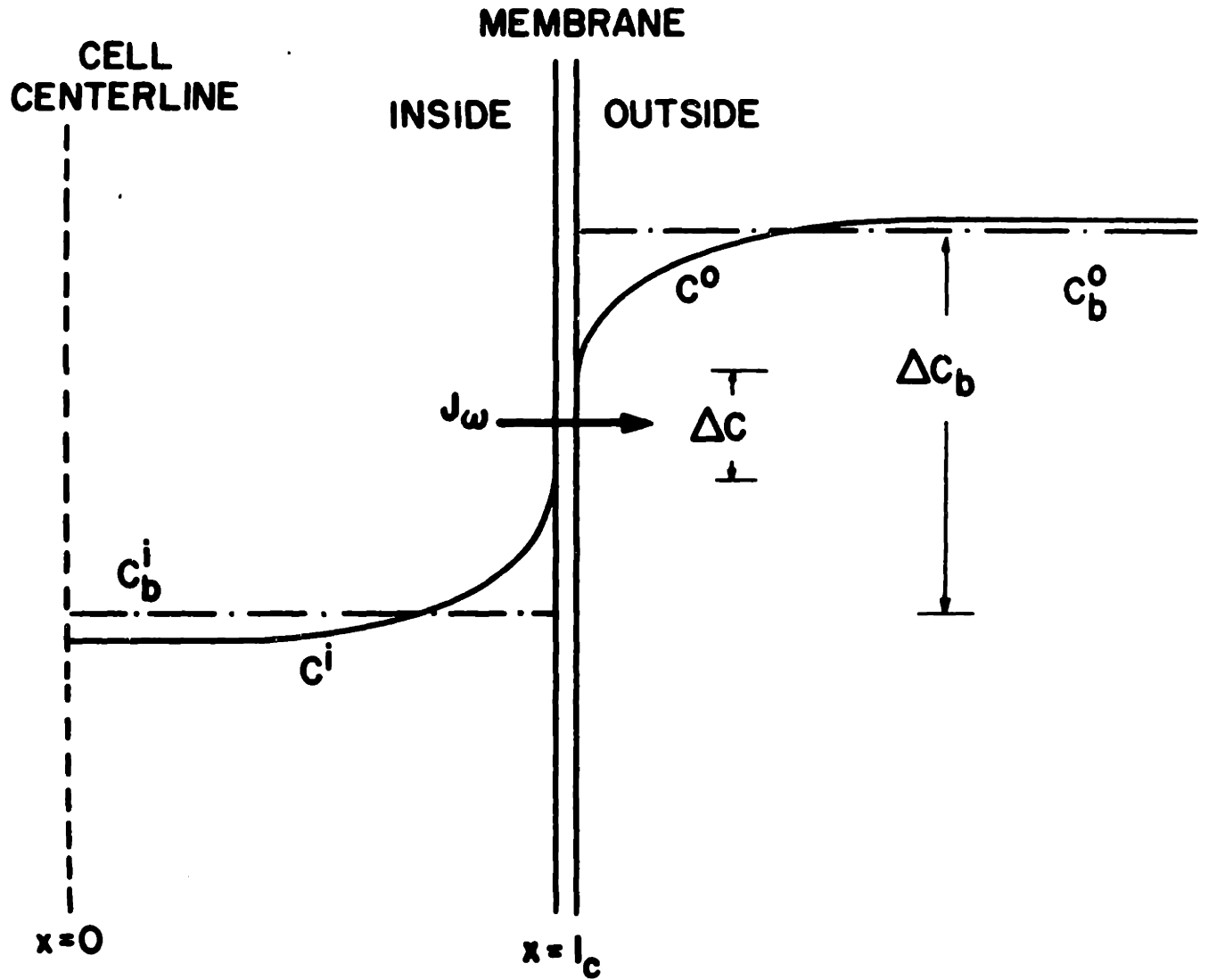


FIGURE 2 Solute polarization

$$D^V \frac{\partial C^i}{\partial x} - J_w^V C^i = 0 \quad x = \ell_c$$

The corresponding non-dimensional equations are

$$\frac{\partial \hat{C}}{\partial \hat{t}} = \frac{\partial^2 \hat{C}}{\partial \hat{x}^2} \quad 0 < \hat{x} < 1$$

$$\frac{\partial \hat{C}}{\partial \hat{x}} = 0 \quad \hat{x} = 0$$

$$\frac{\partial \hat{C}}{\partial \hat{x}} - \alpha \hat{C} = 0 \quad \hat{x} = 1$$

where the non-dimensional groups are defined as

$$\alpha = \frac{J_w^V \ell_c}{D^V} \quad \hat{t} = \frac{t D^V}{\ell_c^2}$$

$$\hat{C} = \frac{C^i}{C^i(t=0)} \quad \hat{x} = \frac{x}{\ell_c}$$

The scaling parameter  $\alpha$  is related to the Sherwood number and represents the ratio of convective to diffusional flow. For small  $\alpha$  we see that concentration polarization at the membrane is negligible

$$\alpha \ll 1 \quad \frac{\partial \hat{C}}{\partial \hat{x}} \sim 0 \quad \hat{x} = 1$$

The maximum water fluxes in each of the present series of experiments, obtained either by evaluating equation 2.25 at  $t=0$  or from computer simulations, range from  $3 \times 10^{-6}$  to  $10 \times 10^{-6}$  mol/cm<sup>2</sup>sec. The characteristic length is again taken to be the ratio of cell volume to surface area,  $.7 \times 10^{-4}$  cm. The mutual diffusion coefficient  $D^V$  is computed in Appendix A and is equal to  $2.6 \times 10^{-7}$  cm<sup>2</sup>/sec for a cell in isotonic saline and  $1.9 \times 10^{-6}$  cm<sup>2</sup>/sec for a cell pre-loaded with concentrated ethylene glycol. We find that  $\alpha$  ranges from  $6.6 \times 10^{-4}$  to a worst case value of  $4.6 \times 10^{-2}$ , and therefore we can reasonably neglect the effect of unstirred layers on measured permeabilities.

**CHAPTER 3**  
**GENERAL SOLUTION MODELS**



### 3.1 Chemical Potential, Activity, Osmolality

The flux equations developed in Chapter 2 relate mass flow through a membrane to differences in bulk solution chemical potentials. The following chapter will present general relations between the chemical potential and accessible concentration scales.

The chemical potential  $\mu$  of the  $i^{\text{th}}$  species in a solution is given by (e.g. [18])

$$\mu_i = \mu_i^* + RT \ln a_i \quad (3.1)$$

where  $a_i$  is the activity. For the solvent  $w$ , the reference state  $\mu_w^*$  is simply equal to the Gibbs free energy per mole of pure substance at the given temperature and pressure. For solutes  $s$ ,  $\mu_s^*$  is equal to the chemical potential of the solute in a hypothetical state in which the amount of solvent in the solution is reduced to zero. Thus, for solutes,  $\mu_s^*$  is a function of temperature and pressure, and may depend on the solvent and other solutes present. However, in neither case is  $\mu^*$  a function of concentration.

In this work we are interested only in differences in chemical potential across a membrane, and, as discussed in section 2.2, this is an isothermal, isobaric situation. Therefore, for the solvent,  $\mu^*$  is irrelevant. As regards solutes, we must make the assumption that they do not interact to any extent and each may be treated as if it were in a binary aqueous solution. The trans-membrane difference in chemical potential is then

$$\Delta\mu_i = RT\Delta\ln a_i \quad (3.2)$$

for both solvent and solutes.

The activity  $a_i$  of  $i$  in a non-ideal solution is defined as

$$a_i = \gamma_i x_i \quad (3.3)$$

where the activity coefficient  $\gamma_i$  approaches unity in the dilute limit  $x_w \rightarrow 1$ . The mole fraction  $x_i$  is given in terms of the mole amounts of all independent entities in solution as

$$x_i = \frac{v_i n_i}{\sum_j v_j n_j} \quad (3.4)$$

where  $v_i$ , the dissociation number, is the number of ions formed from a single molecule of electrolyte.

The activity of the solvent in a binary solution may also be given by

$$\ln a_w = - MW_w \phi v m \quad (3.5)$$

where  $MW_w$  is the solvent molecular weight,  $m$  the solute molal concentration and  $\phi$  the molal osmotic coefficient. When the solvent is water, equation 3.5 becomes

$$\ln a_w = \frac{-18.015 \text{ gm/mol}}{1000 \text{ gm/Kg}} \phi v m \text{ (mol/Kg)} \quad (3.6)$$

Equations 3.5 and 3.6 are actually defining expressions for the osmotic coefficient  $\phi$ , which is solute and solvent specific and a function of solute concentration. The quantity  $\phi v_m$  is commonly termed the solution osmolality and has units of osmol/Kg H<sub>2</sub>O or Osm.

Solvent activity is related to a physically measurable quantity, the solution equilibrium freezing point  $T_f$  by

$$\frac{\partial \ln a_w}{\partial T_f} = \frac{-L_w}{RT_f} \quad (3.7)$$

where  $L_w$  is the latent heat of fusion of pure solvent at that temperature [18]. By using a polynomial expression for  $L_w(T)$ , Levin [4] has integrated equation 3.7 for water and has obtained the following numerical expression

$$\ln a_w = 3.736 \times 10^3 \left( \frac{1}{T_f} - \frac{1}{T_0} \right) + 36.18 \frac{T_f}{T_0} + .1204(T_0 - T_f) + 5.435 \times 10^{-5} (T_f^2 - T_0^2) \quad (3.8)$$

where  $T_0 = 273.15^\circ\text{K}$ . If the latent heat is taken as constant, the following approximate relation is obtained from equation 3.7:

$$-\ln a_w = \frac{L_w(T_0 - T_f)}{RT_0^2} \quad (3.9)$$

The osmometer, a commercial laboratory device which measures solution freezing points, uses this linear expression and equation 3.6 to obtain the osmolality from  $T_0 - T_f$  by the relation 1 osmol/Kg = 1.858 °K. Water activities based on this linear expression differ by less than 1% from those

computed with equation 3.8 in the concentration range 0 - 5.0 osmol/Kg.

In the absence of an adequate solution theory and in light of the data of Katchalsky and Alexandrowicz [19] it is reasonable to assume that equation 3.6 may be extended to solutions containing multiple solutes,

$$\ln a_w = \frac{-18.015}{1000} \sum_s \phi_s v_s m_s \quad (3.10)$$

The osmotic coefficients  $\phi_s(m_s)$  used in equation 3.10 are those measured separately for each solute in a binary aqueous solution. In writing equation 3.10 we are again assuming that solute/solvent interactions are more important than solute/solute effects.

The water activity computed from equation 3.8 or 3.9 will be the activity at the freezing point, and to be strictly correct, all activities should be referenced to a standard temperature. However, a comparison of water activity in an aqueous NaCl solution as computed using freezing point data [20] and equation 3.8 or as tabulated at 25°C [21] reveals that the temperature effect is not significant (Figure 3). Lewis and Randall [22] outline a procedure for activity temperature correction, but the necessary thermodynamic data are available only for NaCl. As a check of equation 3.8, this procedure was applied to the freezing point activities shown in Figure 3 and good agreement with the data at 25°C was obtained.

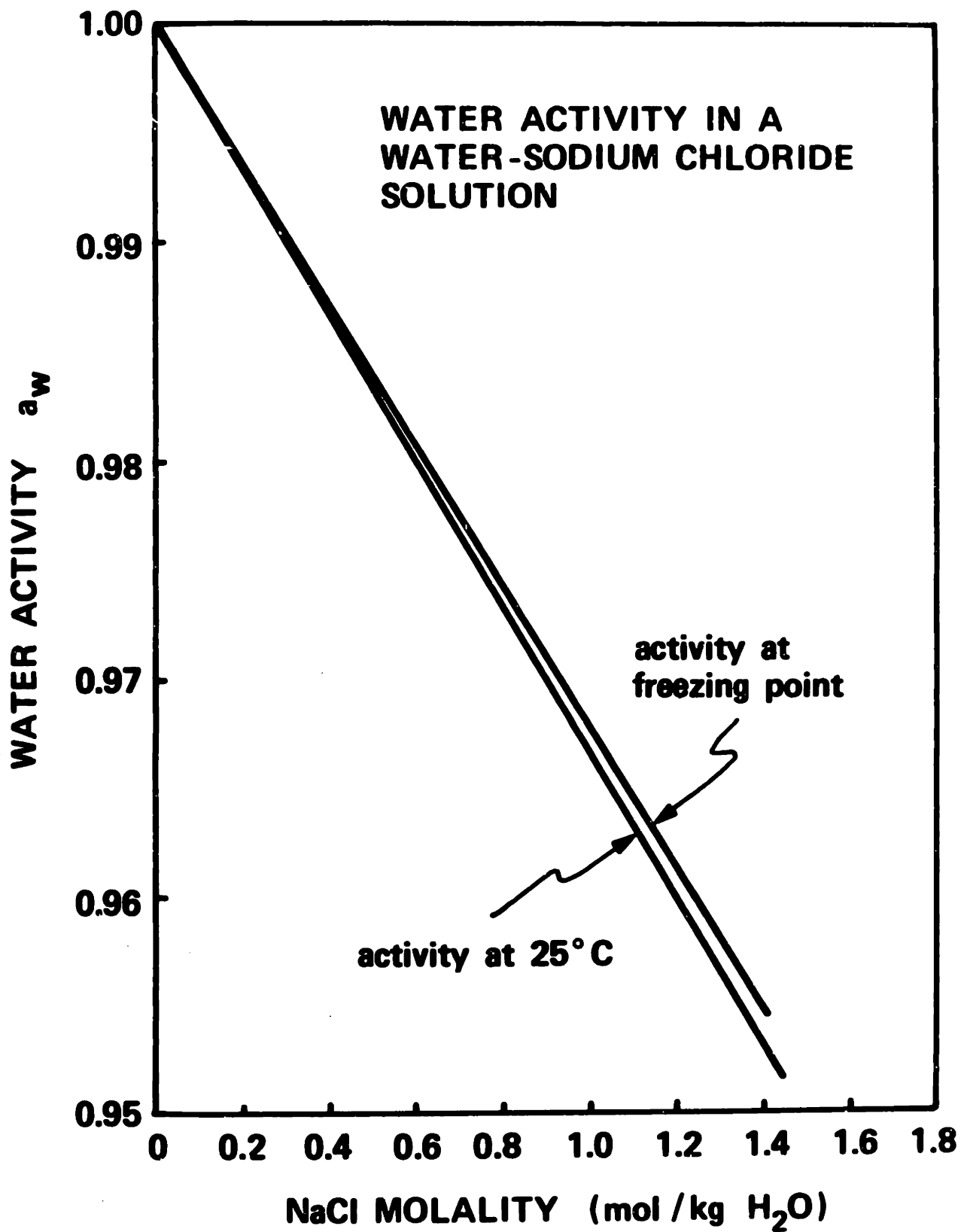


**FIGURE 3** Water activity in a binary NaCl solution

### 3.2 Dilute Approximations

When a solution is dilute it is possible to derive approximate expressions for the chemical potentials of solvent and solute. First, since in the dilute limit the solution approaches ideal behavior and then by definition the activity coefficient  $\gamma \rightarrow 1$ , equation 3.1 becomes

$$\mu_i = \mu_i^* + RT \ln x_i \quad (3.11)$$

The solvent mole fraction  $x_w$  may be expanded to yield

$$\ln x_w = \ln \left[ \frac{n_w}{n_w + \sum v_s n_s} \right] = -\ln \left[ 1 + \frac{\sum v_s n_s}{n_w} \right] \quad (3.12)$$

where  $\sum v_s n_s$  is a summation over all solute species. If the solution is number dilute in that  $n_w \gg \sum v_s n_s$ , the logarithm may be approximated by

$$-\ln \left[ 1 + \frac{\sum v_s n_s}{n_w} \right] \approx \frac{-\sum v_s n_s}{n_w} \approx \sum x_s \quad (3.13)$$

In terms of molal concentration  $m_s$

$$\frac{\sum v_s n_s}{n_w} = \frac{18.015 \text{ gm/mol}}{1000 \text{ gm/Kg}} \sum v_s m_s \quad (3.14)$$

Thus, the chemical potential of the solvent may be approximated as

$$\mu_w = \mu_w^* - \frac{18.015}{1000} RT \sum \nu_s m_s \quad (3.15)$$

which is equivalent to equation 3.10 in the ideal dilute limit  $\phi \rightarrow 1$ .

Similar results for the chemical potential of a non-electrolyte solute may be derived by first approximating the solute mole fraction as

$$x_s \approx \frac{n_s}{n_w} \quad (3.16)$$

where we again consider a number dilute solution. In terms of molal concentrations the solute chemical potential is approximately

$$\mu_s \approx \mu_s^* + RT \ln \left( \frac{18.015 \text{ gm/mol}}{1000 \text{ gm/Kg}} m_s \right) \quad (3.17)$$

An aqueous solution which contains primarily non-protein solutes with molar volumes of 10 - 100 cm<sup>3</sup>/mol will also be volume dilute if it is number dilute. That is, the total volume of solution  $V = \sum \nu_i n_i$  will be approximately equal to the volume of solvent in the solution. In that case, concentrations may be expressed either as molal (mol/Kg H<sub>2</sub>O) or molar (mol/liter solution) without appreciable error. In the latter case we neglect the small temperature variation of water density and set  $\rho_w = 1.00 \text{ Kg/liter}$ . The red cell intracellular solution is not volume dilute, however, even under isotonic conditions and some care must be exercised in the use of different concentration scales. In order to simplify notation, concentration will often be denoted simply as C,

without specifying units unless the choice of scale is significant and not apparent from context.

If we are concerned only with trans-membrane differences, the logarithmic dependence in equation 3.17 may be eliminated by first defining a mean concentration

$$C_s^m = \frac{C_s^i - C_s^o}{\ln\left(\frac{C_s^i}{C_s^o}\right)} \quad (3.18)$$

where, as before, superscript o denotes extracellular and i intracellular. The difference in chemical potential is then

$$\Delta\mu_s = \mu_s^i - \mu_s^o = RT \ln\left(\frac{C_s^i}{C_s^o}\right) = RT \frac{(C_s^i - C_s^o)}{C_s^m} \quad (3.19)$$

For small concentration differences,  $C_s^i/C_s^o \sim 1$ , we may use the first term in the series expansion

$$\ln z = 2 \left\{ \frac{z-1}{z+1} + \frac{1}{3} \left(\frac{z-1}{z+1}\right)^3 + \dots \right\} \quad (3.20)$$

to approximate equation 3.18 with the arithmetic mean

$$C_s^m \approx \frac{C_s^i + C_s^o}{2} \quad (3.21)$$



### 3.3 A Method of Computing Solute Activity

As discussed previously, solvent non-ideality may be easily calculated from freezing point data. The solute activity, though not directly obtainable, may also be computed by the method outlined below.

The Gibbs-Duhem equation [18] describes restrictions on possible changes in constituent masses and chemical potentials in a binary solution

$$n_w \frac{\partial \mu_w}{\partial x_w} + n_s \frac{\partial \mu_s}{\partial x_s} = 0 \quad (3.22)$$

where  $n$  is the quantity (mols),  $\mu$  the chemical potential, and  $x$  the mole fraction of the solvent  $w$  and solute  $s$ . From the definition of chemical potential in terms of activity coefficient  $\gamma$  and mole fraction, the Gibbs-Duhem equation may also be written

$$x_w \left( \frac{\partial \ln \gamma_w}{\partial x_w} \right)_{T,P} + x_s \left( \frac{\partial \ln \gamma_s}{\partial x_s} \right)_{T,P} = 0 \quad (3.23)$$

If one applies the defining relation for the molal osmotic coefficient  $\phi$  and converts mole fractions to solute molal concentration  $m_s$ , equation 3.23 may be integrated to yield the solute activity coefficient at any molality [22]

$$\ln \gamma_s(m_s) = \phi_s(m_s) - 1 + \int_0^{m_s} \frac{\phi_s(m_s) - 1}{m_s} dm_s \quad (3.24)$$

The osmotic coefficient as a function of concentration may be obtained from solution freezing point data and least squares fitted with an  $n^{\text{th}}$  order polynomial

$$\phi_s(m_s) = a_0 + a_1 m_s + a_2 m_s^2 + \dots + a_n m_s^n \quad (3.25)$$

The integral in equation 3.24 may then be directly evaluated

$$\int_0^{m_s} \frac{\phi_s(m_s) - 1}{m_s} dm_s = (a_0 - 1) \ln m_s + a_1 m_s + \frac{a_2 m_s^2}{2} + \dots + \frac{a_n m_s^n}{n} \Bigg|_0^{m_s} \quad (3.26)$$

The first term,  $(a_0 - 1) \ln m_s$ , is undefined at  $m_s = 0$ . However, since by definition  $\phi_s \rightarrow 1$  as  $m_s \rightarrow 0$ , the first polynomial coefficient  $a_0$  should equal one, given a perfect fit, and the first term is thus equivalent to

$$\lim_{x \rightarrow 0} x \ln x$$

This may be transformed to

$$\lim_{y \rightarrow \infty} \frac{-\ln y}{y}$$

which by l'Hôpital's rule is equal to

$$\lim_{y \rightarrow \infty} \frac{-1/y}{1} = 0$$

The right hand side of equation 3.26 is therefore equal to zero at  $m_s = 0$  and the solute activity coefficient is given by

$$\ln \gamma_s(m_s) = (a_0 - 1)(1 + \lambda n m_s) + 2a_1 m_s + (1 + \frac{1}{2})a_2 m_s^2 \dots (1 + \frac{1}{n})a_n m_s^n \quad (3.27)$$

The concentration dependent osmotic coefficient of ethylene glycol in water shown in Figure 4 was computed from freezing point data [20] according to equations 3.8 and 3.6. The method outlined above was then used to compute the activity coefficient and activity, plotted in Figure 5. Polynomial least squares curve fits of this data are listed in Appendix F, as are similar data for glycerol/water solutions.

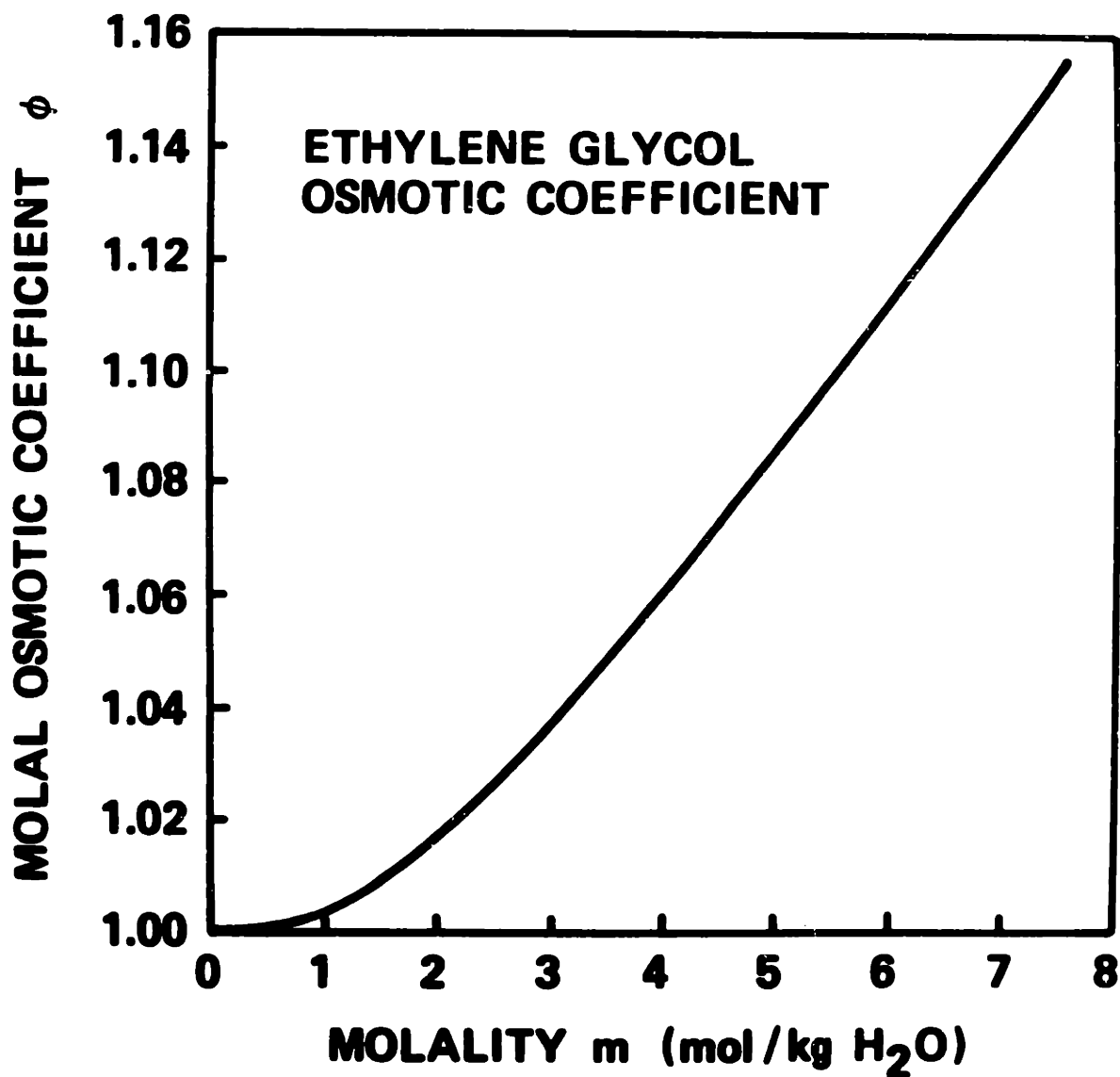


FIGURE 4 Molal osmotic coefficient of ethylene glycol in the aqueous solution

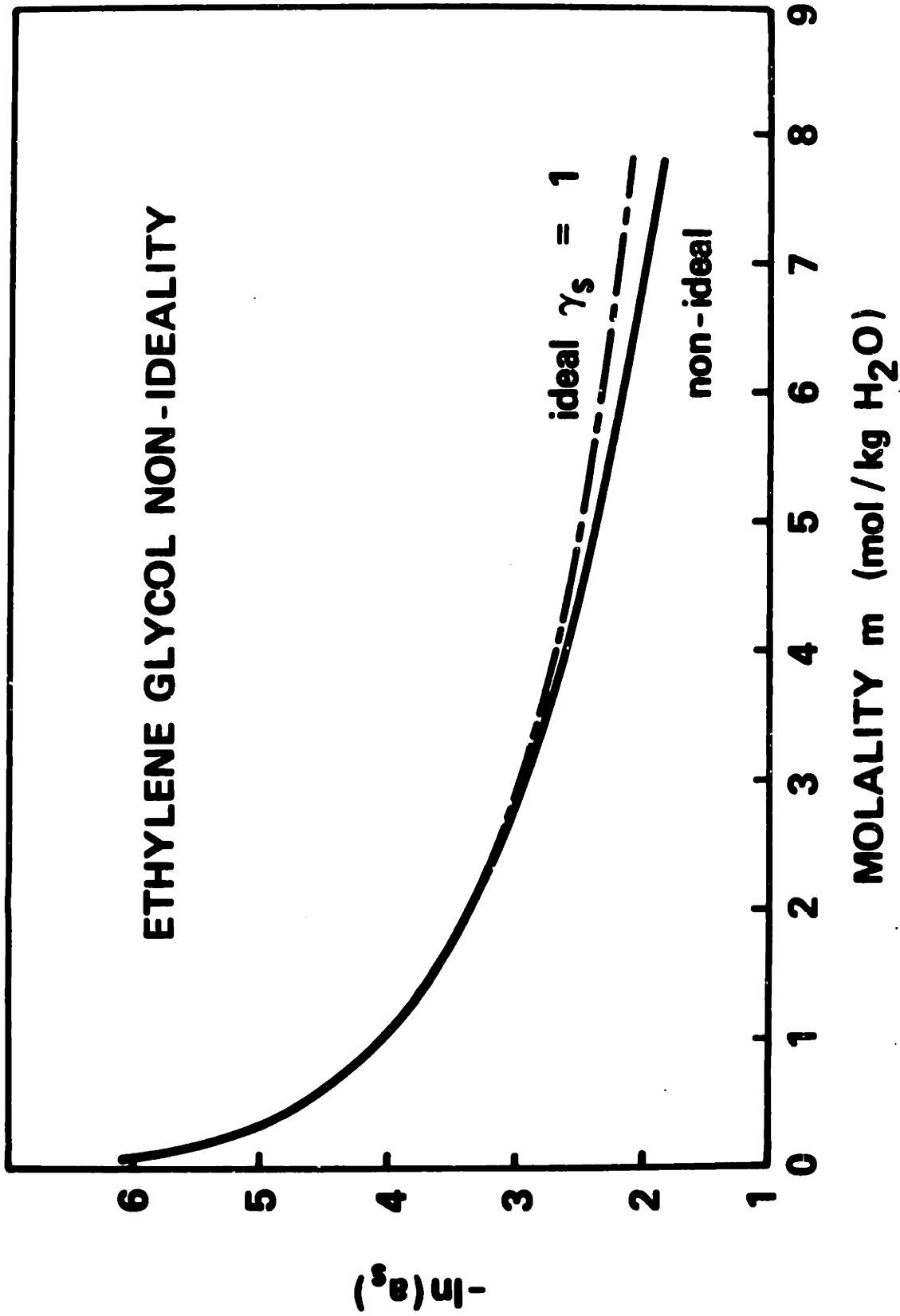


FIGURE 5 Ethylene glycol activity in an aqueous solution

**CHAPTER 4**  
**THE PSEUDO-BINARY INTRACELLULAR MODEL**

#### 4.1 The Pseudo-Binary Solution Model

Although the human erythrocyte contains a complex aqueous solution of proteins, electrolytes and sugars, the hydrated pseudo-binary solution model of Levin [4] provides simple descriptions of intracellular solution and cell volume behavior. The model is based on the following assumptions: (1) all impermeable intracellular solutes may be lumped into a single fictitious pseudo-solute (hence, a pseudo-binary solute/water solution); (2) this pseudo-solute may be considered to have the combined properties of hemoglobin, the principal protein, and KCl, the dominant electrolyte; (3) a portion of the cell's water content is tightly bound to hemoglobin and KCl as water of hydration; (4) thermodynamic descriptions of solutions in-vitro apply equally well to the erythrocyte intracellular solution.

In developing this solution model it is first necessary to assign values to the relevant quantities for the cell in the normal isotonic state. Of the total cell volume of  $100.0 \times 10^{-12} \text{ cm}^3$  (Table H2) about 72% is water, as determined by drying with heat or vacuum (Table H3), so the isotonic cell water content is  $4.00 \times 10^{-12} \text{ mol}$ . If the hemoglobin (Hb) molecular weight is taken to be 66,800 gm/mol, and the small quantity of non-hemoglobin proteins is added to the normal cellular hemoglobin content of 33.7 gm/100 ml cells, a value of  $5.2 \times 10^{-16} \text{ mol Hb/cell}$  is obtained. A KCl content of  $1.052 \times 10^{-14} \text{ mol/cell}$  is obtained by calculating the amount necessary to yield a computed solution osmolality of .290 osmol/Kg under isotonic conditions. This agrees well with the value for total electrolyte content,  $1.033 \times 10^{-14} \text{ mol/cell}$  from data in Table H4.

The water of hydration bound to hemoglobin is approximately .30 - .26 gm H<sub>2</sub>O/gm Hb [4] [23], roughly 1260 mol H<sub>2</sub>O/mol Hb. For KCl, the hydration data range from .6 to 1.9 mol H<sub>2</sub>O/mol KCl [21], so a value of 1.0 will be used for the hydration number  $n_{KCl}$ . The hydrated molar volume of hemoglobin  $v_{Hb}^h$  is taken as  $7.0 \times 10^4 \text{ cm}^3/\text{mol}$  [24], and that of KCl computed as  $45.5 \text{ cm}^3/\text{mol}$  by summing its anhydrous molar volume  $27.5 \text{ cm}^3/\text{mol}$  [21] and the volume of the water of hydration. Note that these hydration numbers and molar volumes are derived from static rather than diffusion experiments, and therefore include only the inner, tightly bound, water shell and not the outer shells which are swept along by a moving solute. Also, it is assumed that the hydration numbers and molar volumes are not concentration dependent.

Similar parameters for the pseudo-solute are determined by forming appropriately weighted sums of hemoglobin and KCl data. Noting that KCl is an electrolyte with dissociation number  $\nu = 2$ , the quantity of pseudo-solute in the cell is

$$\begin{aligned} n_{pb} &= 2n_{KCl} + n_{Hb} && (4.1) \\ &= (2)(1.052 \times 10^{-14}) + 5.2 \times 10^{-16} \\ &= 2.156 \times 10^{-14} \text{ mol/cell} \end{aligned}$$

The pseudo-solute hydrated molar volume is



$$v_{pb}^h = \frac{v_{KCl}^h n_{KCl} + v_{Hb}^h n_{Hb}}{n_{pb}} \quad (4.2)$$

$$= 1.710 \times 10^3 \text{ cm}^3/\text{mol}$$

and its hydration number is

$$h_{pb} = \frac{h_{KCl} n_{KCl} + h_{Hb} n_{Hb}}{n_{pb}} \quad (4.3)$$

$$= 30.88 \text{ mol H}_2\text{O/mol solute}$$

The isotonic quantity of free water, that is, water not strongly bound to solute as water of hydration, is given by

$$n_w^f = n_w - h_{pb} n_{pb} \quad (4.4)$$

$$= 3.334 \times 10^{-12} \text{ mol/cell}$$

Even under isotonic conditions, the intracellular solution is non-dilute and non-ideal. Therefore, the solution models of section 3.1 will be used to develop relations between cell water content  $n_w$  and water activity  $a_w$ . First, the pseudo-solute molality is defined by

$$m_{pb} = 2m_{KCl} + m_{Hb} \quad (4.5)$$

where the molality of each species is given as usual by

$$m_i (\text{mol/Kg H}_2\text{O}) = \frac{1000 \text{ gm/Kg}}{18.015 \text{ gm/mol}} \frac{n_i}{n_w}$$

Note that solution properties are in terms of total water  $n_w$ , without regard to the free water/water of hydration partitioning.

Data for the hemoglobin molal osmotic coefficient  $\phi_{\text{Hb}}$  from Adair [25] and McConaghey and Maizels [26] are shown in Figure 6, and were least squares fit with a fifth order polynomial. Similar data for KCl, tabulated by Robinson and Stokes [21], are shown in Figure 7. These data were also fit with a fifth order polynomial in the region of interest, 0.0 to 0.7 molal.

The pseudo-binary solute molal osmotic coefficient  $\phi_{\text{pb}}$  is now defined by the relation

$$\phi_{\text{pb}} m_{\text{pb}} = 2 \phi_{\text{KCl}} m_{\text{KCl}} + \phi_{\text{Hb}} m_{\text{Hb}} \quad (4.6)$$

This follows from the requirement that the water activity be a physical property of the solution, independent of our choice of concentration variables. The pseudo-binary osmotic coefficient may now be calculated as a function of pseudo-solute molality by first noting that, for a given cell water content  $n_w$ , the molalities  $m_{\text{Hb}}$ ,  $m_{\text{KCl}}$  and  $m_{\text{pb}}$  are in fixed ratios set by the constants  $n_{\text{Hb}}$ ,  $n_{\text{KCl}}$  and  $n_{\text{pb}}$ . Given the concentrations of hemoglobin and potassium chloride,  $m_{\text{Hb}}$  and  $m_{\text{KCl}}$ , the osmotic coefficients  $\phi_{\text{Hb}}$  and  $\phi_{\text{KCl}}$  may be computed from the data curve fits. The coefficient  $\phi_{\text{pb}}$  is then easily obtained from equation 4.6.

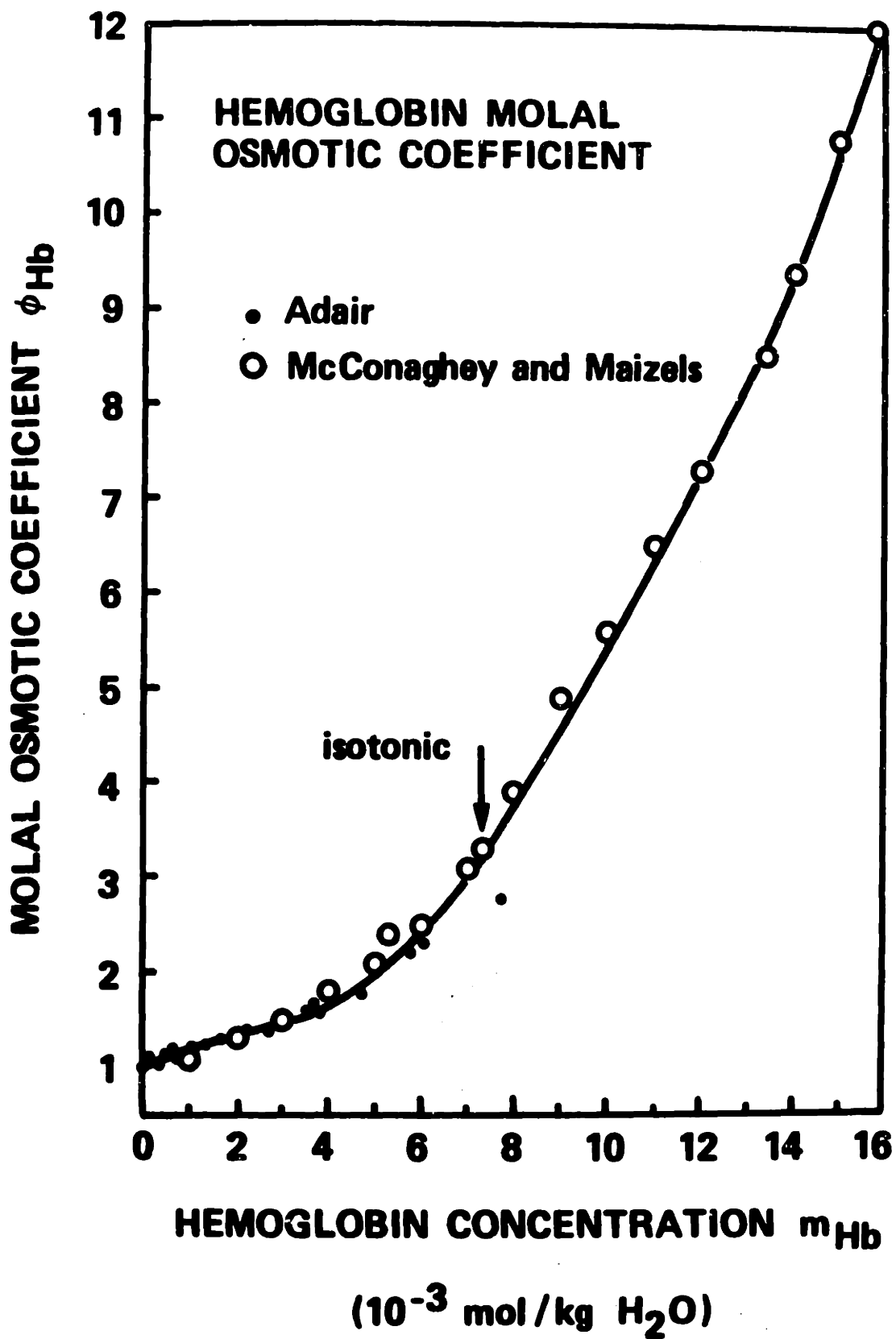


FIGURE 6 Hemoglobin osmotic coefficient

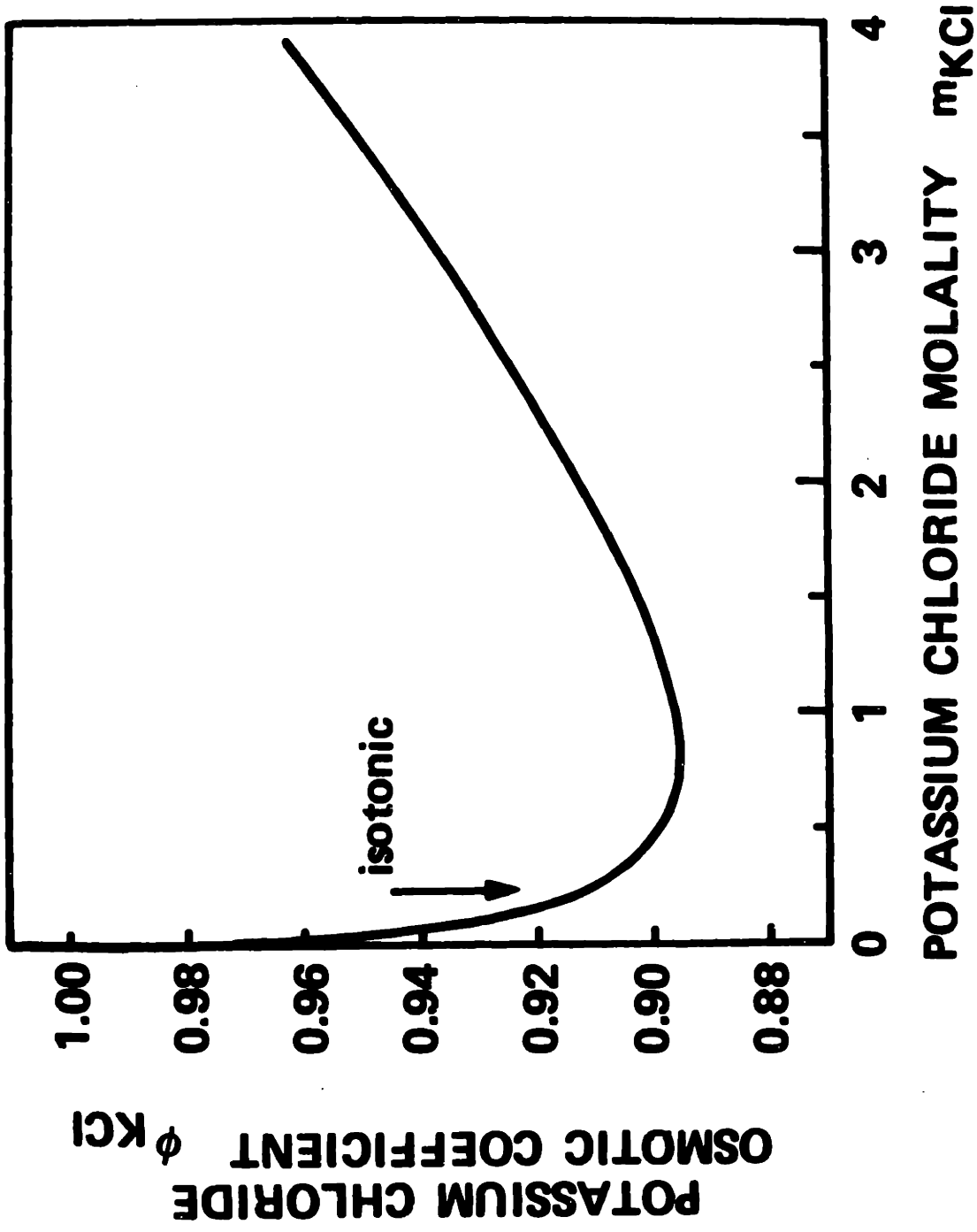


FIGURE 7 Potassium chloride osmotic coefficient

Unfortunately, the data for hemoglobin do not extend to the high concentrations encountered in our experiments. Rather than simply extrapolate the hemoglobin data, Levin [4] suggests a correlation of the van Laar type applied to the pseudo-binary solution. The computational scheme is briefly discussed in Appendix C, and a rationale for the method is presented by Levin. The final results for the pseudo-solute osmotic coefficient are presented in Figure 8 in terms of pseudo-solute molality.

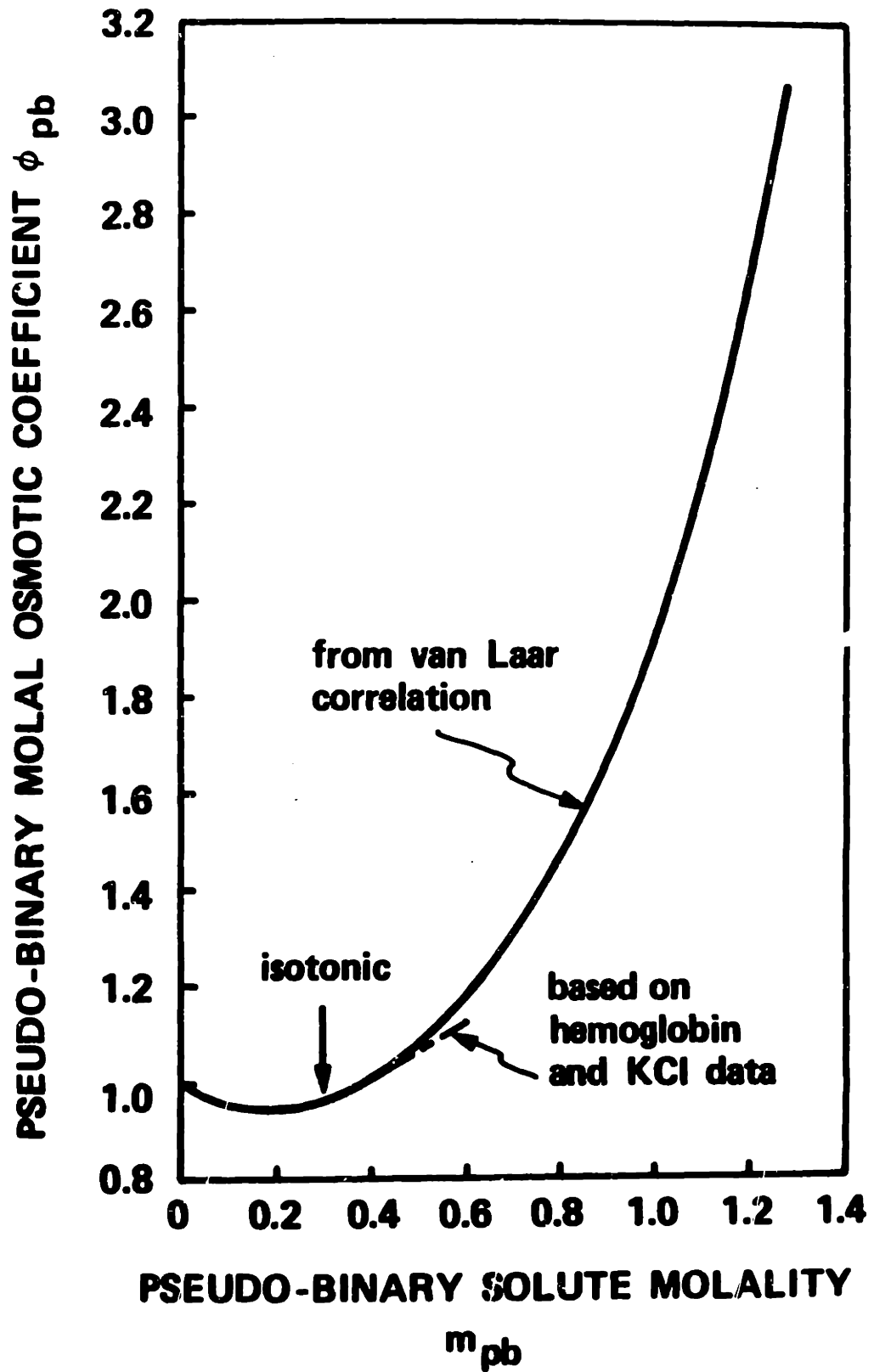


FIGURE 8 The computed osmotic coefficient of the pseudo-binary solute

TABLE 1  
SUMMARY OF PSEUDO-BINARY CONSTANTS

pseudo-solute content	$n_{pb}$	$2.156 \times 10^{-14}$ mol
pseudo-solute molar volume	$v_{pb}^h$	$1.710 \times 10^3$ cm <sup>3</sup> /mol
pseudo-solute hydration number	$h_{pb}$	30.88 mol H <sub>2</sub> O/mol
total water content, isotonic	$(n_w)_{iso}$	$4.000 \times 10^{-12}$ mol
free water content, isotonic	$(n_w^f)_{iso}$	$3.334 \times 10^{-12}$ mol
bound water content	$n_w^b$	$6.658 \times 10^{-13}$ mol

## 4.2 Red Cell Volume

The pseudo-binary solution model also accurately predicts cell volume as a function of cell water content. The cell is pictured as consisting of water, the hydrated pseudo-solute, and a small quantity of membrane material  $V_m$ , so cell volume is

$$V_c = n_w^f v_w + n_{pb} v_{pb}^h + V_m \quad (4.7)$$

From section 4.1 the computed pseudo-solute content is  $n_{pb} = 2.156 \times 10^{-14}$  and the hydrated molar volume is  $v_{pb}^h = 1.710 \times 10^3 \text{ cm}^3/\text{mol}$ . Since we consider the membrane to be completely impermeable to the intracellular electrolytes and proteins, and assume that hydration is not concentration dependent, these values are constant. The cell water content under isotonic conditions was computed to be  $(n_w^f)_{iso} = 3.334 \times 10^{-12} \text{ mol}$ . The erythrocyte membrane is roughly  $100 \times 10^{-8} \text{ cm}$  thick and  $135 \times 10^{-8} \text{ cm}^2$  in area, so the membrane volume is  $V_m = 1.35 \times 10^{-12} \text{ cm}^3$ . Thus from equation 4.7, the pseudo-binary model predicts an isotonic cell volume of  $98.3 \times 10^{-12} \text{ cm}^3$ . To simplify later calculations and reconcile the computed volume with the initial data value, the isotonic cell volume is set equal to  $100.0 \times 10^{-12} \text{ cm}^3$  by including a small correction of  $1.7 \times 10^{-12} \text{ cm}^3$  in the fixed volume term  $n_{pb} v_{pb}^h + V_m$ . The resulting cell volume equation is

$$V_c = n_w^f \times 18.015 \text{ cm}^3/\text{mol} + 39.94 \times 10^{-12} \text{ cm}^3 \quad (4.8)$$



where we have assumed that the partial molar volume of water in the intracellular solution is equal to the pure substance molar volume.

The pseudo-binary solution and cell volume models now contain the information necessary to calculate the equilibrium volume of a cell suspended in a solution of known composition. Suppose the cell is immersed in a solution of water and an impermeable solute such as NaCl. Since we assume that there is no temperature or pressure differential across the membrane, the equilibrium condition is equality of water activity in the extracellular and intracellular solutions,  $a_w^o = a_w^i$ . The equilibrium condition may also be expressed in terms of solution osmolalities

$$\phi_{pb} m_{pb} = C_{si}^o \Big|_{\text{equilibrium}} \quad (4.9)$$

where  $C_{si}^o$  is the extracellular impermeable solute concentration (osmol/Kg),  $m_{pb}$  the pseudo-binary solute molality, and  $\phi_{pb}$  the pseudo-solute molal osmotic coefficient. Cell volume as a function of extracellular concentration may now be calculated from the equilibrium condition equation 4.9, the definition of molality with constant  $n_{pb}$ , the curve fit for  $\phi_{pb}(m_{pb})$  listed in Appendix F and the cell volume relation, equation 4.8.

A simple correlation may be obtained if we note that for constant  $\phi_{pb}$  the cell volume relation takes the form

$$V_c \sim a_o + a_i \frac{i}{C_{si}^o}$$

where the intercept  $a_0 \sim n_{pb} u_{pb}^h + V_m$ . Figure 9, therefore, is a plot of calculated cell volume, normalized to the isotonic volume  $100 \times 10^{-12} \text{ cm}^3$ , as a function of inverse extracellular concentration. The data points ( $n = 57$ ) were obtained in the course of nine calibration sets, as described in Chapter 7, performed over a three month period.

It is interesting to note that the fixed volume predicted by the pseudo-binary model,  $40 \times 10^{-12} \text{ cm}^3$ , has roughly the same numerical value as the so called "osmotic dead volume" commonly obtained by extrapolating data such as are shown in Figure 9 to the limit  $1/C_{si}^0 \rightarrow 0$ . It should be emphasized, however, that the pseudo-binary model does not depend a priori on such experiments, but is developed solely from data for cells under isotonic conditions and well established physical chemistry data and theory.

When cells are immersed in a solution which contains a permeable solute  $sp$  as well as an impermeable species  $si$ , cell volume will be a function both of water content and solute uptake. This may be expressed as

$$V_c = n_w^f u_w + n_{sp} u_{sp} + n_{pb} u_{pb}^h + V_m \quad (4.10)$$

where  $n_{sp}$  is the amount (mols) and  $u_{sp}$  the molar volume ( $\text{cm}^3/\text{mol}$ ) of permeable solute in the intracellular solution.

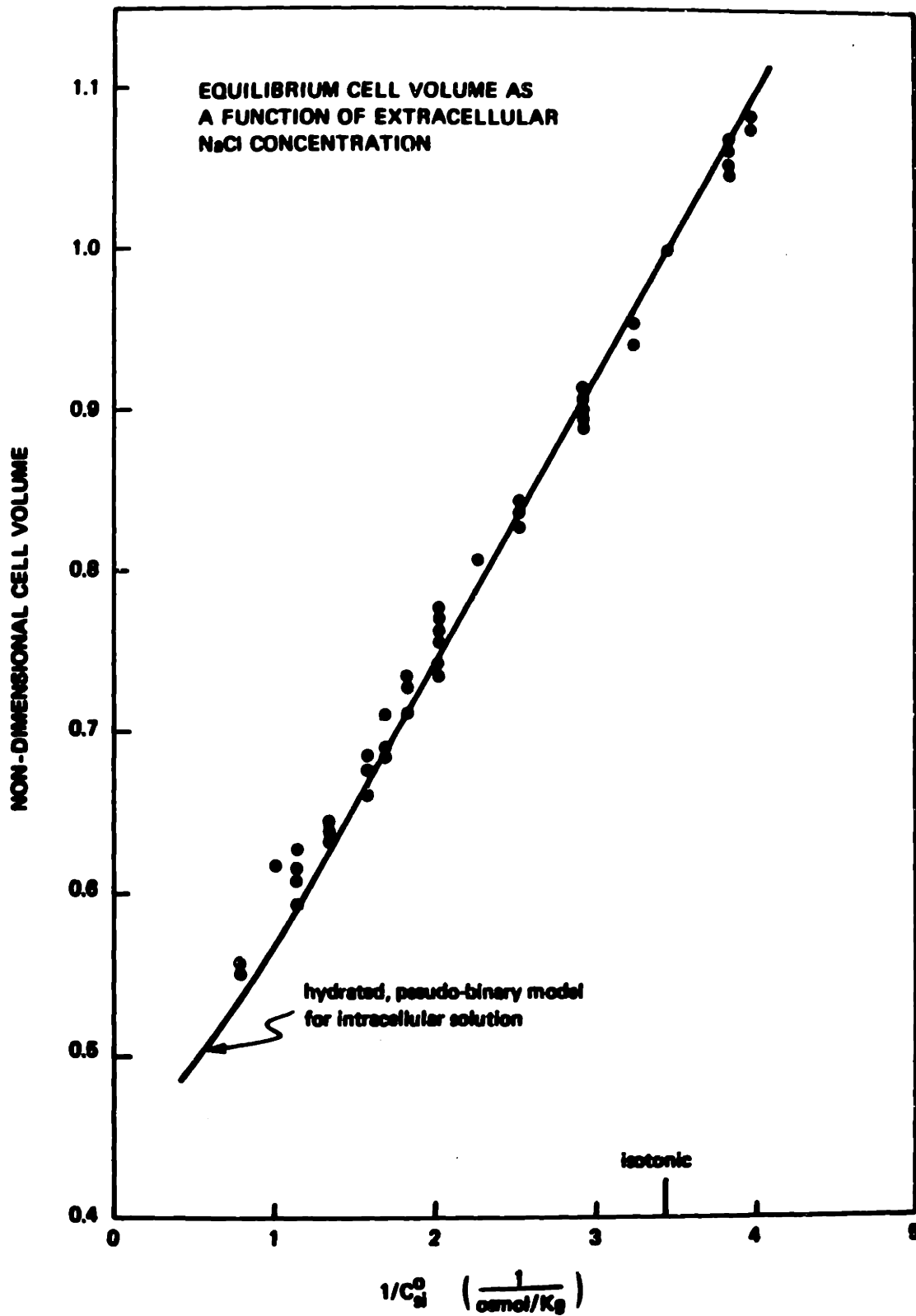


**FIGURE 9** Equilibrium red cell volume as a function of extracellular NaCl concentration

The partial molar volume of a species  $i$  in a solution with total volume  $V$  is defined as the change in volume per mol of  $i$  added at constant temperature, pressure, and quantity of all other species

$$v_i = \left( \frac{\partial V}{\partial n_i} \right)_{T,P,n_j} \quad j \neq i \quad (4.11)$$

Since the volume of intracellular solution, apart from the small membrane volume, is equal to the cell volume, equation 4.10 may be differentiated to yield

$$v_{sp} = \left( \frac{\partial V_c}{\partial n_{sp}} \right)_{T,P,n_w^f,n_{pb}^h} \quad (4.12)$$

assuming constant molar volumes  $v_w$  and  $v_{pb}^h$ . Thus  $v_{sp}$  is strictly the solute partial molar volume. However, there is no reason to expect that the partial molar volume of a solute in the complex non-dilute intracellular solution corresponds to the molar volume of pure substance, or even to its partial molar volume in a binary aqueous solution.

The solute partial molar volume may be measured experimentally by suspending cells in solutions containing a constant concentration of impermeable solute  $C_{si}^0$  and known concentrations of permeable solute. At equilibrium, two conditions pertain:

$$\mu_w^i = \mu_w^0 \Big|_{\text{equilibrium}} \quad (4.13)$$

$$\mu_{sp}^i = \mu_{sp}^0 \Big|_{\text{equilibrium}} \quad (4.14)$$

Since we neglect solute-solute interactions, for this isothermal, isobaric case the solute reference chemical potentials will be equal,  $(\mu_{sp}^*)^i = (\mu_{sp}^*)^0$ . In addition, the solute activity  $a_{sp}$  will be a single valued function of

the molality  $m_{sp}$ , Thus the second equilibrium condition implies

$$m_{sp}^i = m_{sp}^o \Big|_{\text{equilibrium}} \quad (4.15)$$

The reference state for the solvent  $\mu_w^*$  is a function of temperature and pressure only so the first condition becomes

$$a_w^i = a_w^o \Big|_{\text{equilibrium}} \quad (4.16)$$

If we again assume that permeable solute properties are a function only of permeable solute concentration, the osmotic coefficients  $\phi_{sp}^i$  and  $\phi_{sp}^o$  will be equal. Writing the water activities in terms of solution osmolalities leads to the equilibrium condition

$$\phi_{pb} m_{pb} = C_{si}^o \Big|_{\text{equilibrium}} \quad (4.17)$$

We see therefore that the equilibrium cell water content  $n_w$  depends only on the extracellular impermeable solute concentration, which in this experiment is held fixed. Temperature, pressure, and intracellular impermeable solute content  $n_{pb}$  are also constant, so this experiment satisfies the conditions of equation 4.12.

In terms of solute molality  $m_{sp}$ , the cell volume relation may be written

$$V_c = \frac{18.015 \text{ gm/mol}}{1000 \text{ gm/Kg}} m_{sp}^u n_w + n_w^f + n_{pb}^u + V_m \quad (4.18)$$

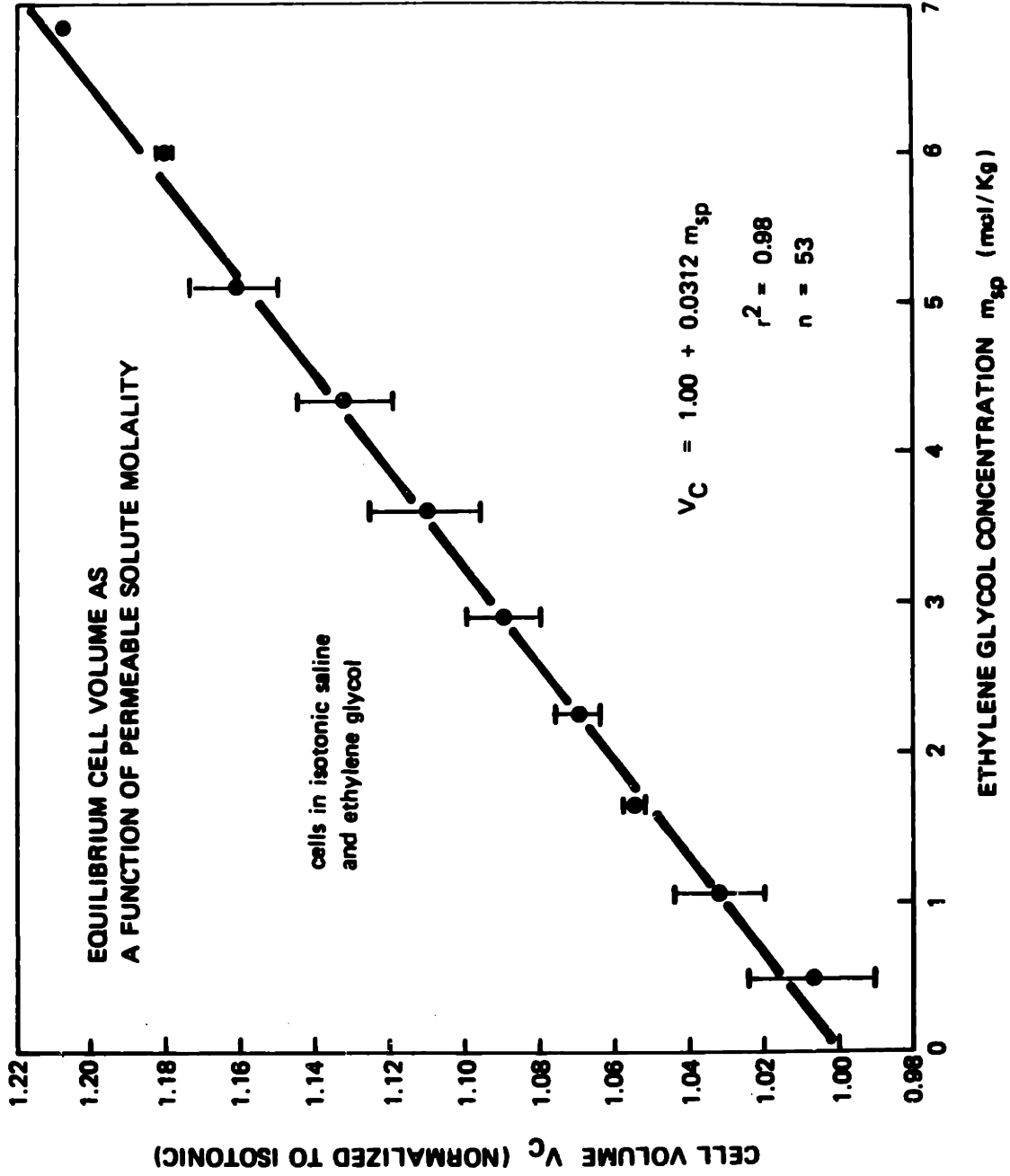


FIGURE 10 Equilibrium cell volume as a function of ethylene glycol concentration

In order to verify this formulation, cells were suspended in solutions of isotonic sodium chloride (.290 Osm) and varying concentrations of ethylene glycol, and the final volumes measured using the method described in Chapter 7. The data are presented in Figure 10 in terms of cell volume  $V_c$  normalized to  $100 \times 10^{-12} \text{ cm}^3$ , as a function of ethylene glycol molality  $m_{sp}$ .

From the slope of the least squares fit line one may use equation 4.18 to calculate the ethylene glycol partial molar volume  $v_{sp} = 42.3 \text{ cm}^3/\text{mol}$ , compared to the pure substance molar volume of  $55.9 \text{ cm}^3/\text{mol}$ . Given the high correlation coefficient ( $r^2 = .98$ ) for the linear regression, one may also conclude that the ethylene glycol partial molar volume is constant in the concentration range 0 to 7.0 mol/Kg. Similarly, the excellent agreement between theory and experiment for cells in equilibrium with varying impermeable solute concentrations (Figure 9) justifies the earlier assumption that the partial molar volume of water in the intracellular solution is constant and equal to the specific molar volume.

As a further check of the volume model, cells were suspended in solutions of 4 M ethylene glycol and varying NaCl concentration, with the results shown in Figure 11.

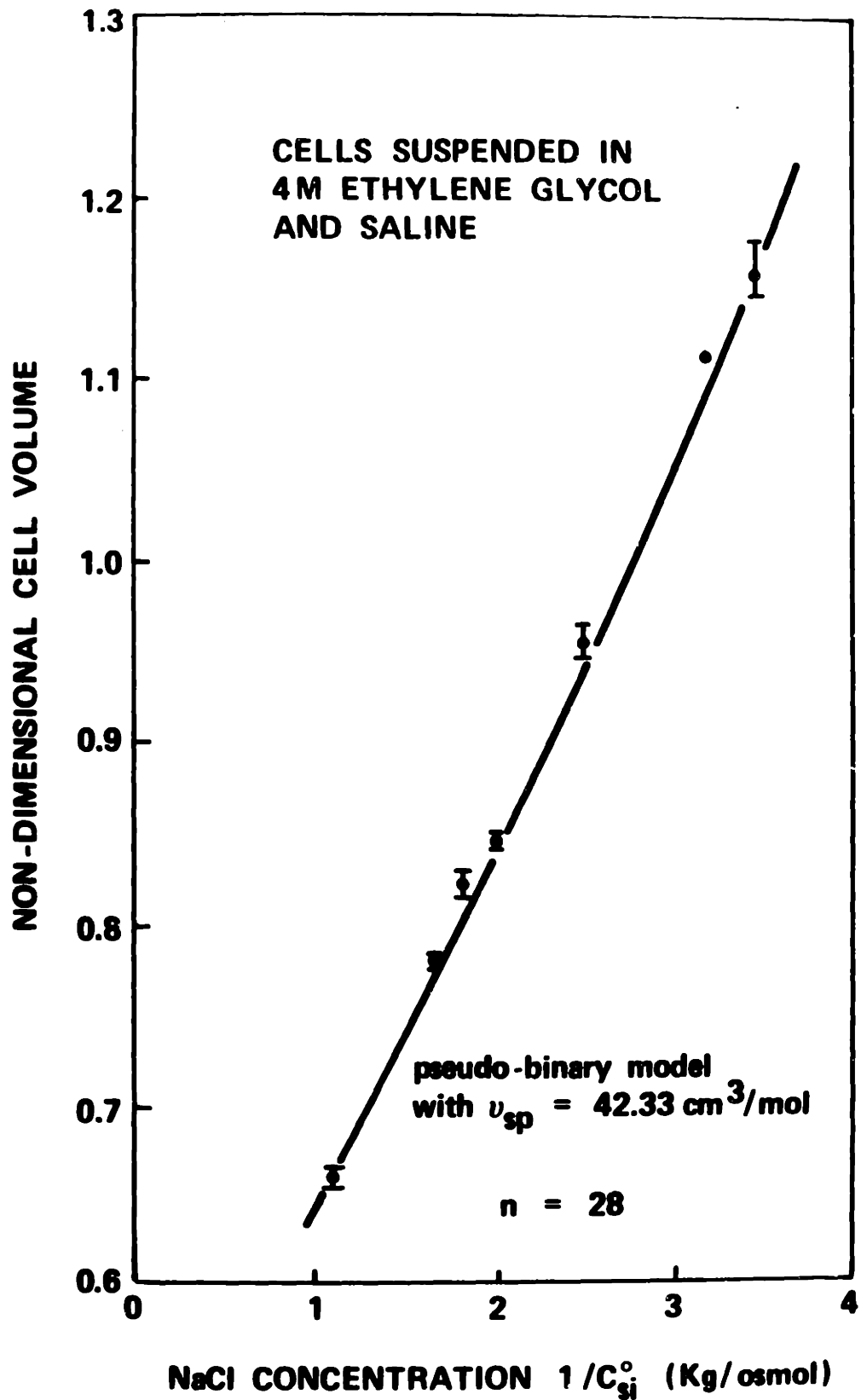


FIGURE 11 Equilibrium cell volume as a function of NaCl concentration, in the presence of 4 M ethylene glycol



**CHAPTER 5**  
**NON-DIMENSIONAL FORMS OF THE MODELLING EQUATIONS**

The membrane transport equations of Chapter 2 and the pseudo-binary solution and volume models of Chapter 4 are written in terms of physical variables. There are several advantages to be gained by casting them in non-dimensional form: (1) the equations will be more compact, easing numerical computations; (2) proper scaling will improve the accuracy of computer algorithms; (3) dimensionless groups will give us some insight into system time constants and the relative importance of different terms.

We begin with the modified Kedem-Katchalsky flux equations 2.25 and 2.26. As the first step in simplifying them we examine the repeated term  $1 + \theta - \theta\sigma$ . The organic solutes typically encountered in erythrocyte membrane research have reflection coefficients  $\sigma$  between 0.5 and 0.9 [27] and molar volumes of about 40 to 100 cm<sup>3</sup>/mol. As a worst case, consider cells exposed to an ethylene glycol solution with  $C_{sp}^m = 4$  M,  $v_{sp} = 42.3$  cm<sup>3</sup>/mol,  $\sigma \approx .8$ . Even for this concentrated solution  $1 + \theta - \theta\sigma = 1.03$ , so little error will result from setting  $1 + \theta - \theta\sigma$  equal to one.

We next apply the mass conservation equations 2.29 and 2.30 to obtain the rate equations for intracellular water and solute

$$\frac{dn_w}{dt} = \frac{-A_c L_p RT}{v_w} \left\{ \left[ 1 + \frac{\theta v_{sp} \omega}{L_p} \right] \frac{\Delta \ell n a_w}{v_w} + \left[ (1-\sigma) - \frac{v_{sp} \omega}{L_p} \right] C_{sp}^m \Delta \ell n a_{sp} \right\} \quad (5.1)$$

$$\frac{dn_{sp}}{dt} = -A_c L_p RT \left\{ \left[ C_{sp}^m (1-\sigma) + \frac{\theta \omega}{L_p} \right] \frac{\Delta \ell n a_w}{v_w} + \left[ C_{sp}^m (1+\sigma)^2 + \frac{\omega}{L_p} \right] C_{sp}^m \Delta \ell n a_{sp} \right\} \quad (5.2)$$

Notice that chemical potentials are now given in terms of activities

$$\Delta\mu_i = RT \Delta \ln a_i$$

where

$$\Delta \ln a_i = \ln a_i^i - \ln a_i^0$$

In the pseudo-binary solution model, only that portion of cell water which is not bound as water of hydration is free to cross the membrane, so

$$\frac{dn_w}{dt} = \frac{dn_w^f}{dt} \quad (5.3)$$

The non-dimensional free water content is now defined with respect to the isotonic free water content as

$$\hat{n}_w^f = \frac{n_w^f}{(n_w^f)_{iso}} \quad \frac{[\text{mol}]}{[\text{mol}]} \quad (5.4)$$

Similarly, the dimensionless permeable solute content is defined by

$$\hat{n}_{sp} = \frac{n_{sp}}{(n_w^f)_{iso} v_w C_c} \quad \frac{[\text{mol}]}{[\text{mol}][\text{cm}^3/\text{mol}][\text{mol/liter} \times 10^{-3}]} \quad (5.5)$$

The characteristic permeable solute concentration  $C_c$  (mol/liter) is introduced for scaling purposes and is taken to be either the initial intracellular concentration or the constant extracellular value  $C_{sp}^0$ , whichever is greater. If no permeable solute is present,  $C_c$  is set equal

to the concentration of pure water, 55.509 mol/liter, so  $v_w C_c = 1$ .

For convenience we also introduce the characteristic solute volume

$$\text{fraction } \theta_c = v_{sp} C_c [\text{cm}^3/\text{mol}][\text{mol/liter} \times 10^{-3}]. \quad (5.6)$$

A physically meaningful time constant  $\tau$  may be formed as

$$\tau = \frac{(n_w^f)_{iso} v_w}{A_c RT L_p C_c} [\text{sec}] = \frac{[\text{mol}][\text{cm}^3/\text{mol}][10^3 \text{ cm}^3/\text{liter}]}{[\text{cm}^2][\text{dyne cm/mol}^\circ\text{K}][^\circ\text{K}][\text{cm}^3/\text{dyne sec}][\text{mol/liter}]} \quad (5.7)$$

and a non-dimensional time defined by

$$\hat{t} = \frac{t}{\tau} \quad \frac{[\text{sec}]}{[\text{sec}]} \quad (5.8)$$

The solute permeability  $\omega$  is non-dimensionalized as

$$\hat{\omega} = \frac{\omega}{L_p C_c} \frac{[\text{mol/dyne sec}]}{[\text{cm}^3/\text{dyne sec}][\text{mol/liter} \times 10^{-3}]} \quad (5.9)$$

Finally we define a dimensionless mean solute concentration

$$\hat{C}_{sp}^m = \frac{C_{sp}^m}{C_c} \quad (5.10)$$

where  $C_{sp}^m$  is the arithmetic mean

$$C_{sp}^m = \frac{C_{sp}^i + C_{sp}^o}{2} \quad (5.11)$$

If we now apply all of the above definitions to the rate equations we obtain the dimensionless formulations

$$\frac{d\hat{n}_w^f}{d\hat{t}} = - \left[ 1 + \theta_c^2 \hat{C}_{sp}^m \hat{\omega} \right] \frac{\Delta \ell n a_w}{C_c v_w} - \left[ (1-\sigma) - \theta_c \hat{\omega} \right] \hat{C}_{sp}^m \Delta \ell n a_{sp} \quad (5.12)$$

$$\frac{d\hat{n}_{sp}}{d\hat{t}} = - \left[ \hat{C}_{sp}^m (1-\sigma) - \theta_c \hat{C}_{sp}^m \hat{\omega} \right] \frac{\Delta \ell n a_w}{C_c v_w} - \left[ \hat{C}_{sp}^m (1-\sigma)^2 + \hat{\omega} \right] \hat{C}_{sp}^m \Delta \ell n a_{sp} \quad (5.13)$$

Several alternate scalings, such as one employing  $1/v_w$  in place of  $C_c$ , are also possible.

The linear flux equations, 2.4 and 2.5, may be similarly non-dimensionalized. First, we apply a scale factor  $L_{ij} = L_{ij}^* v_w RT$  so the transport equations are simply

$$J_w = \frac{1}{v_w RT} \left\{ L_{11} \Delta \mu_w + L_{12} \Delta \mu_{sp} \right\} \quad (5.14)$$

$$J_{sp} = \frac{1}{v_w RT} \left\{ L_{12} \Delta \mu_w + L_{22} \Delta \mu_{sp} \right\} \quad (5.15)$$

and the  $L_{ij}$  have the convenient units cm/sec.

We next apply the mass conservation expressions to these flux equations, and write chemical potentials in terms of activities to obtain the rate equations

$$\frac{dn_w^f}{dt} = \frac{-A_c}{u_w} \left\{ L_{11} \Delta \ln a_w + L_{12} \Delta \ln a_{sp} \right\} \quad (5.16)$$

$$\frac{dn_{sp}}{dt} = \frac{-A_c}{u_w} \left\{ L_{12} \Delta \ln a_w + L_{22} \Delta \ln a_{sp} \right\} \quad (5.17)$$

The following simple non-dimensional groups are now defined:

$$\hat{n}_w^f = \frac{n_w^f}{(n_w^f)_{iso}} \quad (5.18)$$

$$\hat{n}_{sp} = \frac{n_{sp}}{(n_w^f)_{iso}} \quad (5.19)$$

$$\tau = \frac{u_w (n_w^f)_{iso}}{A_c L_{11}} \quad [\text{sec}] = \frac{[\text{cm}^3/\text{mol}][\text{mol}]}{[\text{cm}^2][\text{cm}/\text{sec}]} \quad (5.20)$$

$$\hat{t} = \frac{t}{\tau} \quad (5.21)$$

and the non-dimensional rate equations may be written directly

$$\frac{d\hat{n}_w^f}{d\hat{t}} = -\Delta \ln a_w - \frac{L_{12}}{L_{11}} \Delta \ln a_{sp} \quad (5.22)$$

$$\frac{d\hat{n}_{sp}}{d\hat{t}} = -\frac{L_{12}}{L_{11}} \Delta \ln a_w - \frac{L_{22}}{L_{11}} \Delta \ln a_{sp} \quad (5.23)$$

A note concerning units is appropriate here. Although the water permeability  $L_p$  has dimensions  $\text{cm}^3/\text{dyne sec}$  as it is used in the modified Kedem-Katchalsky equations 2.25 and 2.26, we will present our data in terms of  $\text{cm}/\text{sec}$  by applying the conversion

$$L_p(\text{cm}/\text{sec}) = \frac{RT}{v_w} \frac{(8.313 \times 10^7 \text{ dyne cm/mol } ^\circ\text{K})(^\circ\text{K})}{(18.015 \text{ cm}^3/\text{mol})} \times L_p(\text{cm}^3/\text{dyne sec}) \quad (5.24)$$

If we now compare equations 2.25 and 5.14 we see that if there is no permeable solute present  $L_p(\text{cm}/\text{sec})$  is identical to  $L_{11}(\text{cm}/\text{sec})$ . The solute permeability  $\omega$  is similarly scaled by

$$\omega(\text{cm}/\text{sec}) = RT (8.313 \times 10^7 \text{ dyne cm/mol } ^\circ\text{K})(^\circ\text{K}) \times \omega(\text{mol}/\text{dyne sec}) \quad (5.25)$$

It is also necessary to derive simple expressions relating the non-dimensional solute and water contents to the physical concentrations used in computing water and solute activities. In developing the pseudo-binary formulation we considered the total cell water  $n_w$  to consist of a portion  $n_w^f$  which is free to cross the membrane under normal conditions and a fraction  $n_w^b$  tightly bound to solutes. It is important to remember that this division only reflects water's ability to leave the cell, and that solution properties are always based on the total intracellular water.

The pseudo-solute molal concentration is, therefore

$$m_{pb} = \frac{n_{pb}}{n_w^f + n_w^b} \times \frac{1000 \text{ gm/Kg}}{18.015 \text{ gm/mol}} \quad (5.26)$$

Since  $n_w^b$  is constant we may also write

$$m_{pb} = \frac{n_{pb}}{\left[ \hat{n}_w^f + \frac{n_w^b}{n_w^f \text{ iso}} \right] (n_w^f)_{\text{iso}}} \times \frac{1000}{18.015} \quad (5.27)$$

which reduces to

$$m_{pb} (\text{mol/kg}) = \frac{.3590}{\hat{n}_w^f + .1997} \quad (5.28)$$

when we insert the numerical values of  $n_{pb}$ ,  $n_w^b$  and  $(n_w^f)_{\text{iso}}$  listed in Table 1. Similarly, the permeable solute molality may be written

$$m_{sp} (\text{mol/Kg}) = \frac{\hat{n}_{sp} C_c}{\hat{n}_w^f + .1997} \quad (5.29)$$

where  $C_c$  is in mol/liter and we have again assumed a constant water density  $\rho_w = 1 \text{ Kg/liter}$ .

The cell volume  $V_c$  is non-dimensionalized with respect to the isotonic cell volume  $100 \times 10^{-12} \text{ cm}^3$

$$\hat{V}_c = \frac{V_c}{(V_c)_{\text{iso}}} \quad (5.30)$$



so the cell volume relation, equation 4.10, becomes

$$\hat{V}_c = (\hat{n}_w^f + C_{c,u,sp} \hat{n}_{sp}) \frac{v_w(n_w^f)_{iso}}{(V_c)_{iso}} + \frac{v_{pb}^h n_{pb} + V_m}{(V_c)_{iso}} \quad (5.31)$$

If we use the numerical values given in Table 1 and section 4.2 this becomes

$$\hat{V}_c = .6006 (\hat{n}_w^f + \theta_c \hat{n}_{sp}) + .3994 \quad (5.32)$$

**CHAPTER 6**  
**THE EXPERIMENTAL APPARATUS**

## 6.1 Introduction to Stop Flow; The Fluid Handling System

The theoretical models of the previous chapters allow one to describe the volume response of a cell following a step change in extracellular concentration. The experimental task is to produce such a step change in the extracellular environment of a population of cells and then measure their volume as a function of time. Though simple in concept, the practical implementation is non-trivial because of the short time scales involved, often less than 500 msec, and the small size of the erythrocyte. These problems were resolved by applying the stop flow technique to achieve very rapid mixing of a cell suspension with a different solution, and a light scattering technique to measure cell volume. The overall configuration of the apparatus shown in Figures 12 and 13 is similar to that of stop flow systems used by chemists to study rapid reaction kinetics. The apparatus may be divided into several subsystems: (1) a fluid handling system which contains and mixes the experimental solutions; (2) an optical system which measures cell volume; (3) a data acquisition system which stores and manipulates the signals from the optical system; (4) a thermal system which maintains the apparatus and experimental solutions at the desired temperature. Each of these subsystems will be discussed in turn below, and further details may be found in a previous work by the author [28].

The stop flow operating concept is quite straightforward. The drive syringes are loaded with the reactant solutions, in this case a cell suspension and another solution of different composition, and the

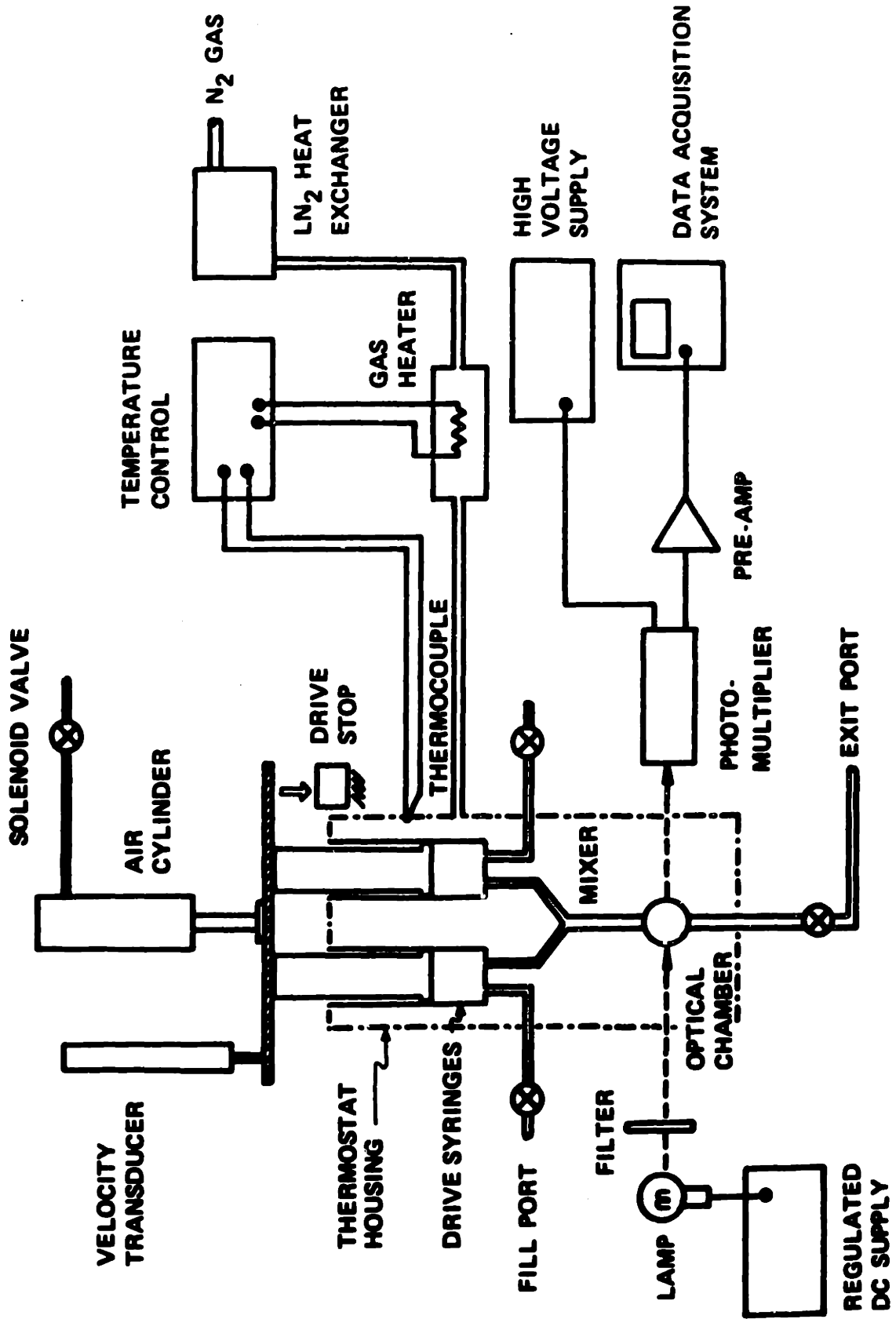
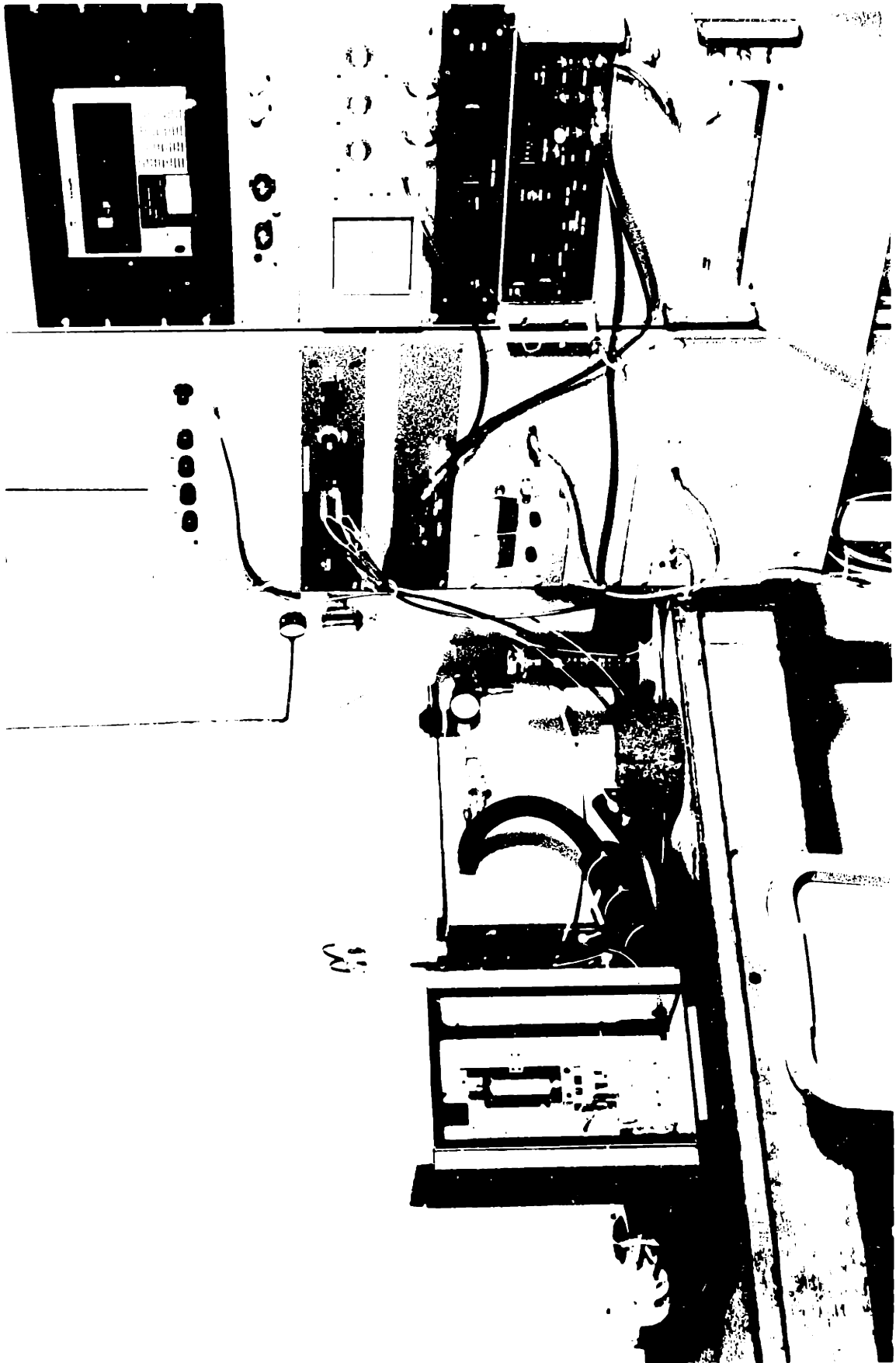


FIGURE 12 Overall schematic of the experimental apparatus



fill valves are closed. The air cylinder drive is actuated, pushing the ram and the drive syringes down and forcing the solutions through the mixer and optical chamber and out the exit port. After a 1-2 second interval during which residual contaminants are swept from the fluid path, the ram hits a mechanical stop and fluid flow abruptly ceases. The optical chamber now contains the solutions which, apart from a small delay time, have just been instantaneously mixed. The instant at which flow is stopped is taken as the datum time  $t=0$  of the experiment, which may now be monitored in the optical chamber.

The details of the drive may be seen in Figures 14 and 15. The air supply to the cylinder is pressure regulated to maintain a uniform ram velocity from run to run, and air flow is controlled with a fast acting solenoid valve. To insure equal delivery rates from the two syringes, the drive bar houses small plastic bushings which ride on the guide rods, and teflon pins projecting from the bar mate with a hole in each syringe plunger. Photometric dye dilution tests showed that the delivery rates of the two syringes were equal within a few percent. In order to eliminate the effect of even this small difference, throughout any series of experimental runs one drive syringe always contains the cell suspension and the other contains the solution. The voltage output of a velocity transducer attached to the drive bar allows one to monitor drive velocity; a typical trace is shown in Figure 16. The drive stop is a small removable aluminum block which brings the bar to a complete halt in about two msec with negligible rebound. The velocity transducer is also connected to a

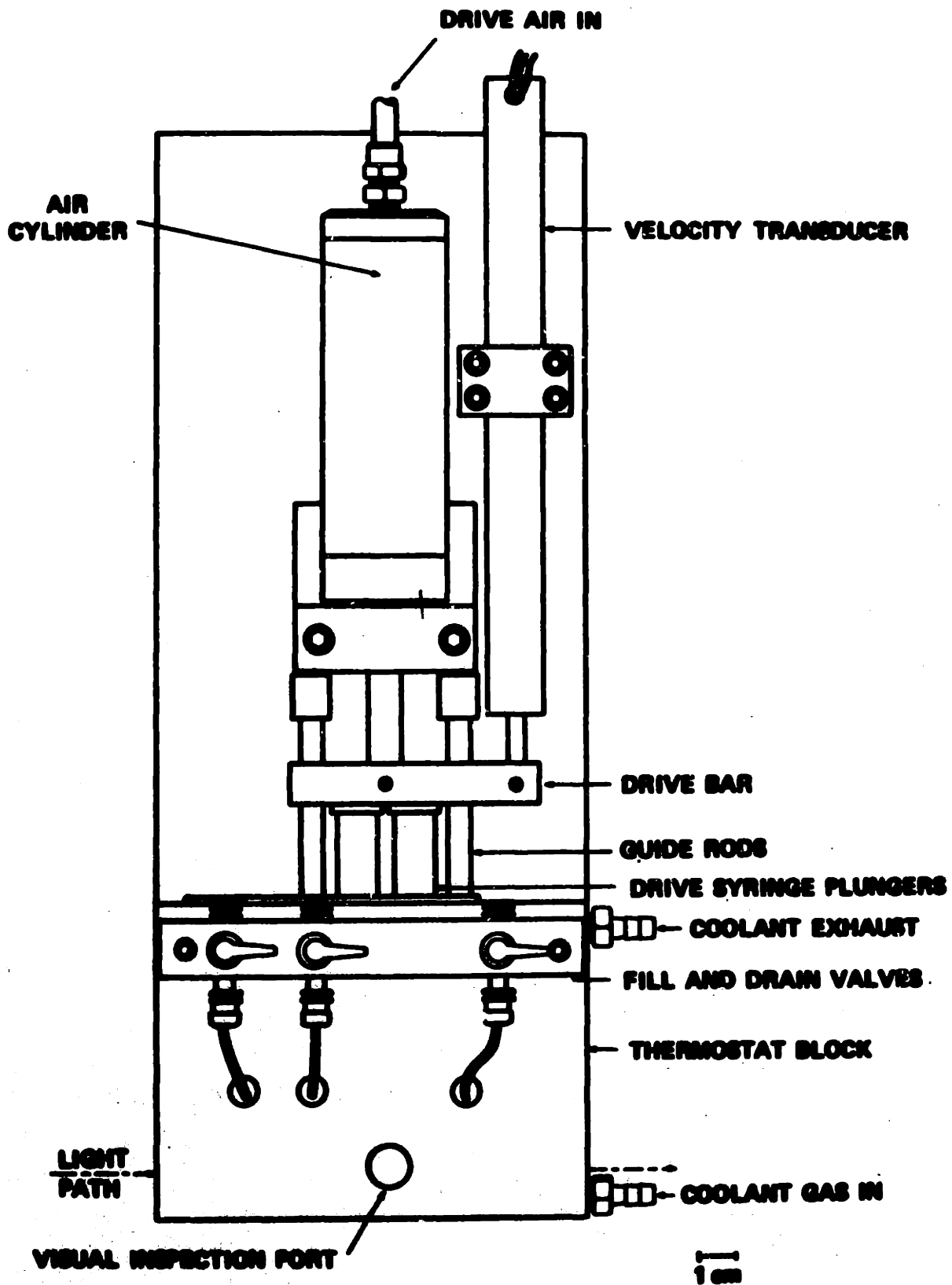
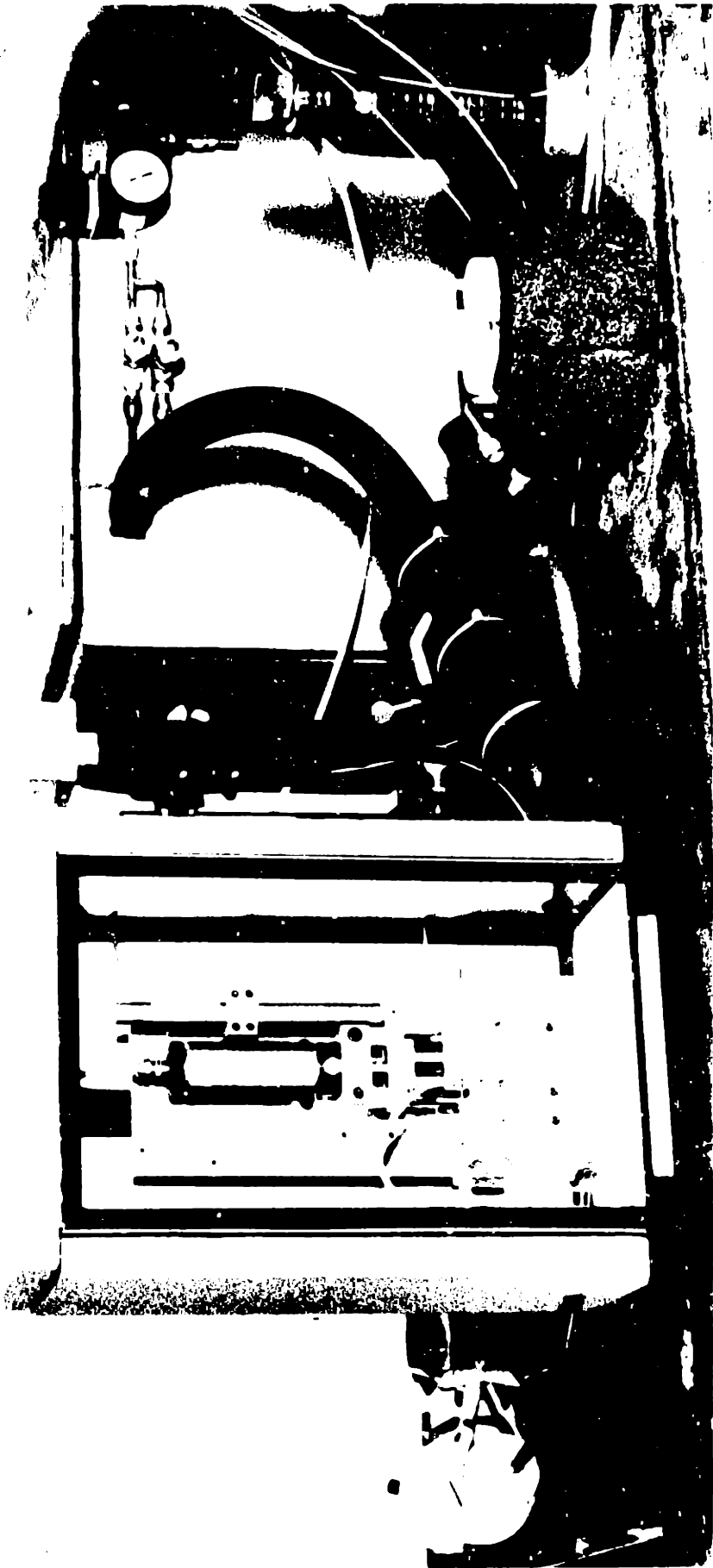


FIGURE 14 The stop flow drive system



4/5



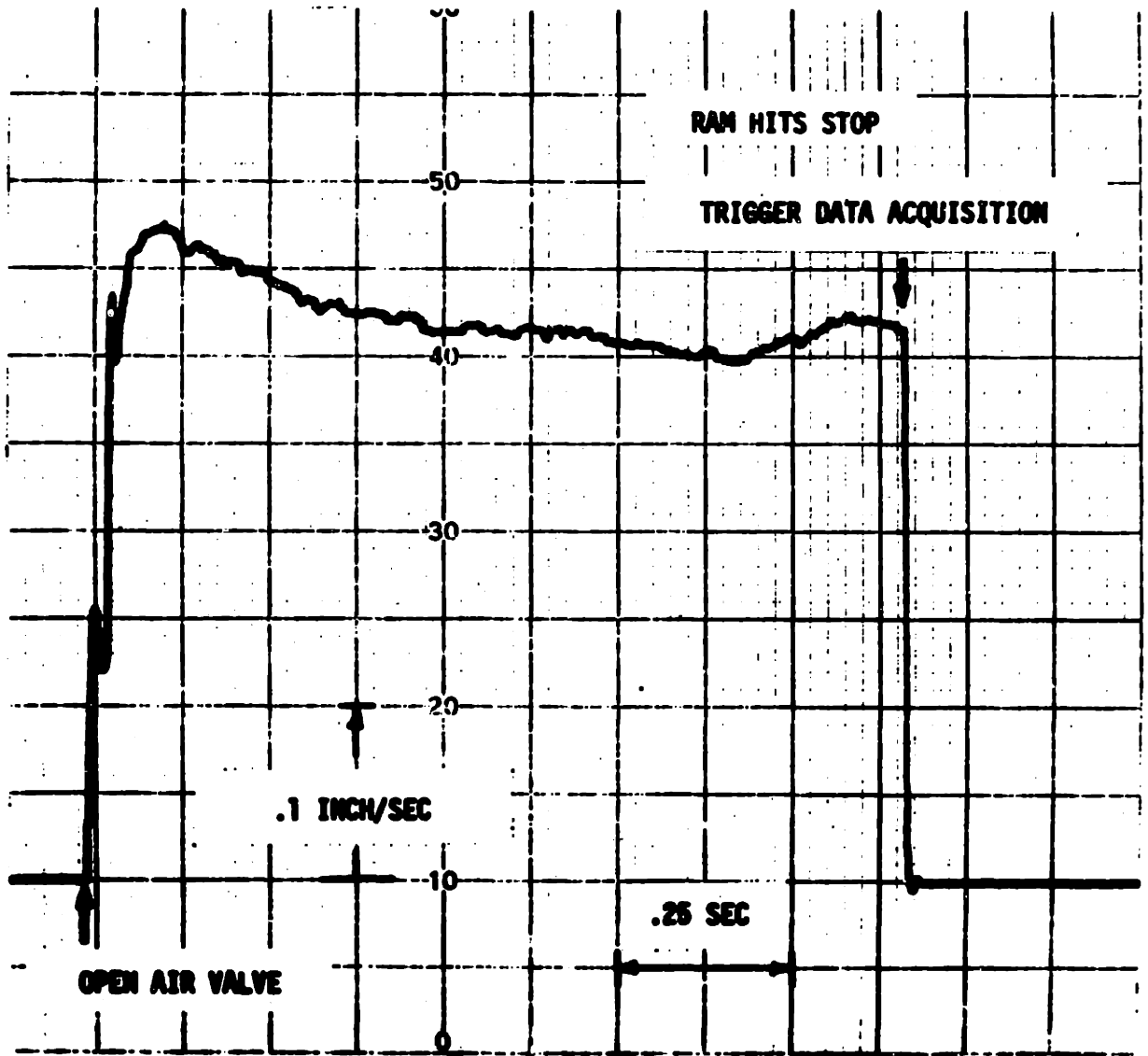


FIGURE 16 Typical drive ram velocity history

level sensing circuit when provides a pulse used to trigger the data acquisition device at roughly the mid-point of the 2 msec deceleration period.

The entire fluid handling subsystem is encased within the solid aluminum thermostat block, as shown in Figure 17. The syringe barrels are machined from standard plastic disposable syringes and pressed into bores in the block. Their lower ends are closed with teflon plugs sealed with rubber O-rings. Retaining plates at top and bottom prevent vertical movement of the barrels. The syringe plungers are machined stainless steel coated with a thin layer of epoxy and also sealed with O-rings. The shape of the plunger ends and teflon plugs and position of the O-rings is designed to minimize residual trapped fluid volume. This, along with the fill procedure outlined in Chapter 7, virtually eliminates cross contamination when experimental conditions are changed. The fluid path from fill valves to syringes and from syringes to mixer assembly is via small bore PYC tubing. A miniature flare compression fitting, leak tight to 100 psig, was designed for all connections.

The mixer and optical chamber are combined in a single assembly, shown in exploded view in Figure 18. The mixer is a simple Y junction constructed by drilling holes in a small teflon block. The upstream flow passages are .102 cm diameter and the passage downstream of the junction is .132 cm diameter. The optical chamber, described in section 6.2, is sandwiched between the mixer and the teflon exit block. A glass plate on the far side of the exit block makes it possible to inspect the chamber for air bubbles or contamination. Teflon

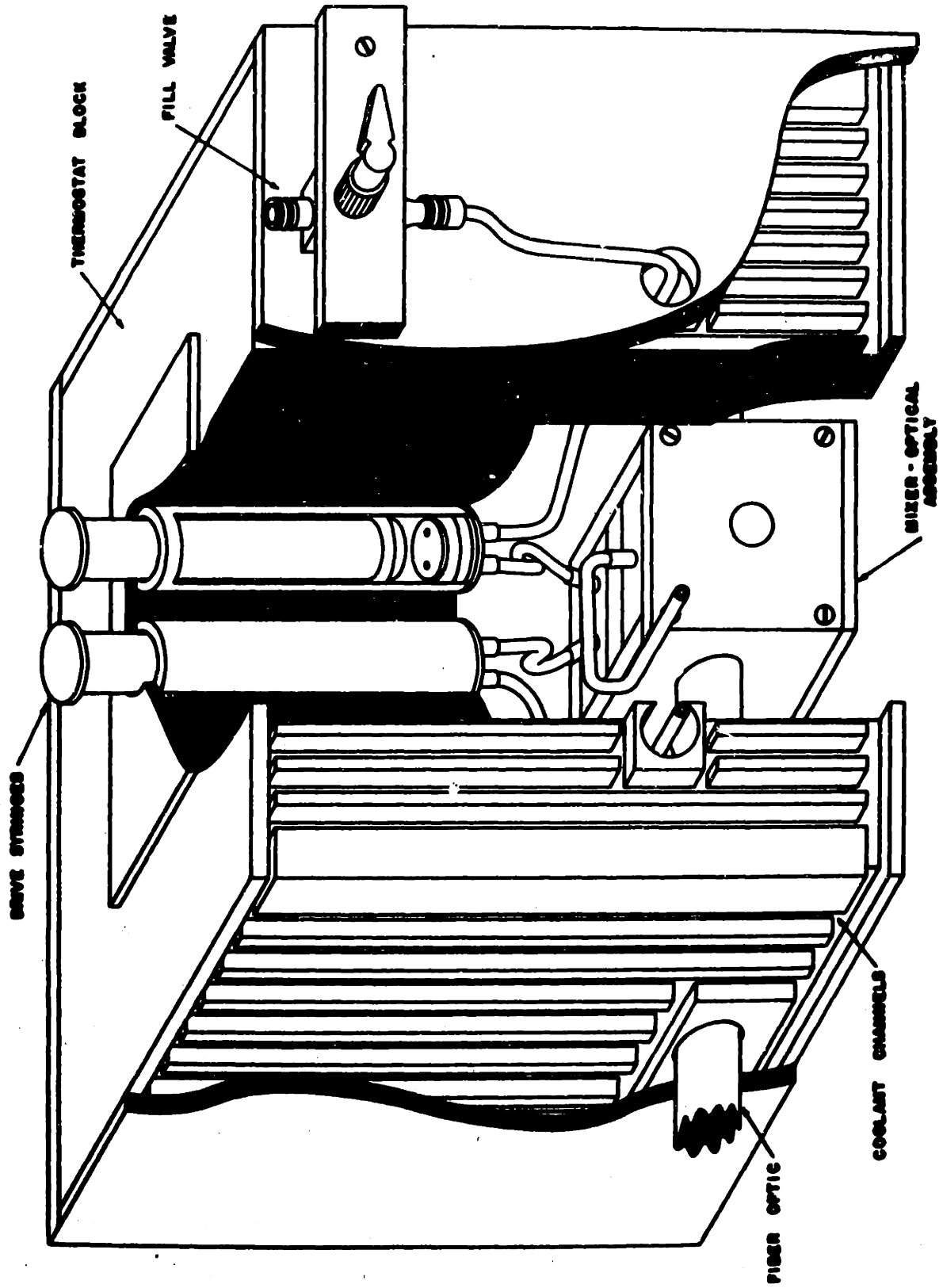


FIGURE 17 The stop flow thermostat block and fluid system

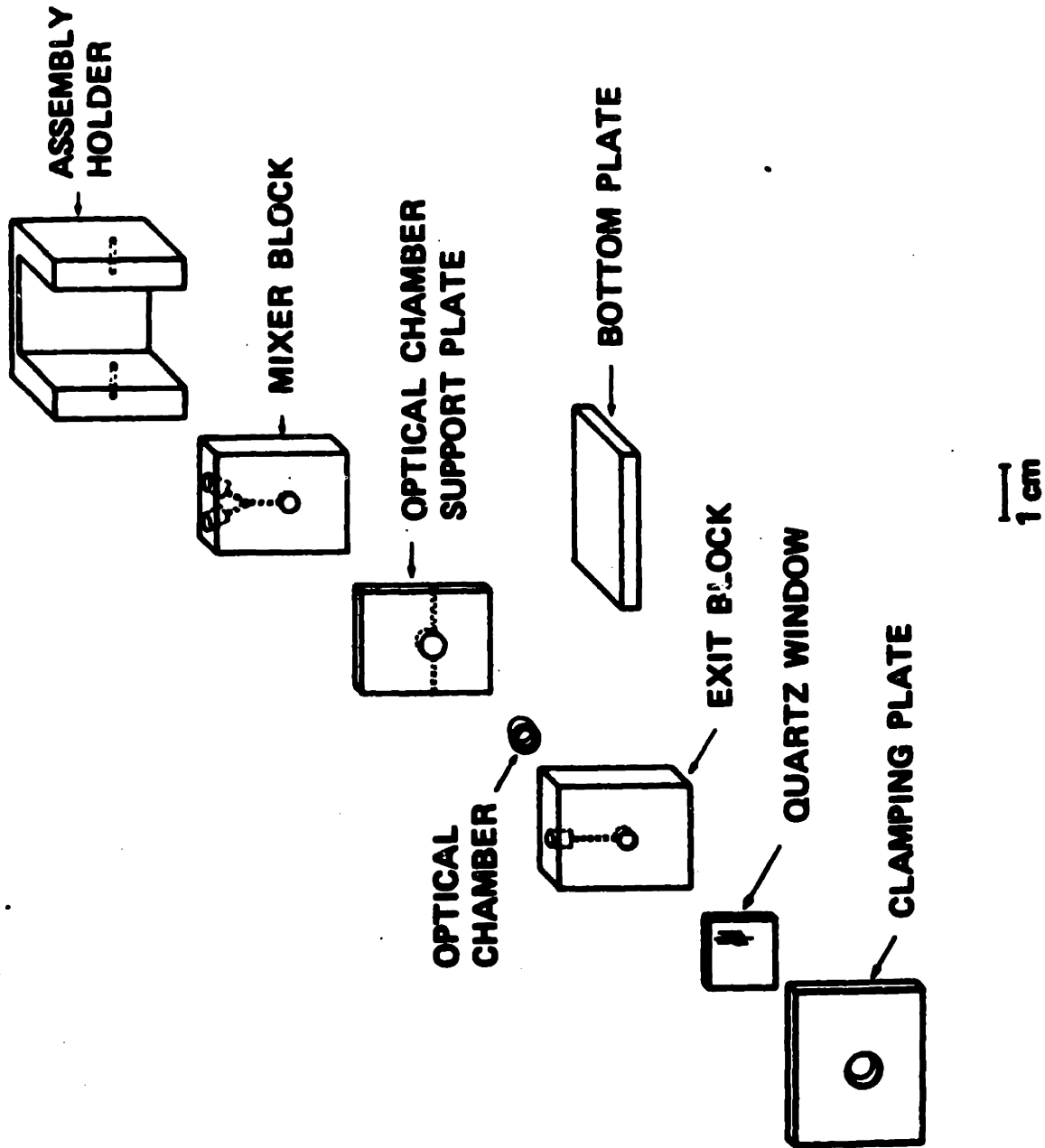


FIGURE 18 The mixer-optical assembly

film gaskets keep the sandwich leak tight when compressed by the clamping plate. After the assembly is connected to the syringes it is tightly inserted into a cavity in the thermostat block.

In the beginning of this section we stated that when flow is stopped the optical chamber contains instantaneously mixed reactants. Actual stop flow performance, however, is degraded by several effects. (1) The mixer may not be efficient, in which case there will be a significant delay after flow stops during which solutions are brought together by diffusion. The present system was tested by photometric measurements of an acid-base reaction with dye indicator [28] and it appears that there is no measurable mixing delay. (2) Stop flow experiments are also limited by system dead time, here operationally defined as the difference between the stop time and actual reaction initiation. The dead time of this system was measured (Appendix E) and found to be due primarily to the finite time required for fluid to travel between mixer junction and observation point. All experimental times were corrected for this transit time, which was computed for each experiment from fluid system dimensions and measured drive ram velocity. Transit dead times were typically 6-10 msec. (3) Because of the finite size of the optical beam and the non-uniform velocity profile of fluid traveling from mixer to observation chamber, optical measurements really represent an average over reactions of different age. However, estimates of this time smear effect [28] indicate that it is less than 1 msec and may safely be ignored.

## 6.2 Optical System

Light incident on a suspension of small particles is attenuated by two mechanisms - absorption and scattering. Absorption at any wavelength will depend on the nature and concentration of substances within the particle. Scattering amplitude and angular distribution will depend on particle size and shape, surface characteristics and index of refraction relative to the medium, the number of particles per unit volume, and optical system geometry. If absorption is reduced by suitable selection of incident wavelength, particle count is held fixed, and shape, surface parameters and internal index of refraction assumed to be unique functions of particle size, it should be possible to relate scattering to cell volume. Unfortunately, the question of light extinction as a function of non-spherical macro particle dimensions has received little theoretical attention, and what work has been done (e.g. [29] [30] [31] [32]) does not successfully predict the experimentally observed relations. Despite this, it is still possible to empirically relate measured light intensity to cell size for a given system geometry, and thus follow the time course of cell volume changes.

The components of the optical system were seen in Figure 12 as part of the overall stop flow apparatus. A lamp powered by a regulated DC supply provides a stable light source. This light is filtered, then transmitted via a fiber optic light pipe to illuminate the red cell suspension inside the optical chamber. Another fiber optic carries the transmitted and forward scattered light to a photomultiplier. The output of the photo-

multiplier is amplified, filtered, and passed to the data acquisition system. The source lamp, stop flow apparatus, and detector assemblies are all rigidly mounted to a steel frame.

The source lamp is a 12 volt 60 watt tungsten filament bulb ordinarily used as a Zeiss microscope illuminator. The standard illuminator housing has been modified to block ambient light and the lamp is force air cooled. The original spring loaded electrical contacts have been removed and the power leads soldered directly to the bulb to eliminate fluctuations by changing contact resistance.

The lamp is powered by a Hyperion Industries model SI 15-10 D.C. supply. Since filament resistance may drift with age or changes in temperature, normal current or voltage regulation is inadequate. The circuit shown in Figure 19 senses both lamp current and voltage, and uses the auxiliary inputs of the supply to regulate lamp power. After a twenty minute warm-up period, this scheme limits optical system drift to less than 0.5% in six hours, and at 10 V output supply noise is only 2 mV peak to peak.

Hemoglobin, the principal absorbing species in the red cell, normally exists in several forms, each with a unique absorption spectrum. None, however, absorbs significantly at wavelengths above 600 nm. Thus, by illuminating the cell suspension only with light of wavelength greater than 600 nm, almost all attenuation will be due to scattering, and the proportion of each hemoglobin type will not be an experimental variable. Figure 20 shows the absorption spectra of the two most prevalent forms,

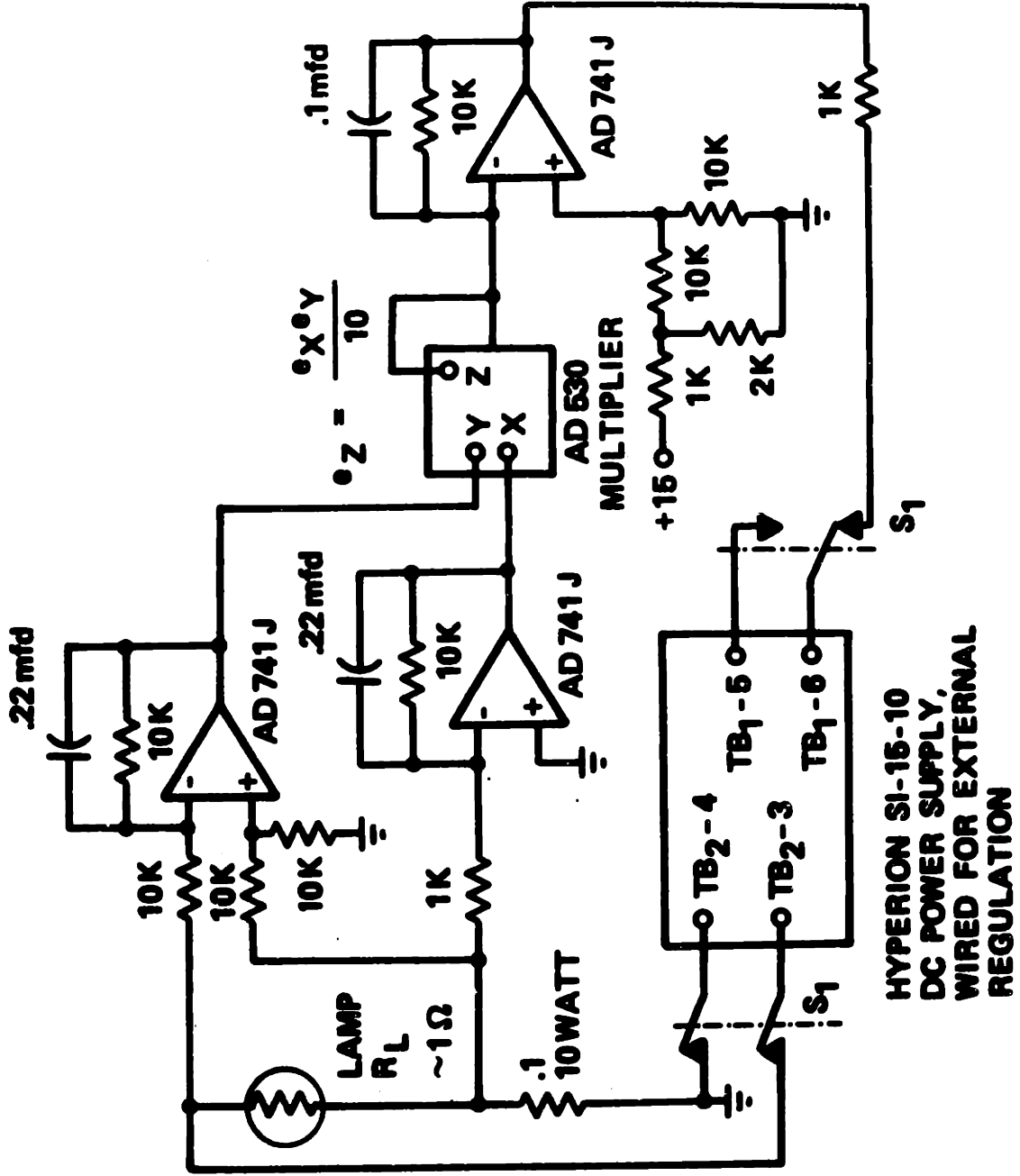


FIGURE 19 Lamp power regulation circuit



oxygenated HbO and reduced hemoglobin Hb [33], and the spectral characteristics of the optical filter and photomultiplier. The filter, a high pass glass sandwich interference filter, is contained in an aluminum housing coupled to the lamp assembly. A fiber optic light pipe inserted into the fiber housing at the focal point of the illuminator lens carries the light to the stop flow optical chamber.

The optical chamber was designed with the following objectives in mind: small sample volume; biological compatibility; maximum sensitivity to cell volume changes. The chamber configuration was shown in Figure 18. The chamber itself is a section of pyrex tubing .25 cm ID, .40 cm OD, .32 cm long, sandwiched between the teflon mixing and exit blocks. An aluminum support plate surrounds the glass tube, and holes through the support plate and assembly holder serve as optical slits .19 cm in diameter and 2.22 cm long. The slits and the inner surface of the support plate surrounding the glass are coated with flat black paint, with the result that only transmitted light or light with a small forward scattering angle will reach the face of the detector fiber optic.

The detector is an RCA 8645 assembly, a sealed unit containing a type 8644 photomultiplier tube and its associated dynode voltage divider resistors and electrostatic and magnetic shielding. The tube is an end window type with S-20 spectral response extending from 300 to 800 nm, a dark current of  $10^{-9}$  amp and a  $10^{-8}$  second rise time. As the shield is held at cathode potential, typically 1 KV, the entire assembly is encased in a phenolic cylinder which also accepts the detector fiber

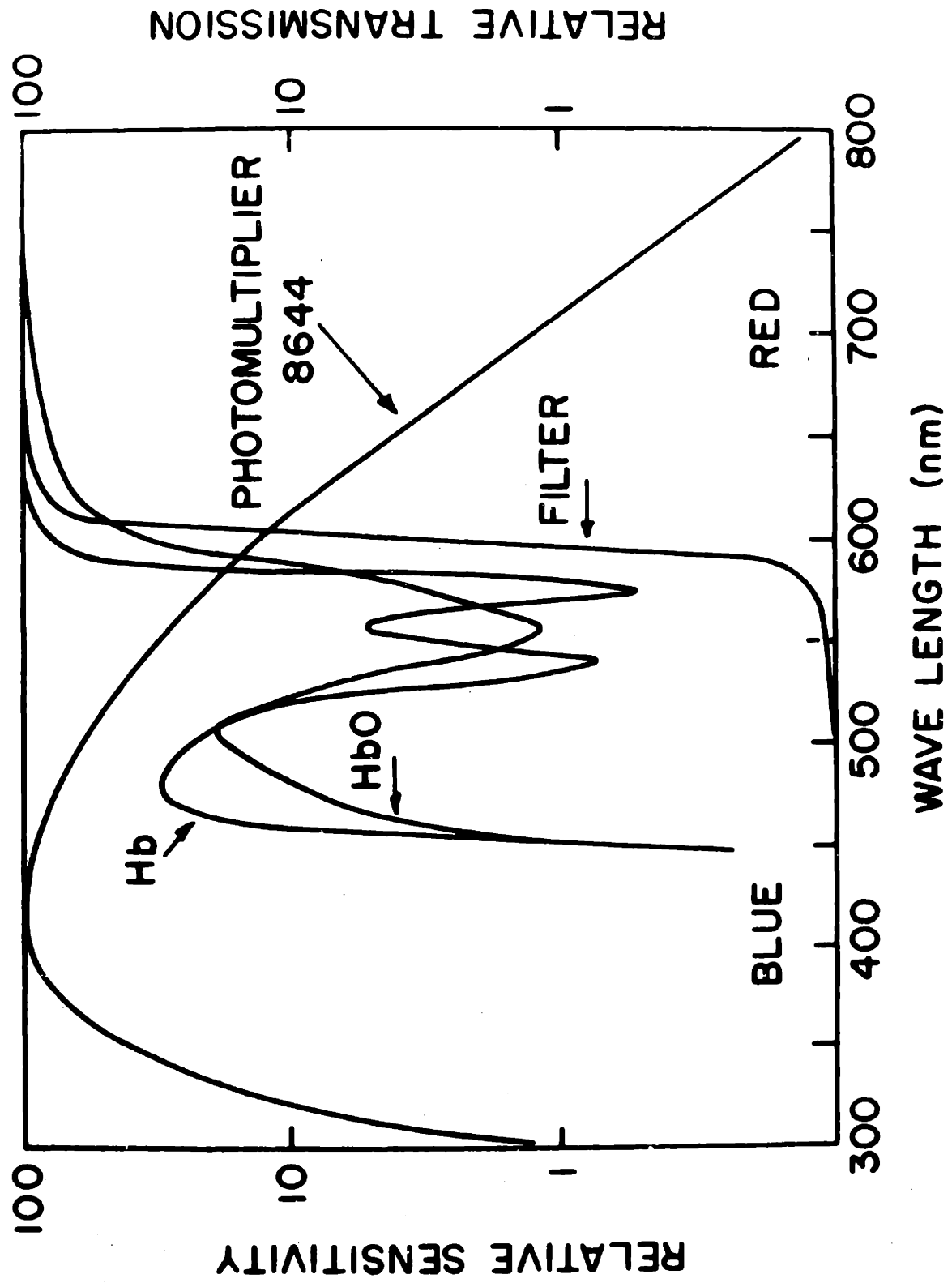


FIGURE 20 Spectra of hemoglobin and optical system components

optic. The other end of the casing is closed with a grounded metal cap to which is attached a chassis box containing the photomultiplier signal pre-amplifier.

A photomultiplier amplifies light by repeated secondary emission and acceleration of electrons through the dynode stages. Tube gain is determined by the voltage applied to the dynodes through the voltage divider resistor string. For the 8645 assembly, tube gain  $G$  increases as the external supply voltage is raised to the 8.0 power. The dynode voltage is provided by a Keithly Instruments model 246 regulated supply with stated ripple and noise of 1 mV and regulation of .002% through its 0-3000 volt range.

In order to reduce the effect of noise pickup from external sources, the photomultiplier anode is coupled directly to a shielded pre-amplifier. Since a photomultiplier is a nearly ideal current source with very high output impedance, the pre-amp also serves as a current to voltage converter and impedance buffer. The pre-amplifier is based on an Analog Devices model 52K op-amp, an FET input design with 130 dB open loop gain, rolling off at 6 dB/octave above 4 Hz,  $10^{12}$  ohm input impedance, and excellent input noise and offset characteristics. It is used in a standard inverting configuration, with a  $10^5$  ohm precision metal film resistor and 100 pF capacitor in the feedback loop. This gives the amplifier a DC closed loop gain of about  $10^5$  volt/amp with 6 dB/octave rolloff at frequencies above 130 Hz.

The pole frequency of this passive first order filter was selected to be above the characteristic frequency of most experimental signals, and in the worst case the filter contributes less than 0.5% signal distortion. When illuminated with a 100 Hz square wave modulated LED, no distortion was apparent in the amplified photomultiplier output.

Because the light impinging on a photomultiplier is made up of photons randomly distributed in time there is an unavoidable noise current at the photo-cathode, often termed shot noise. The photomultiplier signal to noise ratio SNR is given by [28]

$$\text{SNR} = \sqrt{\frac{I_A}{E G \pi f_p}} \quad (6.1)$$

where  $I_A$  is the anode current,  $E$  the charge of an electron ( $1.6 \times 10^{-19}$  coulomb),  $G$  the internal tube gain, and  $f_p$  the filter pole frequency (Hz). The photomultiplier is typically operated with a 900 volt dynode supply producing a gain  $G = 1.3 \times 10^3$ , and an anode output current of  $10^{-6}$  amp. For these conditions the signal to noise ratio, either measured or computed, is about  $10^3$ .

When setting the optical system operating parameters several constraints must be kept in mind.

- 1) Pre-amp output should be 10 mV or more, as there is roughly 0.1 mV (peak to peak) noise pickup in the pre-amp circuit, external leads and data acquisition system.
- 2) Photomultiplier anode currents greater than 5 micro amps.

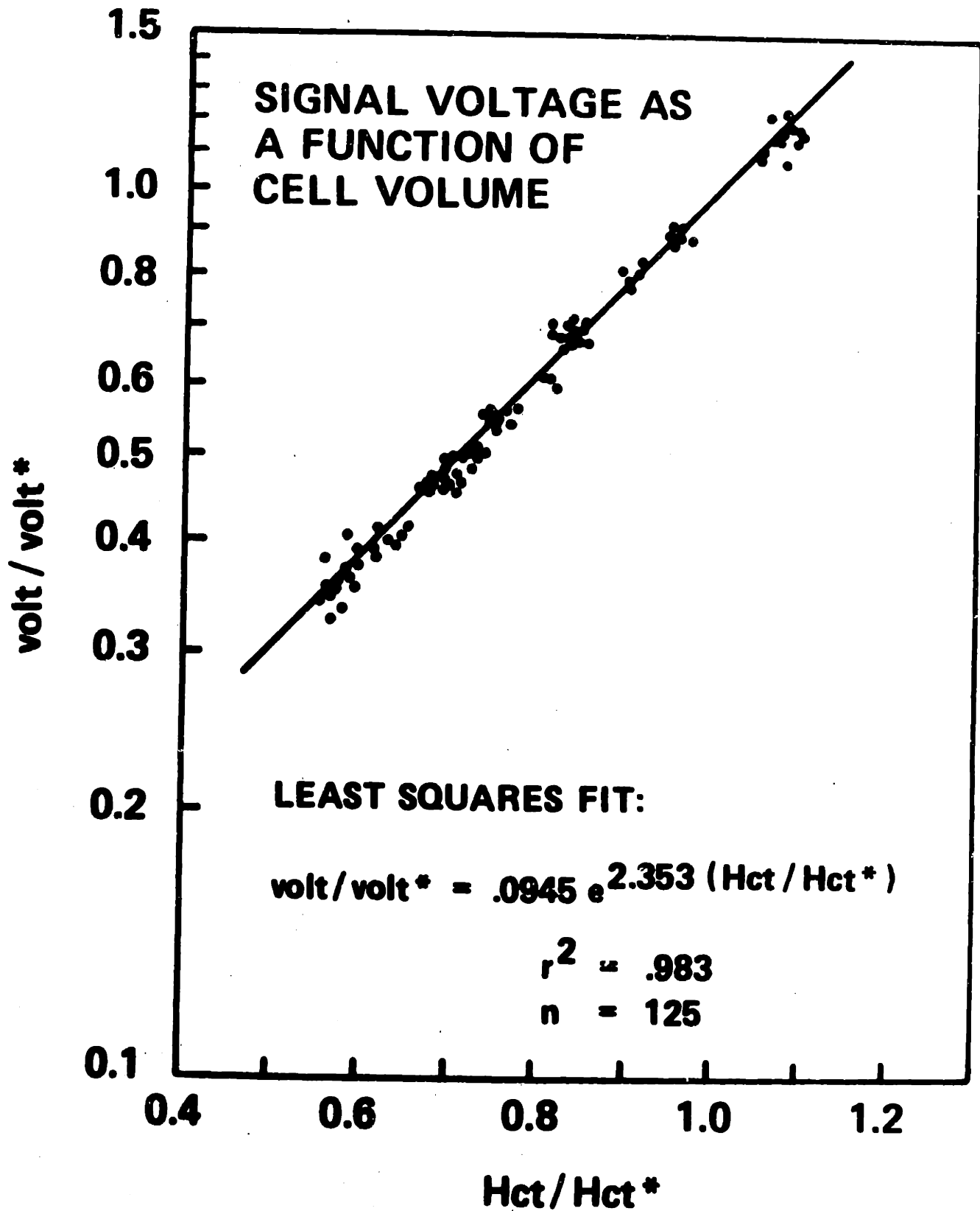


**FIGURE 21** Photomultiplier output as a function of cell volume

corresponding to a pre-amp output of 0.5 volt, will degrade tube stability and should be avoided.

- 3) Source lamp intensity should be as great as possible to maximize the signal to noise ratio. However, lamp life will be increased if it is operated somewhat below its rated 60 watts.
- 4) For linear photomultiplier operation, dynode supply voltage should be greater than 400 volts. The absolute rated maximum dynode supply of the 8645 assembly is 1800 volts. Remember, however, that changing the tube gain does not affect the signal to noise ratio.

The relationship between red cell volume and photomultiplier pre-amp output voltage was determined in the course of a series of calibration experiments described in Chapter 7. Briefly, cell volume was varied by allowing cells to come to equilibrium in a series of solutions with different impermeable solute concentrations. The clinical index of red cell volume is the hematocrit Hct, given by

$$\text{Hct}(\text{ml cells}/100 \text{ ml suspension}) = N_c(\text{cells}/100 \text{ ml}) \times V_c(\text{ml}/\text{cell}) \quad (6.2)$$

By maintaining the number of cells per unit volume  $N_c$  constant within a calibration set, the cell volume would be proportional to the measured hematocrit. The results of 24 independent calibration sets performed over a three month period are shown in Figure 21. The data includes calibrations performed under a variety of conditions: cells in saline only; in solutions containing

up to 4 M ethylene glycol or .25 M glycerol; at temperatures ranging from 25°C to -10°C; with values of Hct\* from 4 to 12 ml cells/100 ml. All data points lie within the 95% confidence limits of the regression

$$\frac{\text{volt}}{\text{volt}^*} = .0945 \exp(2.353 \frac{\text{Hct}}{\text{Hct}^*}) \quad (6.3)$$

The results of each set were normalized with respect to values (denoted \*) obtained for cells immersed in isotonic saline and whatever permeable solute was present.

If there is no permeable solute, the non-dimensional cell volume  $\hat{V}_c$  is simply equal to the measured relative hematocrit Hct/Hct\*, since in this case Hct\* = (Hct)<sub>iso</sub>. If there is a permeable solute in the calibration solutions, the cell volumes corresponding to measured values of Hct/Hct\* may be found by concurrently measuring the hematocrit of cells in an isotonic saline suspension with the same cell number density and computing

$$\hat{V}_c = \frac{V_c}{(V_c)_{iso}} = \frac{\text{Hct}}{\text{Hct}^*} \times \frac{\text{Hct}^*}{(\text{Hct})_{iso}} \quad (6.4)$$

Alternatively, the non-dimensional cell volume corresponding to the normalizing \* condition may be obtained from data such as are shown in Figure 10, and then we have

$$V_c = \frac{\text{Hct}}{\text{Hct}^*} \times V_c^* \quad (6.5)$$

The volume-voltage relationship shown in Figure 21 may be used to evaluate the cell volume resolution of the apparatus. The voltage resolution of the data acquisition system is better than .1 mV, and a typical signal level is 50 mV. From the least squares regression it is possible to compute a corresponding volume resolution of 0.1%. The system accuracy can be evaluated by examining the 95% confidence limits on future observations. That is, given a measured value of  $\text{volt/volt}^*$ , the probability is 95% that the corresponding value of  $\text{Hct/Hct}^*$  lies within these limits. These statistics are computed in Appendix J, and we find an uncertainty in non-dimensional cell volume of roughly  $\pm .04$ . For cell volumes ranging from .5 to 1.1, this corresponds to an error of 3.5% to 7.5%.

In addition to changing with cell volume, the measured light intensity is also a function of several other cell and solution properties.

Certainly as the number of cells in the light path increases, light intensity will diminish. This was measured experimentally by preparing cell suspensions with varying cell number density but constant cell volume. Blood was collected, washed, and packed as usual and suspensions were made up with 10 ml of NaCl solution and between .2 and 1.4 ml of packed cells. These suspensions were injected directly into the stop flow optical chamber and the resulting photomultiplier signals recorded. Three separate experimental sets were performed, each with a different



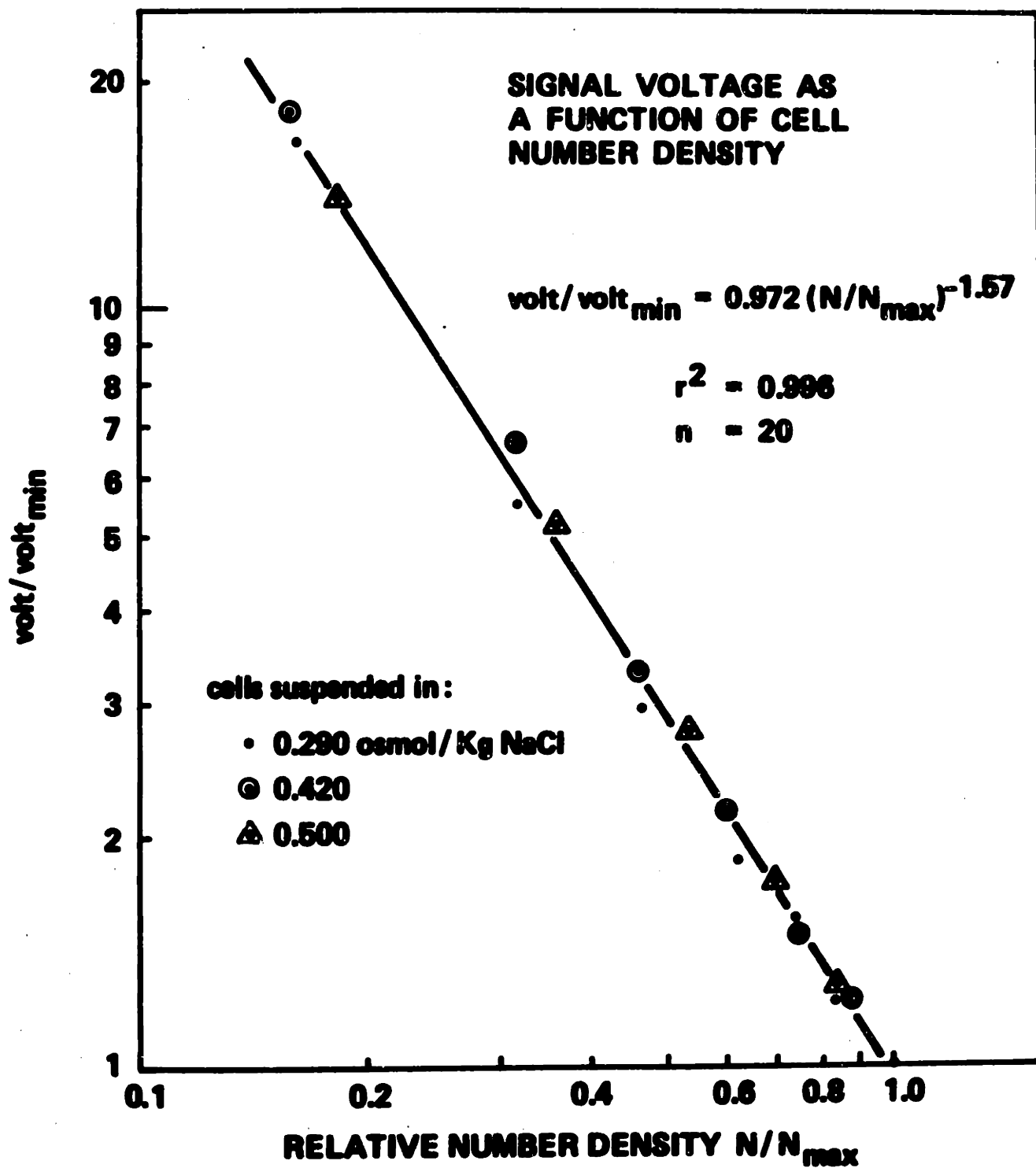


**FIGURE 22** Photomultiplier output as a function of cell number density

NaCl concentration and therefore a different cell volume. Within each set the signal levels and cell concentrations were normalized with respect to the value corresponding to the most concentrated cell suspension with the results shown in Figure 22.

Signal levels are not a function of temperature, and volume-voltage calibrations performed at  $-10^{\circ}\text{C}$  were identical to those at  $25^{\circ}\text{C}$ . It is important, however, to maintain the apparatus and experimental solutions at a uniform temperature, or variations in fluid indices of refraction within the optical chamber produce anomalous results.

Light extinction in cell free saline solutions was found to be a very weak function of NaCl concentration. Measured light intensity decreased less than 2% as the concentration was varied from .2 to .6 osmol/kg.

Although not a normal result of the experimental procedure, occasionally a fraction of the cell population rupture and lose their intracellular hemoglobin (hemolyze). Excessive shear during the mixing phase of stop flow operation may mechanically damage cell membranes, but in general, ram velocities of less than 5 cm/sec did not induce measurable hemolysis in this apparatus. If cell volume exceeds 1.3 times the isotonic volume, hemolysis usually follows immediately. This places a lower limit on impermeable solute concentration of about .20 osmol/Kg. High concentrations of solute may also result in hemolysis, though on a longer time scale. Typically, 10% of the cells will hemolyze (denoted 10% H) after immersion for one hour in 2 Osm NaCl, or isotonic saline plus 5 M ethylene glycol or 4M glycerol. It is this sensitivity

to high solute concentrations which determines the minimum temperature at which one can perform the experiments. Cells which have been stored for longer than three weeks after collection are usually more susceptible to all modes of injury.

In the preliminary stages of apparatus development it had been noted that photomultiplier output was extremely sensitive to the percentage of cells hemolyzed. This was later quantified by first preparing a washed cell suspension (Hct ~ 8) in isotonic saline, then dividing the suspension into two equal aliquots. One was left unaltered, and taken to be un-hemolyzed (0% H). The other fraction was rapidly cooled by immersion in liquid nitrogen, then rewarmed in air to ambient temperature. The cells in this suspension were assumed to be totally destroyed (100% H). By mixing varying proportions of these two stock suspensions different ratios of hemolyzed to un-hemolyzed cells were obtained. These % H values were verified by the standard clinical cyanmethemoglobin spectrophotometric technique, with good agreement. The various %H suspensions were then manually injected into the stop flow optical chamber and the resulting signals, normalized to the value for the 0% H suspension, are shown in Figure 23, plotted vs  $1 - \frac{\%H}{100}$ . The experiment was later repeated with cells suspended in a solution of isotonic saline and 3 M glycerol, with results within 2% of those shown [34]. The similarity between the hemolysis data and those obtained for varying cell number density suggests that for light scattering from red cells to be significant a large difference must exist between the intra-

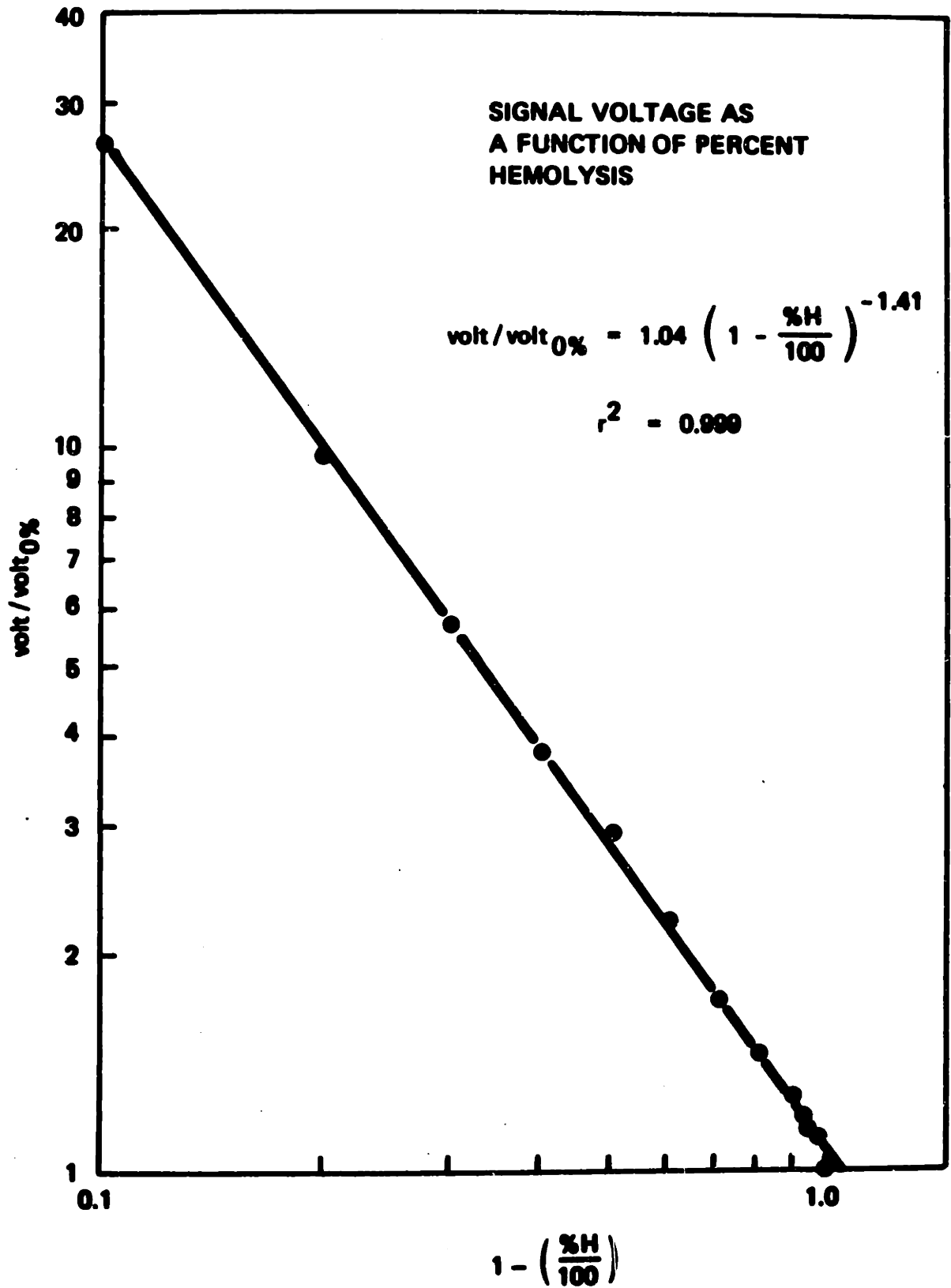


**FIGURE 23** Photomultiplier output as a function of percentage of cells hemolyzed

cellular and extracellular indices of refraction. Thus, when cells lyse and lose their contents they are no longer effective scattering objects.

It would be expected, therefore, that light intensity would also vary as a function of the extracellular solution index of refraction. This was confirmed by suspending identical aliquots of packed cells in solutions of isotonic saline and varying ethylene glycol concentrations. Again, the suspensions were manually injected into the stop flow optical chamber. The measured signal levels, normalized to the value for cells in isotonic saline alone, are shown in Figure 24. Also shown for reference is the variation in signal predicted on the basis of solute induced volume changes, derived from the data of Figures 10 and 21. It is because of this considerable index of refraction effect that all volume-voltage calibrations were performed in solutions with the same permeable solute concentration as found in the corresponding experimental post-mix extracellular solution.

In conclusion, the data presented in this section demonstrate that all the measured effects on light intensity are independent and that the actual intensity will appear to be a product of those functions. Also notice that in every case the normalizing procedure eliminates the effects of source lamp intensity and photomultiplier gain.

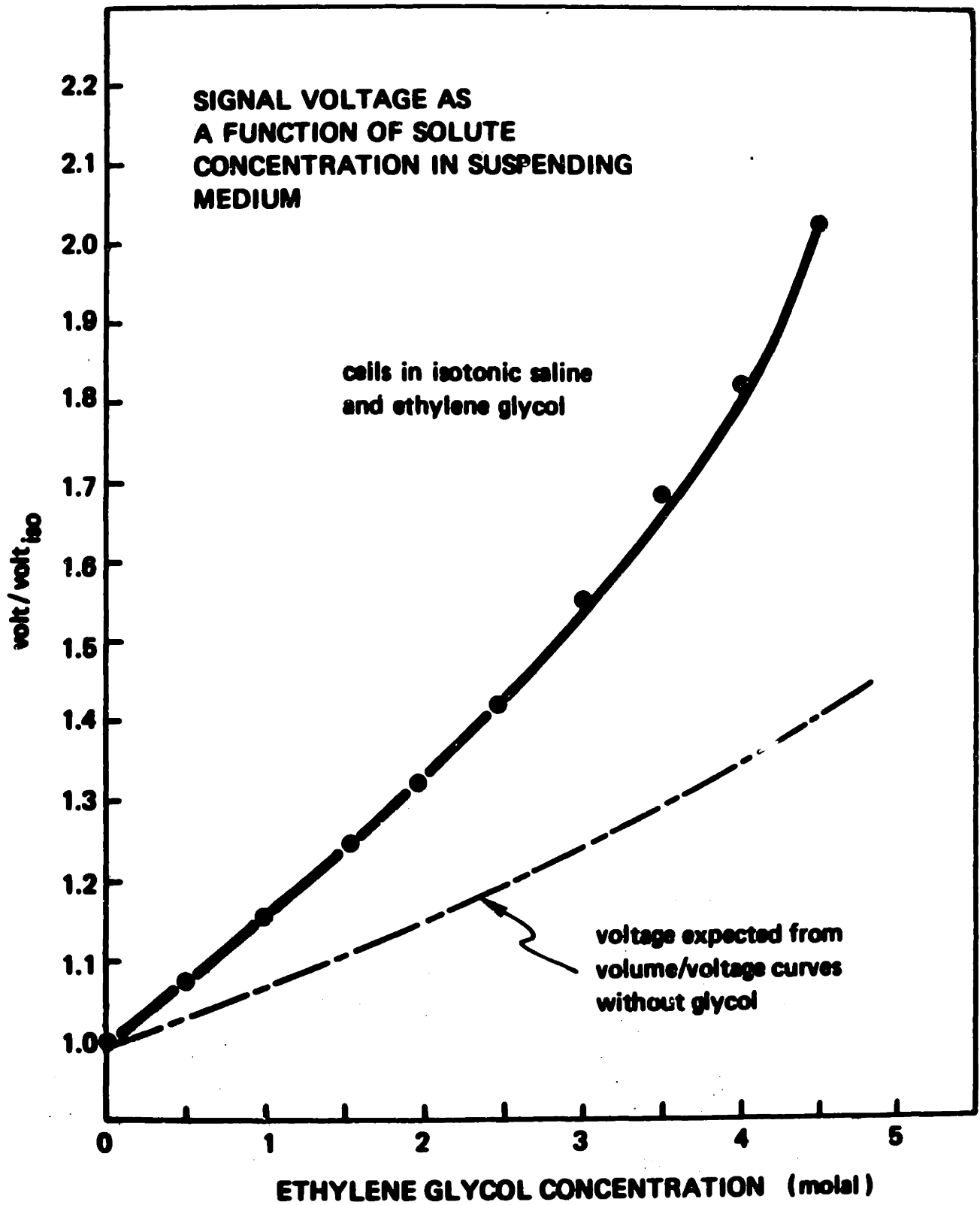


**FIGURE 24** Photmultiplier output as a function of suspending medium solute concentration

### 6.3 Data Acquisition

As cell volume changes during the course of an experiment, the optical system produces a proportionally varying voltage. The task of recording these signals for analysis is not an easy one. In many experiments one wishes to examine both events occurring on a millisecond time scale and an overall picture which encompasses tens of seconds. Also, one is often interested in volume changes producing signal variations which are only a small fraction of the nominal voltage level. Oscilloscopes and chart recorders simply do not have the necessary dynamic range and resolution, so a high speed digital data acquisition system was designed and built to our specifications by Rollins Associates of Lincoln, Massachusetts. The data system samples the incoming analog signal, converts it to digital form, and stores the discrete points in semiconductor memory. After the experiment is completed, memory may be accessed and the stored signal examined at leisure.

Two identical analog input channels, which may be used separately or multiplexed, have switch selectable input ranges of 0 - 0.8 and 0 - 8.0 volts, input impedance of  $6 \times 10^7$  ohm, and front panel polarity selection. Analog input is sampled and converted to 14 bit digital words, providing resolution of 1 part in 16,000.

The sampling rate may be set from .1 to 999.9 msec per memory location. The 4096 word memory thus allows one to record experiments with durations

ranging from .4 second to over an hour. (In multiplex mode, the two input channels share memory, halving the number of locations available to each.) Regardless of the sampling rate, that is, interval between samples, the duration of each sample is about 7 microseconds. All timing is quartz oscillator controlled and .01% accurate.

Triggering may be either manual or by an external signal, in which case controls similar to an oscilloscope's adjust for trigger level, polarity, and slope. Because of the memory structure, it is also possible to capture events occurring prior to a trigger. When the device is armed, incoming signals are continuously sampled, digitized, and loaded into the top of the memory stack, rolling down previous data. When a trigger is received, acquisition continues for another 4096 samples, then stops. In the pre-trigger mode acquisition continues for only 2048 or 3072 samples after triggering, and thus the first half or quarter of memory contains input before the trigger.

Once stored, data may be displayed in several ways. In CRT mode, memory is repetitively scanned and the digital values converted to a stepwise analog signal which is displayed on a conventional oscilloscope. Slewing controls allow the operator to shift the display on the screen, and any portion of memory may be time expanded simply by positioning it at the left of the screen and increasing the sweep rate of the oscilloscope. The operator may also manually scan memory with the same slewing controls and read the voltage stored in each location on a five digit LED display. Consistent with the 14 bit A/D resolution, the display reads to  $\pm .05$  mV in the .8 volt range. The location being accessed is indicated by a cursor



on the oscilloscope display and the location number may be read from another LED display. Knowing the original sampling rate, it is a simple matter to convert location number to time. It is these manually read voltage/time pairs which are then used in subsequent data reduction. Memory contents may also be dumped in analog form on a strip chart recorder to produce hard copy of the stored signal. Just as in CRT mode, time and voltage scales may be expanded or compressed as desired after the experiment is performed. The oscilloscope and strip chart recorder may also be used independently or in parallel with the digital system. Memory contents may also be stored off-line on magnetic tape, using standard audio cassettes. Each experimental data block is assigned a code as it is loaded which allows the system to locate it later. When reloaded into memory these tapes provide all the data of the original experiment. Future plans include an interface which will make it possible to dump tape records directly into a computer for data reduction.

Because of the numerous sources of noise in the experimental signals and the small variations from run to run, it was felt that it would be advantageous to average results of several replicate experiments prior to data reduction. Signal averaging is performed electronically by a dedicated microprocessor constructed and programmed by Rollins Associates. The microprocessor is based on a Signetics 2650 CPU and has 16 K bytes of 8 bit RAM storage and 2 K bytes of ROM available for programming. It is connected directly to the data acquisition memory with a serial data

bus and control interlocks which prevent inadvertent destruction of data or program interrupts. Although at present only the signal averaging algorithm has been written and stored in PROM, other data manipulation subprograms could be compiled and later called with existing front panel switches. With the addition of a keyboard and alphanumeric CRT display, FORTRAN or BASIC languages could be implemented.

After each replicate experiment  $n$  of a set, the average value  $\bar{S}_{m,n}$  at each memory location  $m$  is computed as

$$\bar{S}_{m,n} = \frac{n-1}{n} \bar{S}_{m,n-1} + \frac{1}{n} S_{m,n}$$

where the previous average  $\bar{S}_{m,n-1}$  is stored in microprocessor memory. This 4096 location subset of memory may be accessed in exactly the same modes as the data acquisition memory. The average program is written in double precision (16 bit) arithmetic so that even after the maximum ten averages, the accumulated numerical error is less than the resolution of the data system. The efficacy of the averaging process may be seen in Figure 25. Nine snapshots of the original signal, a repetitive sine wave with superimposed noise, were taken with the data system and averaged with the microprocessor. A square wave synchronous with the signal triggered the data system at the same point in the cycle so the nine sine waves are time correlated. (The limited slew rate of the hard copy recorder has heavily filtered the original noisy signal; when viewed with an oscilloscope it was impossible to discern any wave shape buried in the noise.)

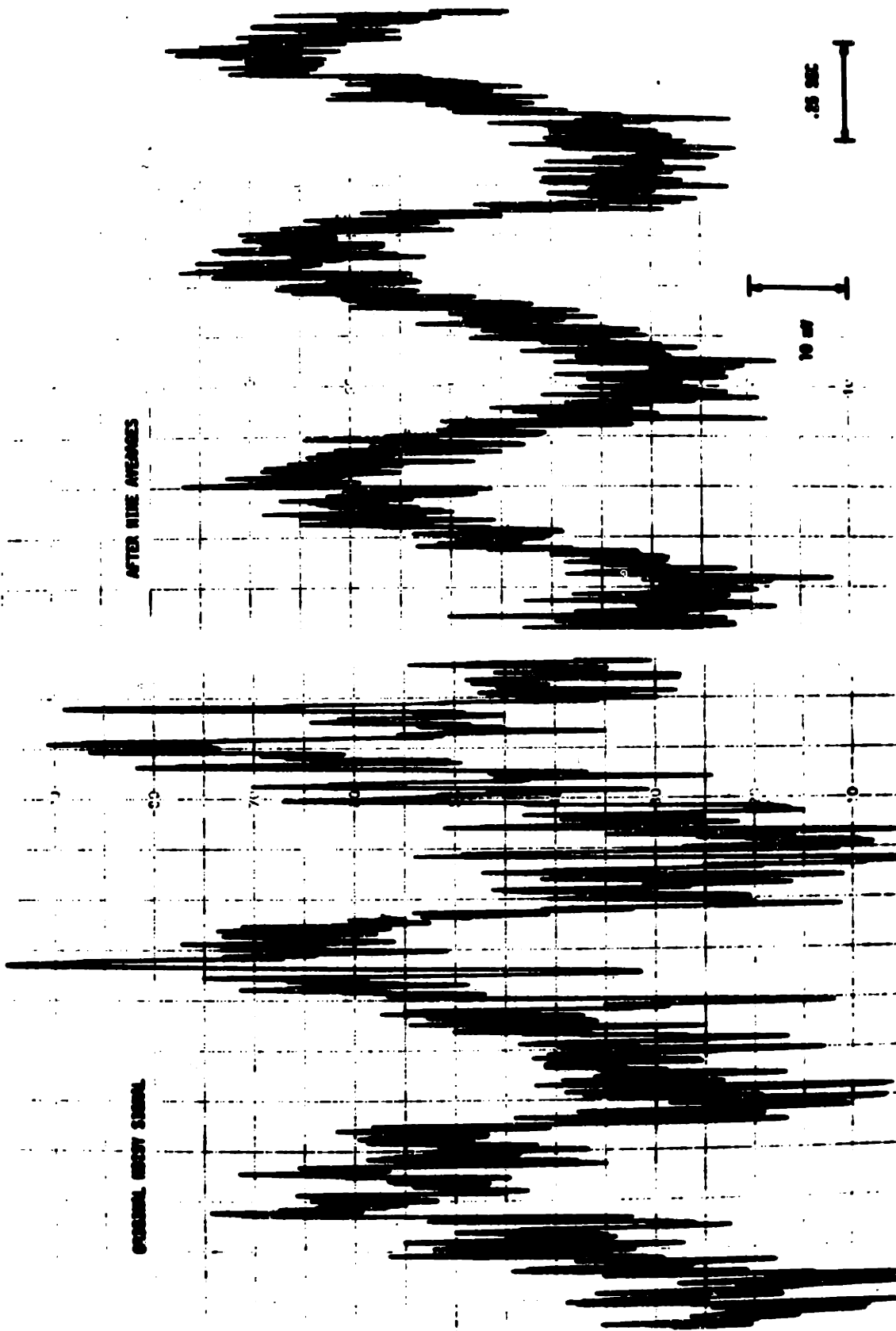


FIGURE 25 Microprocessor average of a repeated sine wave with superimposed noise

#### 6.4 Thermal Control System

A thermal system, designed as an integral part of the stop flow apparatus, allows the user to run experiments at any temperature between  $-30^{\circ}\text{C}$  and  $+35^{\circ}\text{C}$ .

Nitrogen gas, selected as coolant because of its ready availability in this laboratory, is first passed through a heat exchanger immersed in liquid nitrogen and cooled to  $-190^{\circ}\text{C}$ . The heat exchanger is a folded array of copper tubing housed in a stainless steel tank insulated with rigid urethane foam. The tank holds twelve liters of liquid nitrogen and has a boil off rate of about three liter/hour under normal operating conditions. Gas flow rate is adjusted depending on operating temperature and is typically .5 Kg/hour. The cold gas then passes through a heater consisting of a ni-chrome coil encased in a sealed phenolic tube. The electronic controller described below regulates power input to the heater coil and hence the temperature of the gas flowing into the thermostat block. Grooves milled in the block, and attached cover plates, form small gas channels over the entire surface (see Figure 17). At steady state, point to point temperature variations within the stop flow apparatus are less than  $0.5^{\circ}\text{C}$ . However, the time constant for thermal equilibrium of fluid loaded into the drive syringes is over five minutes, so a pre-cooler was devised. The pre-cooler is an aluminum cylinder machined to accept several bottles of experimental solutions and surrounded by a copper coil fed by a portion of the gas stream



exiting the heater. When the system reaches its operating point, the pre-cooler is typically within less than 1°C of the thermostat block temperature. To reduce coolant load, all exposed gas tubing, the heater, and the pre-cooler are heavily insulated. Extensions of the frame which supports the source lamp and photomultiplier assemblies form a box which surrounds and clamps the main stop flow assembly. The box framework is covered with an aluminum skin and polystyrene insulation, and includes an easily removable front access panel.

The electronic controller shown in Figure 26 measures the thermostat block temperature and modulates power dissipation in the gas heater to maintain the desired steady state. The copper-constantan measuring thermocouple is inserted into a deep well in the thermostat block and the reference thermocouple is immersed in liquid nitrogen, so the resulting thermal emf is always unipolar. Both thermocouple leads are enclosed in grounded shielding cable to reduce noise pickup. The copper leads of the thermocouples are connected to a high performance instrumentation amplifier with gain of 1:1000. A first order low pass filter with unity gain then removes most of the noise from the amplified thermocouple signal. Controller set point voltage is produced by a unity gain buffer and precision ten turn potentiometer. After referring to a table of thermocouple emf vs. temperature, the operator simply adjusts the potentiometer until the value displayed in the digital panel meter is equal to the desired tabulated voltage. A summing point amplifier then outputs an error signal proportional to the difference

between set point voltage and amplified thermocouple voltage. As the gas cooled thermostat block is essentially a first order system, proportional control should be adequate; however, even when the system is at set point, heater power is required to offset the cold gas stream. Therefore, the next stage incorporates proportional-integral control, with gains and time constant which represent a compromise between stability and offset error. The proportional-integral stage is followed by a bound limiter which rejects negative error signals (the heater can only add energy, not remove it) and limits output to less than ten volts to prevent saturation of the power stage.

The power amplifier, located on a separate chassis, is essentially a Darlington amplifier with cascaded transistors in a common collector configuration. The feedback resistor and base driver op-amp produce linear amplifier current response over its zero to ten volt input range. An overheat detection circuit protects the gas heater from burn out. A thermistor attached to the outside of the heater tube forms one leg of a bridge which drives a level detector with hysteresis. When the set bridge imbalance is exceeded the level detector output increases sharply and turns on a transistor which pulls power stage input to ground.

The thermal system start up procedure is as follows: (1) turn on the coolant gas to flush out any water vapor which might cause ice plugs; (2) fill the reference thermocouple dewar and heat exchanger tank with liquid nitrogen; (3) turn on the temperature controller and heater amplifier; (4) adjust the gas flow value and set point potentiometer for the

desired operating temperature. With ambient temperature typically between 22°C and 27°C, steady state is reached in a half hour when the set point is 25°C, and ninety minutes are required for cool down to -10°C. The control system will then maintain the apparatus within 0.5°C of the set point for at least six hours.



**CHAPTER 7**  
**EXPERIMENTAL METHOD**  
**AND TYPICAL RESULTS**

Blood was drawn by venous puncture from random donors at the Massachusetts General Hospital Blood Transfusion Service in conjunction with their normal collection procedure. Acid citrate dextrose (ACD) was the usual anticoagulant in the 25 ml glass collection tubes, though citrate phosphate dextrose (CPD) was used on occasion. Heparin coated tubes were also tried, but discontinued when clotting was noted after only three days storage. The choice of anticoagulant did not appear to affect the experiments in any way [35]. Bloods were stored in their collection tubes at 5°C for one to twelve days prior to use.

Red cells were prepared just before each day's experiments by a simple washing procedure. After discarding any clotted bloods, each aliquot was separately diluted 1:1 with isotonic saline, gently agitated, and centrifuged at 900 x g for ten minutes. The supernatant plasma and saline and the upper white cell layer were removed by aspiration. These washed red cell aliquots could then be combined without concern for agglutination caused by donor type incompatibility. The combined washed packed cells (Hct  $\approx$  90) constituted a stock suspension to be used in that day's experiments and calibration procedure.

Because light scattering theory does not adequately predict the relation between the size of non-spherical scattering objects and light extinction, it was necessary to establish an empirical correlation between erythrocyte volume and the light received at the photomultiplier. In the early phases of this research the volume calibration described

below was performed prior to each experimental set; in later experiments, the least squares fit based on the accumulated data shown in Figure 20 could be used.

A range of cell volumes were easily obtained by allowing cells to come to equilibrium in solutions with varying concentrations of NaCl, an impermeable solute. Typically, five calibration solutions were selected to provide the range of volumes expected in that experimental set. An isotonic NaCl solution was always included for reference. If the experiment involved a permeable solute, all the calibration solutions were made up with the same permeable solute concentration as would be in the post-mix extracellular solution. Thus the index of refraction effect shown in Figure 24 was not a factor in the calibrations.

Saline solutions were made up with reagent grade NaCl and distilled water and their osmolalities measured to  $\pm .002$  osmol/Kg with a freezing point osmometer. As the permeability does not appear to be affected by pH in the range 6-8 [6] we did not feel that the additional experimental complexity involved in using buffered media was justified. Permeable solutes were then added to these stock saline solutions as needed. These solutions were made up to the desired solute molar concentrations on a volume solute/volume solution basis, using buret and volumetric flask. The small volume contribution of the salt was neglected, which at worst leads to a 1% error in solute molarity in a 1.0 osmol/Kg NaCl solution.

Calibration cell suspensions were made up with 1 ml of stock packed

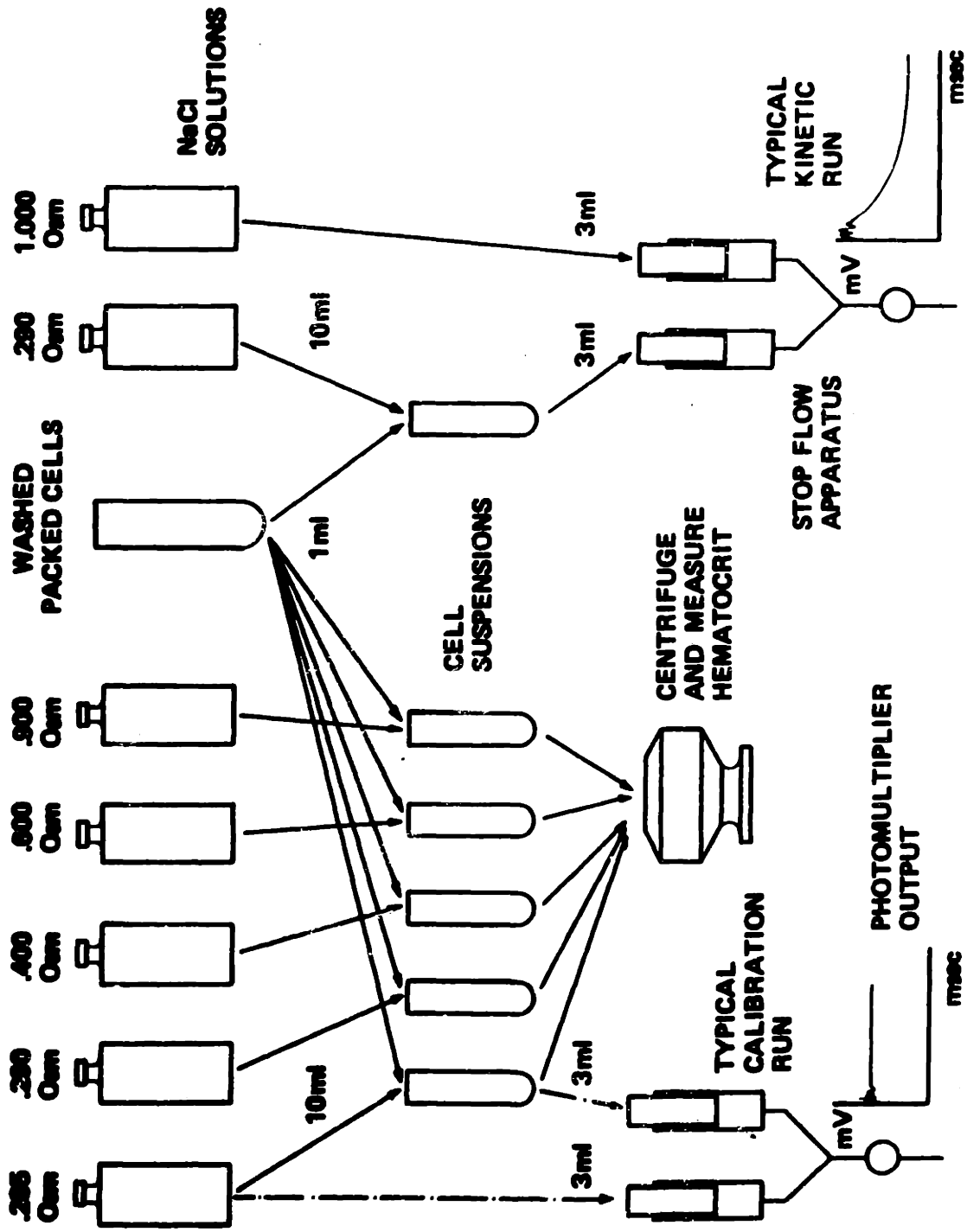
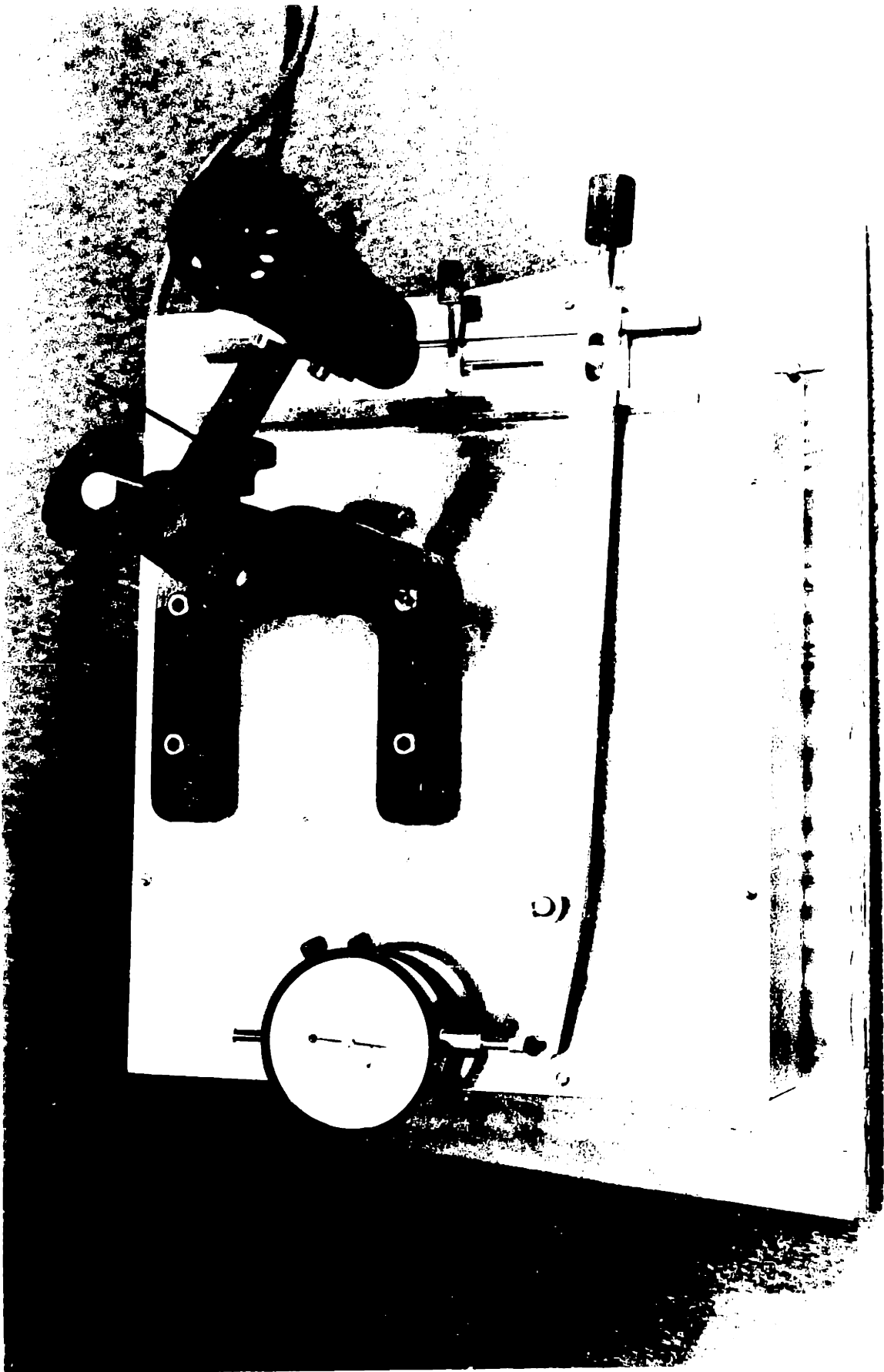


FIGURE 27 Schematic of calibration and experimental protocols

cells in 10 ml of solution, both measured by volumetric pipette. Solutions were measured in the usual manner, while the more viscous cell suspensions were gently blown out of the pipette. The experimental suspensions were prepared in the same tenfold dilution and thus had the same cell number density as the calibration suspensions. If no calibration was performed, the experimental suspension was made up with a dilution between 1:10 and 1:15. As mentioned in Section 6.2, cell volumes are derived from measurements of suspension hematocrits. The hematocrit, Hct, is the product of cell number density and population mean cell volume, and has units ml cells/100 ml suspension. If cell number density is held fixed, as we have been careful to do in our dilution procedure, relative cell volumes will be proportional to relative hematocrits.

After allowing time for cells to reach their equilibrium volumes, hematocrits were measured by first centrifuging the suspensions at 1000 x g for ten minutes in standard clinical micro-hematocrit capillary tubes. The relative volumes of supernatant fluid and packed cells were then measured with the specially constructed optical reader shown in Figure 28. A movable illuminated stage holds the capillary tube, which may be viewed through a low power microscope with fixed cross hairs. The stage is linked to a dial indicator through a lever sized to produce a 1:4 displacement reduction. By moving the stage and reading the displacement shown on the dial indicator, one is able to measure distances along the tube to  $\pm .005$  cm. The hematocrit is taken as the ratio of the height of the packed cell column to the



total fluid height in the capillary. Using this technique, replicate determinations of the same tube or several tubes drawn from the same suspension consistently agreed to within 2% of reading. The experimental suspensions typically had hematocrits ranging from 5 to 12 ml cells/100 ml.

Relative cell volumes were always referenced to the isotonic cell volume, that is, the non-dimensional cell volume is given by

$$\hat{V}_c = \frac{V_c}{(V_c)_{iso}} = \frac{Hct}{(Hct)_{iso}}$$

when the cell count is held constant, and  $(Hct)_{iso}$  is the measured hematocrit of the cells in isotonic saline. If the calibration solutions contained permeable solute, an additional solute free isotonic saline suspension was used as the volume reference, but not injected into the stop flow apparatus.

Stop flow operating procedures are identical for calibration and experimental determinations. The flow path is first thoroughly flushed and filled with isotonic saline. The lamp power supply, photomultiplier high voltage and pre-amp power supplies and data acquisition system are turned on, and the lamp shutter opened sufficiently to produce an approximately 80 mV photomultiplier signal. System output is then measured until it attains steady state, usually within 20 minutes. When experiments are performed at other than ambient temperature, the thermal system start up procedure described in Section 6.4 is also

followed. Throughout the cool down period the experimental cell suspension and solutions are held in the pre-cooler.

The stop flow fill procedure is designed to eliminate trapped air bubbles and fluid cross contamination and is as follows: (1) close the lamp shutter to prevent photomultiplier overload; (2) holding both drive syringe plungers fully down, open the exit valve and inject about 3 ml of solution into one fill valve, flushing the associated drive syringe and the fluid path; (3) close the exit valve and, releasing that drive syringe, continue to inject fluid until it is filled (about 3 ml); (4) follow the same sequence to flush and fill the other drive syringe with cell suspension. When the shutter is now opened the signal voltage will be roughly one third the experimental signal, as the optical chamber contains a cell suspension with double the post-mix number density. The photomultiplier high voltage supply, and thus gain, should be adjusted at this point to obtain a signal level of about 25 mV. This setting will usually provide the maximum experimental signals without exceeding the constraints on operation outlined in Section 6.2. Photomultiplier and lamp power supply settings are, of course, not changed during the course of a set of experiments.

The system is now ready for an experimental run, which is performed by arming the data acquisition system, inserting the drive ram stop block, and actuating the air cylinder drive. (This should be done within three minutes of filling, to preclude the effects of cell settling in the drive syringes.)



In a calibration run, the cell suspension is mixed with a solution containing solutes in the same concentration, so the cell number density is halved but cell volume does not change. Strip chart records of photomultiplier output during several typical calibration runs are shown in Figure 29. These are only a portion of that day's calibration set, which also included two other NaCl concentration levels and repeat runs of each cell volume. The calibration voltage was read to  $\pm .05$  mV roughly 60 seconds after flow stopped, using the data acquisition system in a real time digital voltmeter mode. At least two repeat runs, typically agreeing to better than .5 mV, were then averaged.

The fill and operating procedure is identical for a kinetic run, but the added solution has, of course, a different solute composition. For a given experiment, from two to ten repeat runs were performed and the results numerically averaged with the microprocessor after each run. Roughly forty data points were then read from microprocessor memory, using the manual slewing controls and location and voltage displays. Figures 30 through 35 show some typical experimental results, either as real time strip chart records, digital data acquisition system hardcopy, or microprocessor average hardcopy. Unless otherwise noted,  $T = 25^{\circ}\text{C}$ .

Signal voltages were converted to cell volume by several alternate methods. If a calibration set had been performed, the results were applied directly, using either an exponential fit such as equation 6.3 or linear interpolation between closely spaced volume/voltage data points. In later experimental sets, it was only necessary to know the

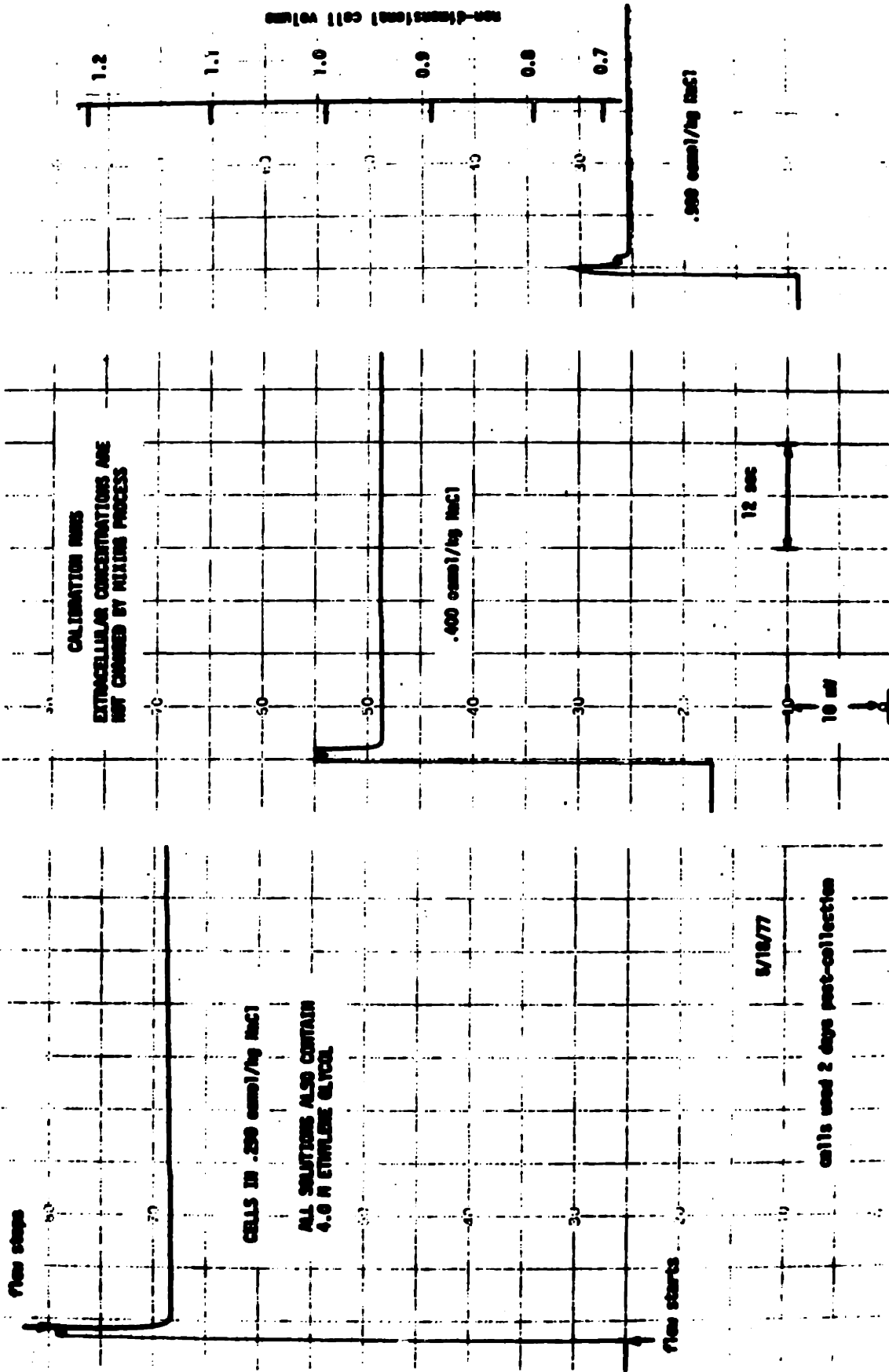


FIGURE 29 Typical calibration results, strip chart records of photomultiplier output

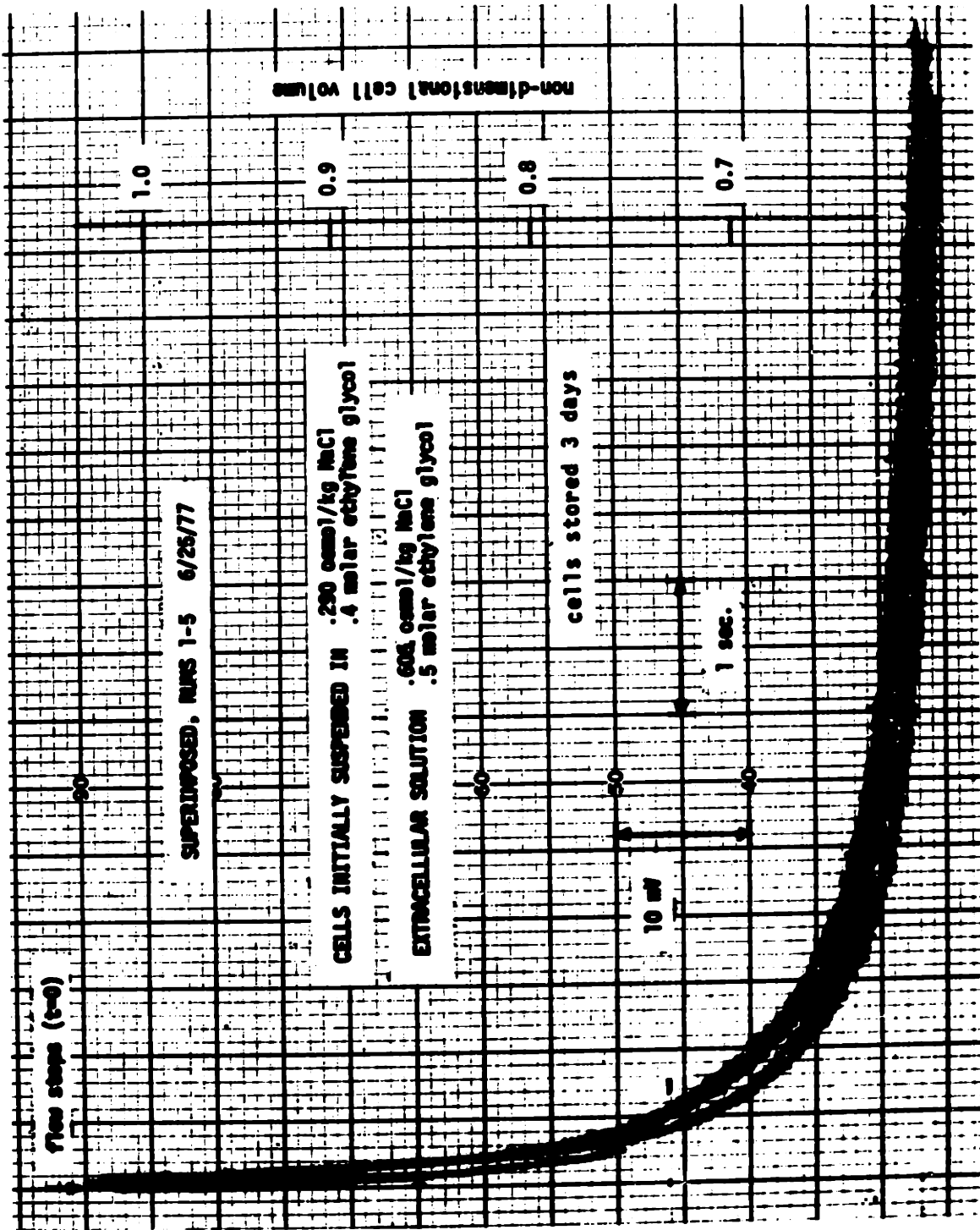


FIGURE 30 System reproducibility, five superimposed repeat runs of a typical experiment (data acquisition system hard copy)

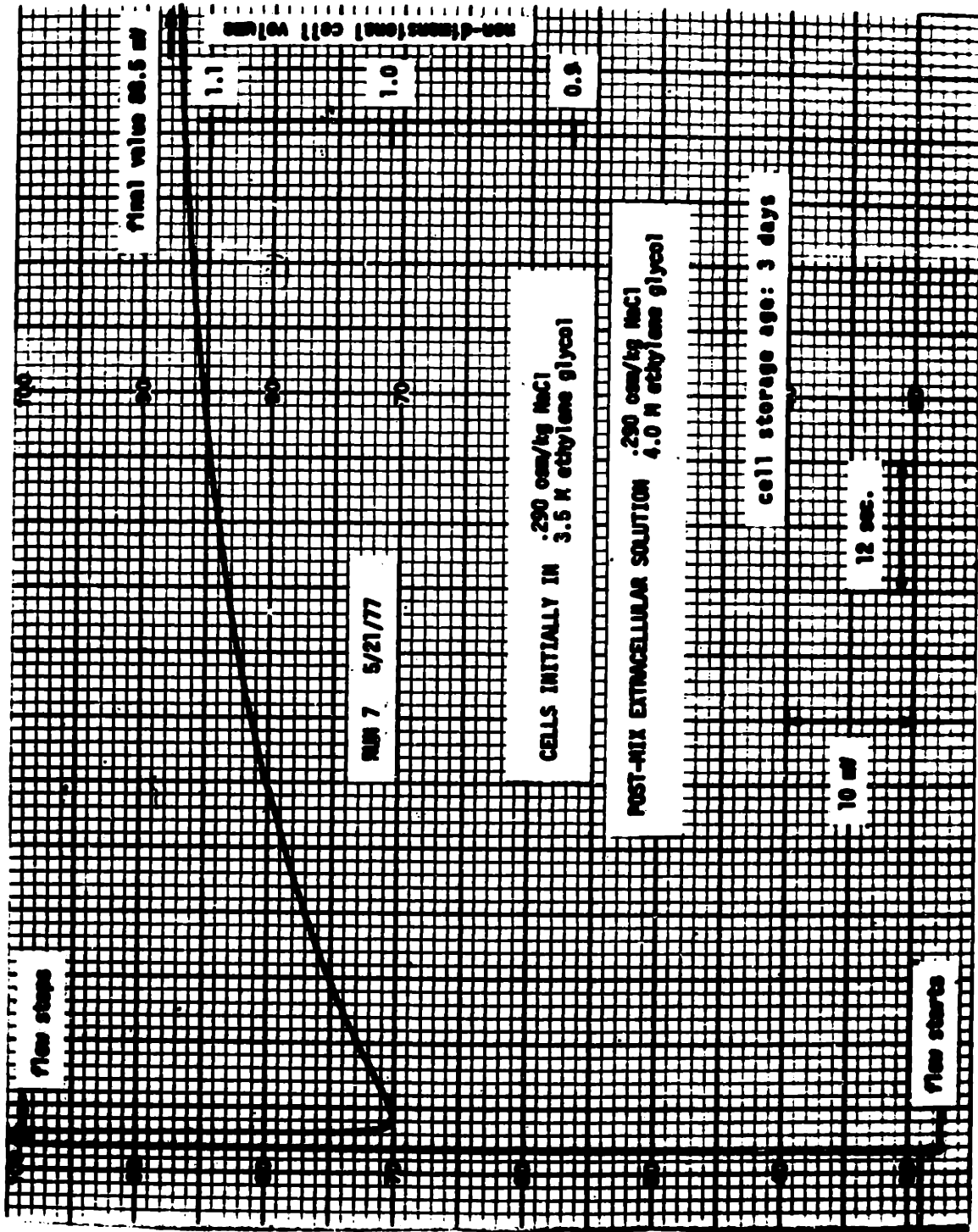
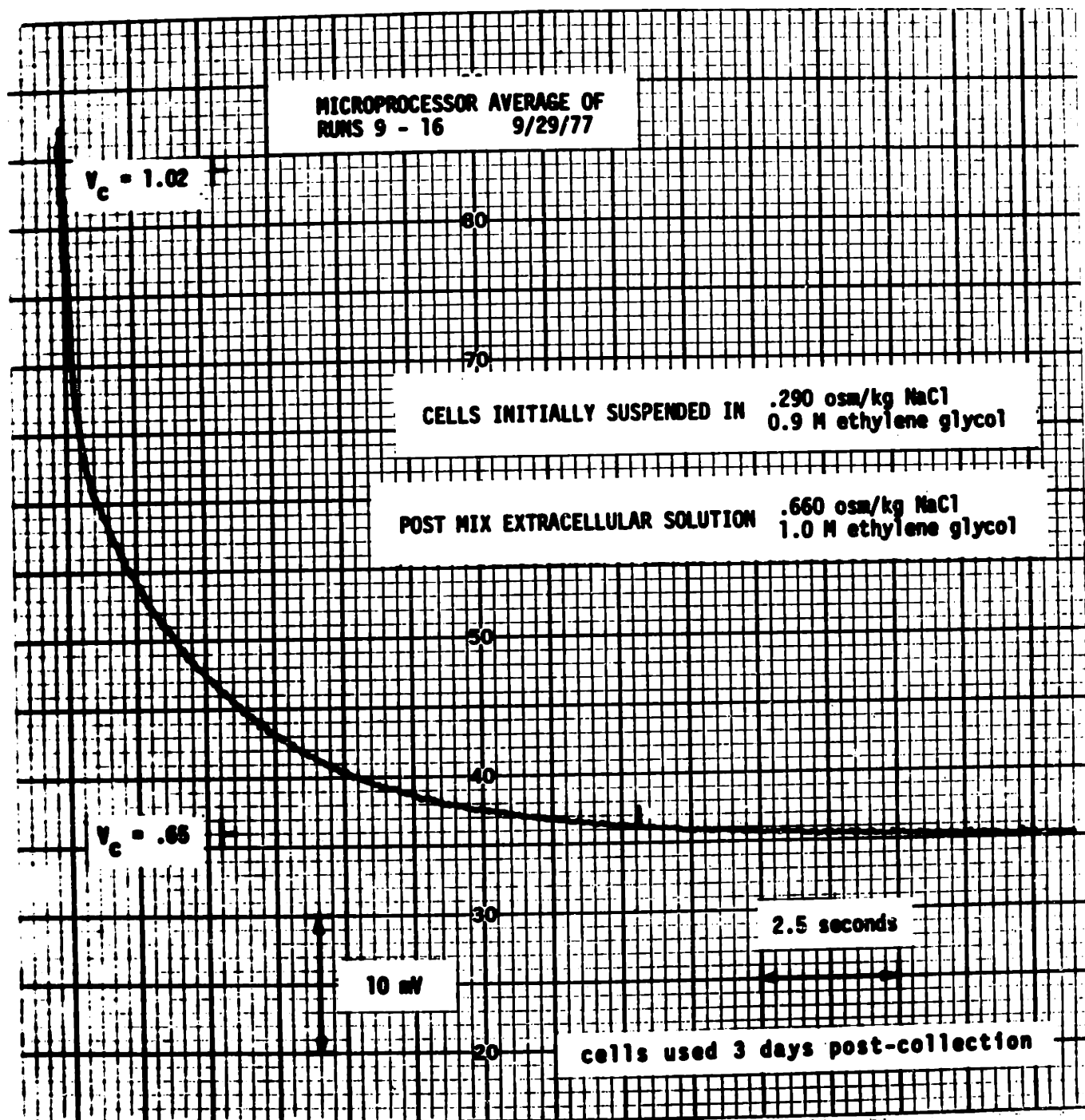


FIGURE 31 Strip chart record of a typical "shrink-swell" experiment



**FIGURE 32**      Hardcopy of microprocessor average of  
eight repeat runs of a typical experiment

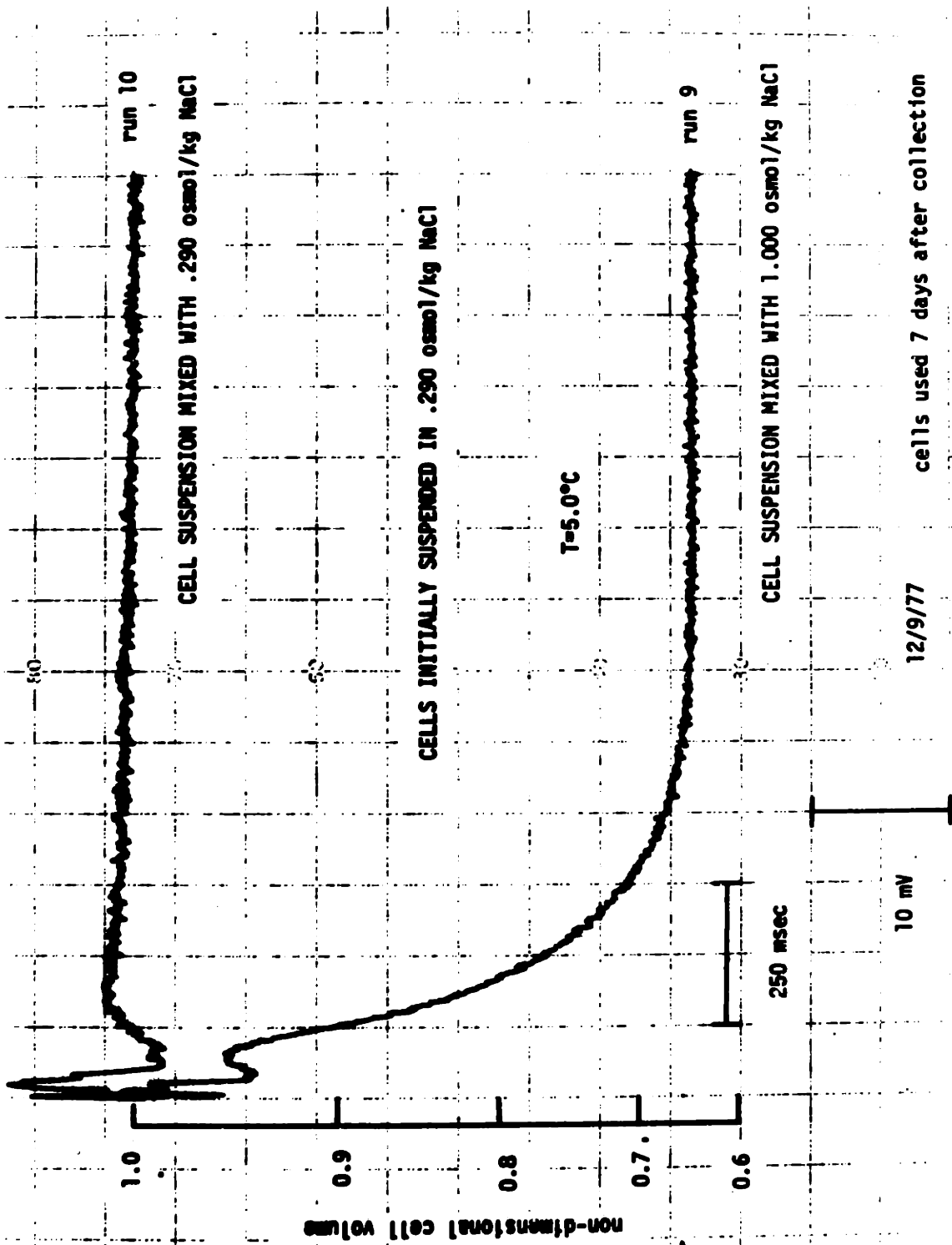


FIGURE 33 Two superimposed runs from a typical experiment set, showing consistency of initial values (data acquisition hard copy)

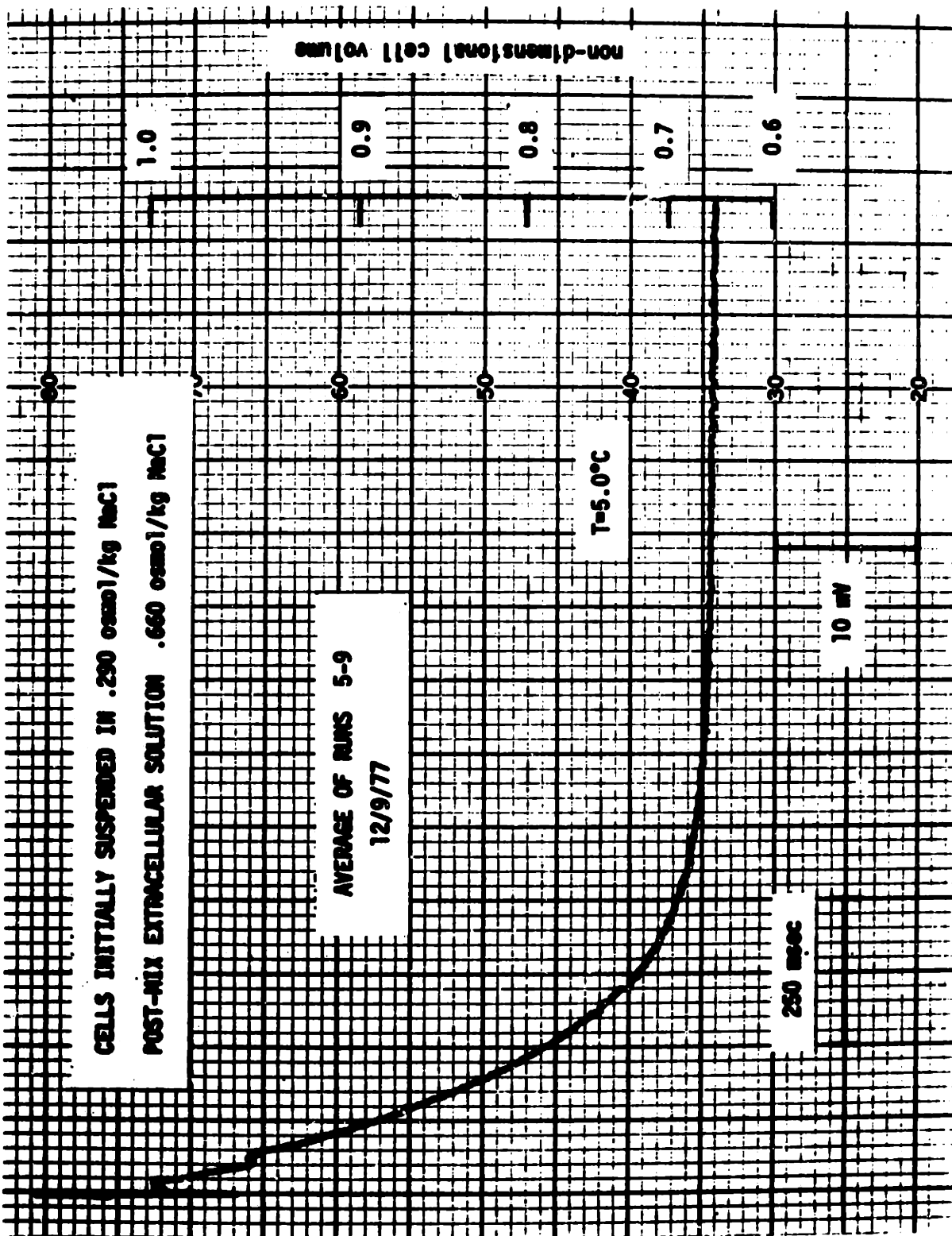


FIGURE 34 Microprocessor average of four repeat runs of experimental type shown in Figure 33

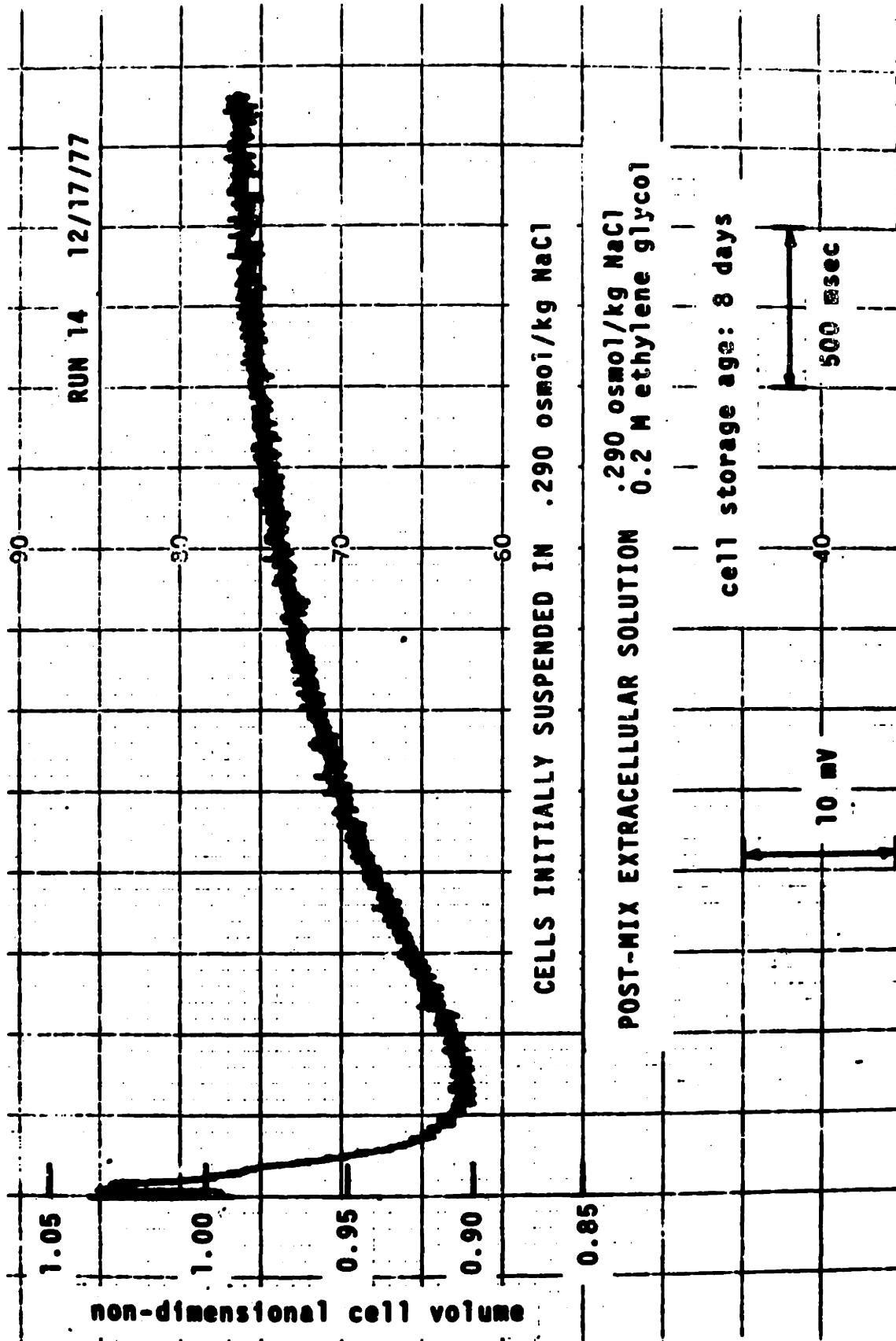


FIGURE 35 System resolution, data acquisition record of a typical experiment with very small volume changes



concentrations of solutes in the solutions; equilibrium cell volumes could then be calculated from the pseudo-binary volume model. If there was only one measurable equilibrium condition in the experiment, as in Figure 35, then equation 6.3 was applied directly. If there were two measurable steady state voltages, as in Figure 33, the form of equation 6.3 was used, but new best fit coefficients computed. The coefficients obtained in this manner were consistently within 10% of those in equation 6.3. The non-dimensional cell volumes, however calculated, were then entered on computer cards for data reduction.

Perhaps the most serious sources of error in stop flow measurements of cellular kinetics are the optical transients seen after flow is stopped. There appear to be two distinct time scales involved - a short oscillatory transient, shown in Figure 36, and the slow monotonic decay seen in Figure 37. Though the mechanisms involved in these transients are not fully clear, the following facts are relevant. (1) Cells carried in a flow field have statistically preferred orientations (e.g. [36] [37]), and light transmission through red cells is orientation dependent [38]. This would explain the shift in level and superimposed small fluctuations seen in the optical signal during the flow phase. (2) The magnitude and time scale of the optical transients do not depend on flow velocity prior to stopping flow, nor on the manner in which flow is halted. Other experimenters with substantially different apparatus configurations have observed identical transients [8] [39] [17].

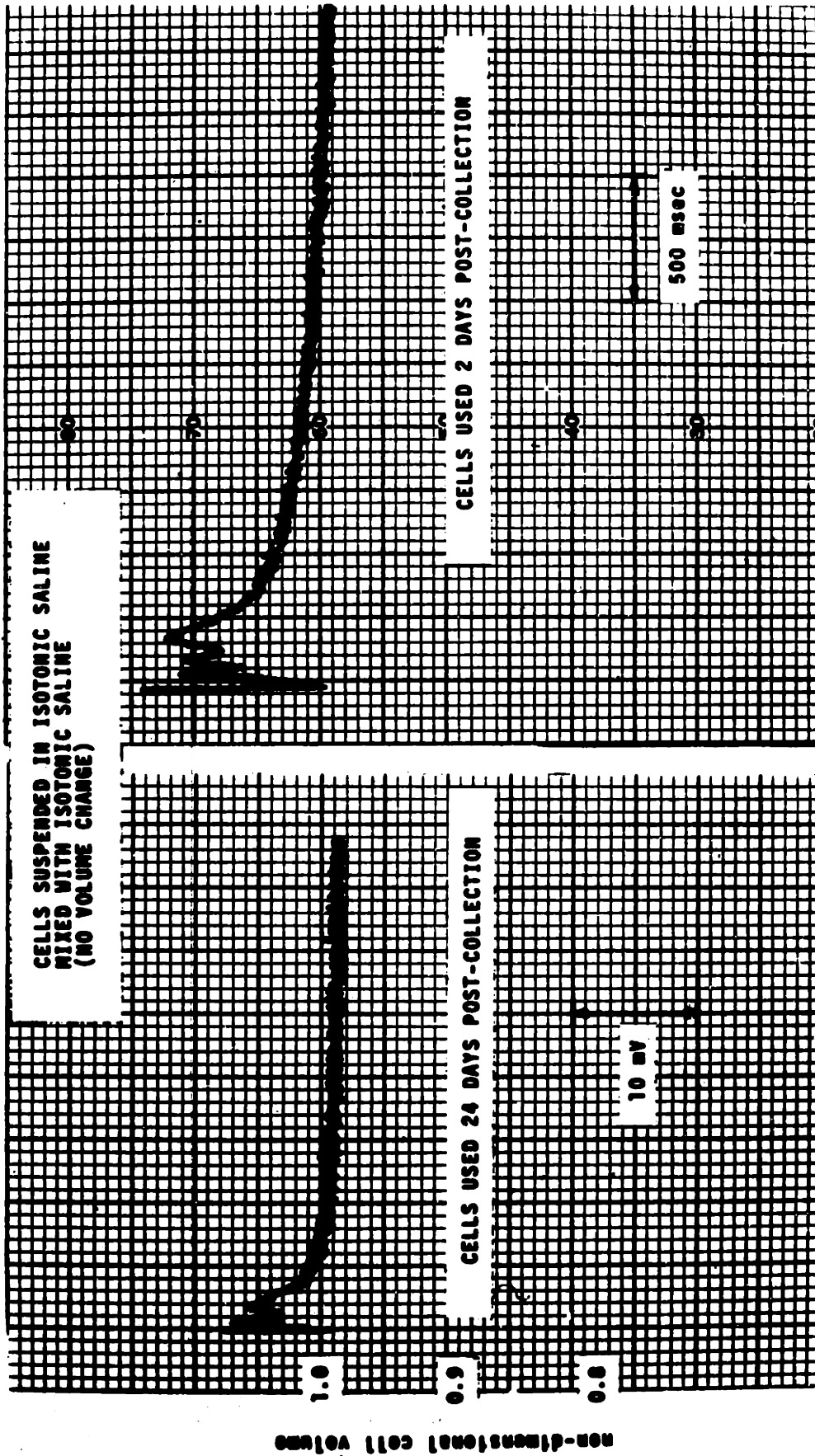


FIGURE 36 The short time optical transient, effect of cell storage age

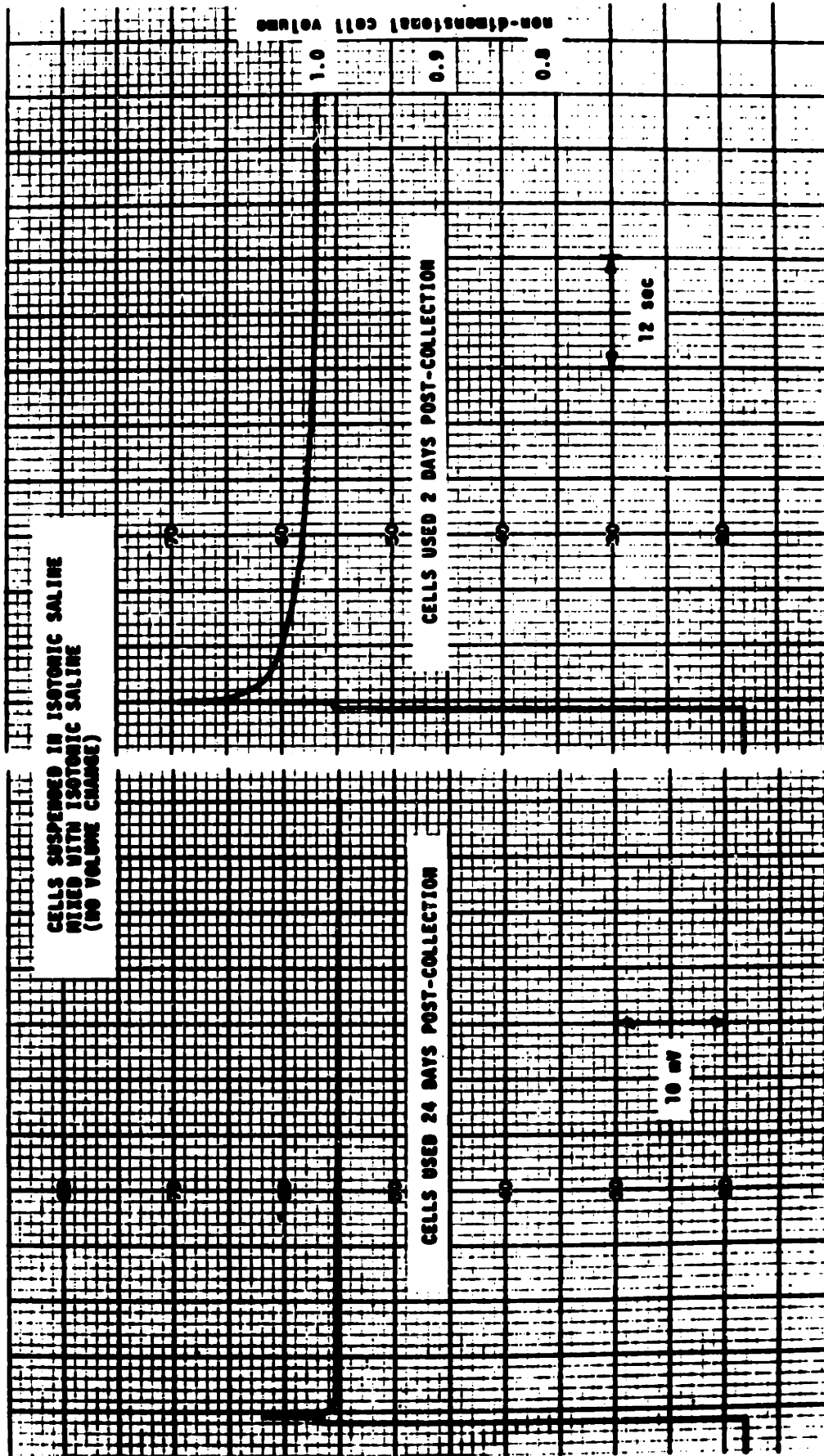


FIGURE 37 The long time optical transient

(3) The transients are also seen when a cell suspension is mixed in the stop flow with the same cell suspension, and are therefore not due to dilution effects. (4) The nature of the transients depends critically on cell storage age, the time between collection and use, as may be seen in Figures 36 and 37. (5) Cells shrunken to crenated spheres in hypertonic saline show a greatly increased transient magnitude, relative to steady state signal level. Cells swollen to spheroids in hypertonic saline produce a reduced transient. (6) Similar short time oscillatory signals are seen with suspensions of glutaraldehyde hardened cells but not when using cells sphered by addition of sodium lauryl sulfate [38]. (7) As cells age *in-vivo* they become increasingly spheroidal [40]. (8) Membrane rigidity, or surface tension, of hypotonically swollen cells is greater than that of normal cells. Cells shrunken to crenated spheres in hypertonic media exhibit reduced membrane stiffness [14]. This is consistent with the notion that membrane surface area is constant during cell volume changes. (9) Addition of high concentrations of permeable solute (e.g. Figure 29) or experimental temperatures below 10°C greatly diminish the transients.

These collected bits of information imply that: (1) the signal oscillations seen during flow and immediately after flow is stopped are due to the rapid changes in cell orientation; (2) the short time transient lasting 100-300 msec is then observed as fluid and cell motions are damped out; (3) the slower monotonic decay is probably due to relaxation of the cell from a perturbed, distorted configuration to

its normal state. It is significant that the time constant for this transient (~10 sec) is approximately equal to that measured by Rand [44] for stress induced membrane changes leading to hemolysis.

What can the experimenter do to reduce the adverse effect of these optical transients? Changes in apparatus configuration, drive velocity or stopping mode have almost no effect. Sphering the cells by the addition of detergents or other agents is clearly undesirable. One common approach is to run "base line" experiments in which cell volume is not changed and then use these to correct the kinetic results. The author disagrees with this approach for two reasons. First, in Section 6.2 we saw that the optical signal appears as a product of numerous uncoupled effects. Thus, the transient correction should be via a multiplicative rather than subtractive manipulation, but it is not obvious how to do this properly. Second, the optical transients are not independent of cell volume or the kinetics of concurrent cell volume changes, so the meaning of a "base line" is ambiguous.

The approach taken in the present work was first to use only cells with storage ages between two and twelve days. Within this range of storage times no correlation was seen between permeability and cell age. This strategy reduces but does not completely eliminate the optical transients. The short time transient may be reduced still further by signal averaging, as may be seen in Figures 32 and 34. Also, it will be shown in Section 8.3 that the first 100 msec of noisy data may be completely discarded without affecting the measured permeability values.

For many experiments with time scales of less than 1 second the long time decay appears as a constant offset. We then simply subtract this offset from the short time record and proceed as usual to reduce the data. There is really no justification for such a procedure, but it does result in correct initial values and consistent time histories, and is the minimum manipulation one could make.

**CHAPTER 8**  
**DATA REDUCTION**

### 8.1 The General Algorithm

Given a set of data points  $y_i$  and a theoretical fitting function  $y(x_i)$ , the correlation between theory and experiment may be measured by the chi-square statistic

$$\chi^2 = \sum_i \left( \frac{y_i - y(x_i)}{\sigma_i} \right)^2 \quad (8.1)$$

where the  $\sigma_i$  are the standard deviations of each data point.

For a fitting function  $y(x_i)$  which depends on unknown parameters  $a_j$ , the optimum  $a_j$  may be obtained by applying the method of least squares and minimizing  $\chi^2$  with respect to all the parameters

$$\frac{\partial \chi^2}{\partial a_j} = \frac{\partial}{\partial a_j} \sum_i \left( \frac{y_i - y(x_i)}{\sigma_i} \right)^2 = 0 \quad (8.2)$$

If, however,  $y(x_i)$  is not a linear function of the parameters, equation 8.2 can not be solved for the  $a_j$  and other less direct methods must be used.

One can imagine equation 8.1 as describing a  $\chi^2$  surface in  $a_j$  coordinates. The least squares problem then becomes one of searching for a local minimum. Although in general the surface may have more than one minimum, physical constraints will dictate a limited parameter region in which to search.

In the gradient method [41], all parameters are adjusted simultaneously by an amount  $\delta a_j$



$$\delta a_j \sim - \frac{\partial \chi^2}{\partial a_j} \quad (8.3)$$

such that the search direction at each step is along the gradient of the  $\chi^2$  surface. Unfortunately, as a local minimum is approached the magnitude of the gradient diminishes, and the search is slow to converge.

Another approach [41] is to linearize the fitting function with a first order Taylor series expansion in the parameters

$$y(x_i) = y_0(x_i) + \sum_j \frac{\partial y_0(x_i)}{\partial a_j} \delta a_j \quad (8.4)$$

The chi-square is then given by

$$\chi^2 = \sum_i \frac{1}{\sigma_i^2} \left\{ y_i - y_0(x_i) - \sum_j \frac{\partial y_0(x_i)}{\partial a_j} \delta a_j \right\}^2 \quad (8.5)$$

For a non-analytic function  $y(x)$ , the derivatives may be evaluated numerically as

$$\frac{\partial y(x_i)}{\partial a_j} = \frac{y(x_i, a_j + \Delta a_j) - y(x_i, a_j - \Delta a_j)}{2\Delta a_j} \quad (8.6)$$

where, for given values of the independent variable and parameters, the fitting function is generated numerically.

If the method of least squares is applied to the parameter increments  $\delta a_j$  in equation 8.5, one obtains

$$\frac{\partial \chi^2}{\partial \delta a_k} = -2 \sum_i \frac{1}{\sigma_i^2} \left\{ y_i - y_0(x_i) - \sum_j \frac{\partial y_0(x_i)}{\partial a_j} \delta a_j \right\} \frac{\partial y_0(x_i)}{\partial a_k} = 0 \quad (8.7)$$

This result may be written in matrix form as

$$\bar{\alpha} \bar{\delta a} = \bar{\beta} \quad (8.8)$$

where the elements of the vector  $\bar{\beta}$  are

$$\beta_k = \sum_i \frac{1}{\sigma_i^2} \left( y_i - y_0(x_i) \right) \frac{\partial y_0(x_i)}{\partial a_k} \quad (8.9)$$

and the elements of the matrix  $\bar{\alpha}$  are given by

$$\alpha_{jk} = \sum_i \frac{\partial y_0(x_i)}{\partial a_j} \frac{\partial y_0(x_i)}{\partial a_k} \quad (8.10)$$

Equation 8.8 is easily solved for the desired parameter increments by matrix inversion

$$\bar{\delta a} = \bar{\alpha}^{-1} \bar{\beta} \quad (8.11)$$

Since the Taylor series expansion is only an approximation to the actual  $\chi^2$  surface, the local minimum must be approached by repeatedly computing the  $\delta a_j$ , moving to the new position  $\chi^2(a_j + \delta a_j)$  and computing improved estimates of the  $\delta a_j$ . In contrast to the gradient search, the expansion method converges rapidly near the minimum, but is not well behaved far away.

A search algorithm which behaves like the gradient method far from the minimum and like the expansion method as the solution converges was developed by Marquardt [42] by forming a modified  $\bar{\alpha}'$  matrix, specified by

$$\alpha'_{jk} = \begin{cases} \alpha_{jk} (1 + \lambda) & j = k \\ \alpha_{jk} & j \neq k \end{cases} \quad (8.12)$$

If the interpolation variable  $\lambda$  is small, the solution method simply follows the Taylor series scheme, but for large  $\lambda$ , the matrix equation 8.11 degenerates into the uncoupled equations

$$\delta a_j = \frac{\beta_j}{\lambda \alpha_{jj}} \quad (8.13)$$

Now, if one defines the chi-square at some point in  $a_j$  space as

$$\chi_0^2 = \sum_i \left( \frac{y_i - y_0(x_i)}{\sigma_i} \right)^2 \quad (8.14)$$

then from equation 8.9

$$\beta_j = -\frac{1}{2} \frac{\partial \chi_0^2}{\partial a_j}$$

Also, since from equation 8.10 the  $\alpha_{jj}$  do not involve the data points  $y_i$ , for a defined fitting function the value of  $\alpha_{jj}$  at any point in  $a_j$  space is invariant. Therefore, within a scaling factor, we see that equation 8.13 is equivalent to the gradient method.

The Marquardt search algorithm is as follows: (1) select some small value of  $\lambda$  and choose some initial  $a_j$ ; (2) compute  $\chi^2(a_j)$  and the  $\frac{\partial y_0(x_i)}{\partial a_j}$  at this point using equations 8.1 and 8.6; (3) for the given  $\lambda$ , compute the  $\delta a_j$  by inversion of the  $\bar{\alpha}'$  matrix; (4) compute the chi-square at the new location  $a_j + \delta a_j$ ; (5) if  $\chi^2$  has increased

return to step 3 with larger  $\lambda$ ; (6) if  $\chi^2$  has decreased, reduce  $\lambda$ , replace the  $a_j$  with the new parameter values  $a_j + \delta a_j$ , and return to step 2; (7) when subsequent decreases in  $\chi^2$  are less than a specified convergence test, terminate the search.

## 8.2 Computer Program Description

The search algorithm outlined above has been implemented in FORTRAN programs RBCPERM, PERM2, and PERM3, which differ only in their theoretical modelling equations. PERM2 is based on the non-dimensional forms of the modified Kedem-Katchalsky transport equations and solution and volume models derived in Chapter 5, and is fully listed in Appendix D. PERM3 uses the linear flux equations 5.22 and 5.23, but is otherwise identical. RBCPERM employs the conventional Kedem-Katchalsky rate equations and the "osmotic dead space" cell volume model. Because these equations apply only in the dilute limit, RBCPERM was not used for data reduction but served as a test and development program. Similar computer algorithms have also been described by Marquardt [42], Bevington [41], and Stusnick [43]. The first two are general purpose and may be applied to any non linear parameter search, while Stusnick specifically examined the problem of membrane transport.

The program is made up of a mainline MAIN which primarily handles input/output, subprograms CURFIT, FDERIV, FCHISQ and MINV which actually perform the Marquardt algorithm, and subroutines VOLFUN, RKI, and MODEL which generate the theoretical cell volume fitting function.

User input to MAIN consists of the experimental conditions such as temperature and solute concentrations, initial guesses of parameter values, and the cell volume data obtained from the stop flow apparatus. In the general case the user would also input SIGMAV as a weighting vector of standard deviations  $\sigma_i$  of each data point. However, the present data acquisition scheme does not produce that statistic, so SIGMAV has been set equal to a constant scalar value of .05, and all data points are equally weighted in computing  $\chi^2$ . MAIN computes post-mix extracellular concentrations and activities, initial intracellular conditions and cell volume, and several parameter independent constants. The parameters contained in vector A(J) are either the scaled Kedem-Katchalsky set  $L_pRT$ ,  $\omega RT$  and  $\sigma$ , or the linear set  $L_{11}$ ,  $L_{12}/L_{11}$  and  $L_{22}/L_{11}$ . MAIN also sets the search convergence criterion HALT, the initial value of the interpolation variable LAMBDA and the integration time step DT. After performing these initialization tasks, MAIN calls subroutine CURFIT to search along the  $\chi^2$  surface. After each iteration of CURFIT, which corresponds to a new position in parameter space, MAIN computes TEST, the percent change in the chi-square statistic. If TEST is less than HALT, typically .01, one assumes that the minimum has been reached and the search is terminated. The program then uses the last set of parameter values to generate and display the theoretical best fit cell volume and intracellular concentration time histories. Data and computer generated best fit lines for three typical experiments are shown in Figures 39, 40 and 41. MAIN also outputs the

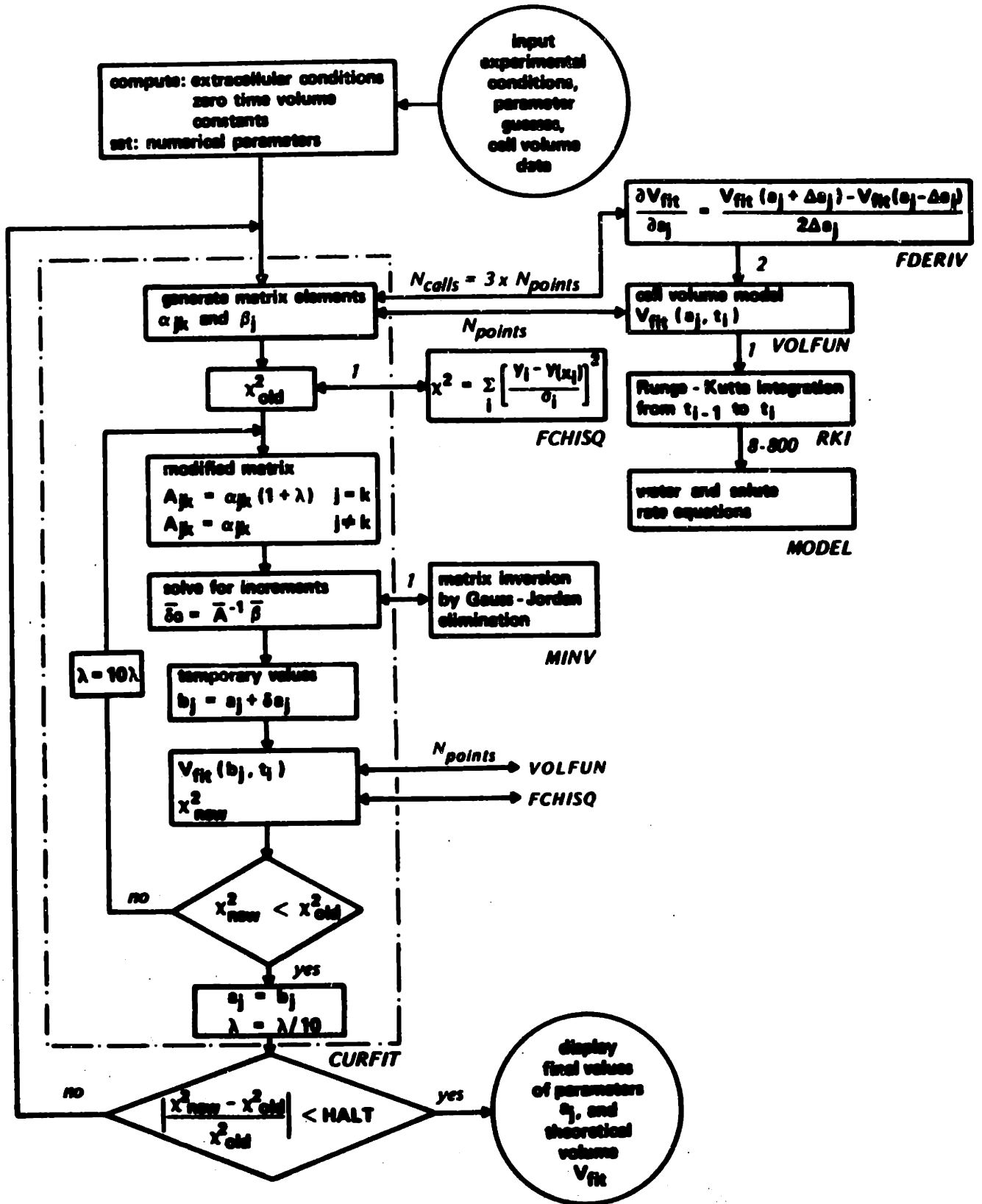


FIGURE 38 Flow chart of data reduction program

estimated parameter uncertainties,  $ERR(J)$ , computed by Bevington's method [41].

Subroutine CURFIT, which embodies the Marquardt algorithm, accepts as input the non-dimensional cell volume data  $V(I)$  as a function of time  $T(I)$ , the number of data points NPTS, the current value of the membrane parameters in vector  $A(J)$  and the current value of LAMBDA. CURFIT first generates the elements of matrices ALPHA and BETA according to equations 8.10 and 8.9. Notice that since  $\bar{\alpha}$  is a symmetric 3 x 3 matrix, only six elements need be computed. The theoretical fitting function  $y(x_i)$  is the non-dimensional cell volume  $VFIT(I)$ , generated for a given set of parameter values by NPTS calls to function subprogram VOLFUN. Derivatives of the fitting function with respect to each of the parameters are computed at each point  $i$  by subroutine FDERIV, using equation 8.6. The finite differences  $\Delta a_j$  are not constant, but are always  $.05 a_j$ . The modified  $\bar{\alpha}'$  matrix ARRAY is filled according to equation 8.12 and the current value of  $\lambda$ . Each element of ARRAY is then scaled by an amount  $S_{jk} = \sqrt{\alpha'_{jj}\alpha'_{kk}}$  to improve the numerical accuracy of the subsequent matrix inversion. This is performed by subroutine MINV, which is based on the IBM SSP program of the same name, but has been rewritten for the particular case of a 3 x 3 matrix. The inverse matrix returned by MINV is first properly rescaled by factors  $S_{jk}$ , then applied in equation 8.11 to compute the parameter increments  $\delta a_j$  and the new parameters  $b_j = a_j + \delta a_j$ . These temporary values, subject to any external constraints such as are contained in equations 2.8, are

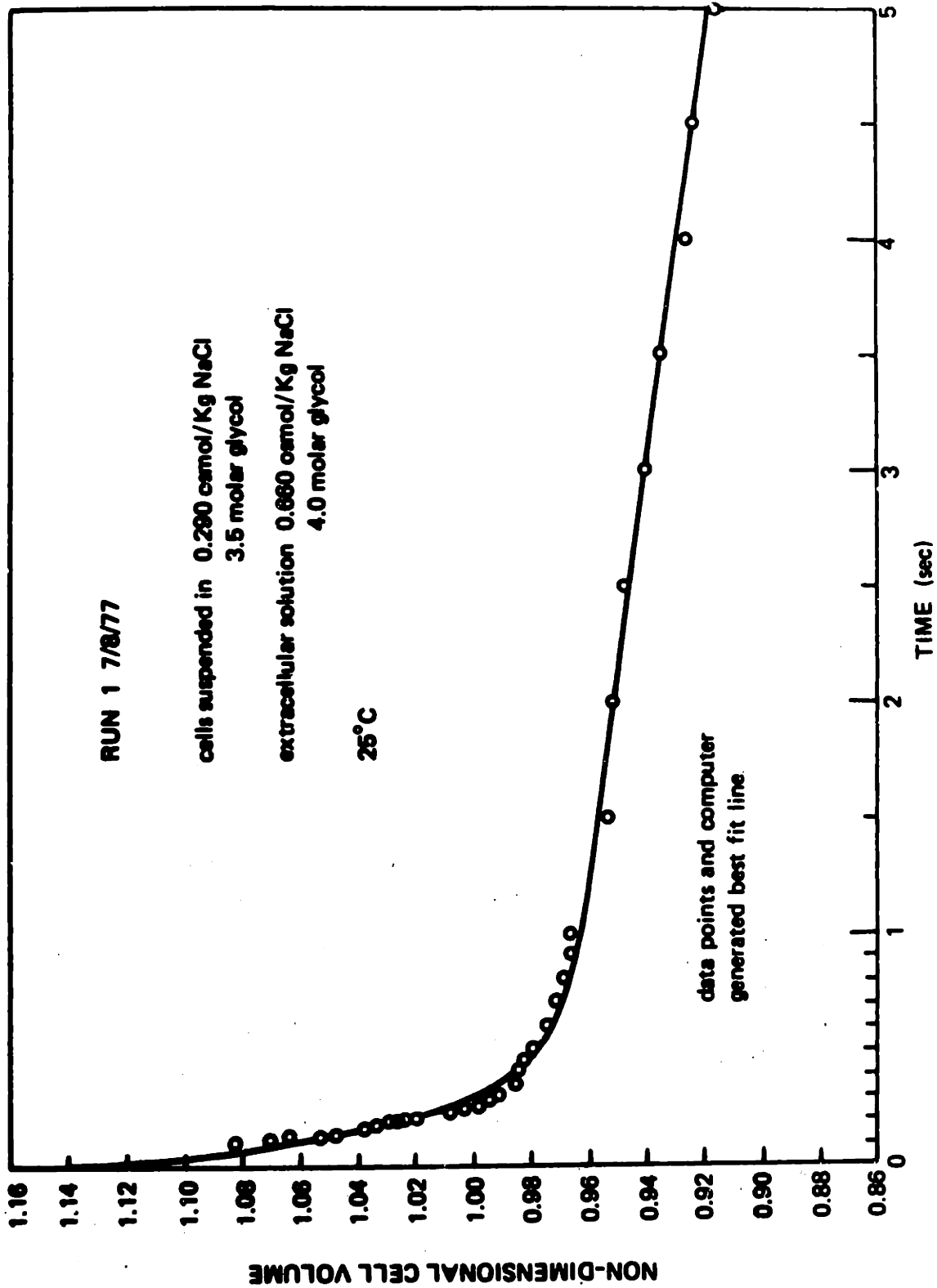


FIGURE 39 Results of a typical data reduction run, experimental data points and computer generated best fit line



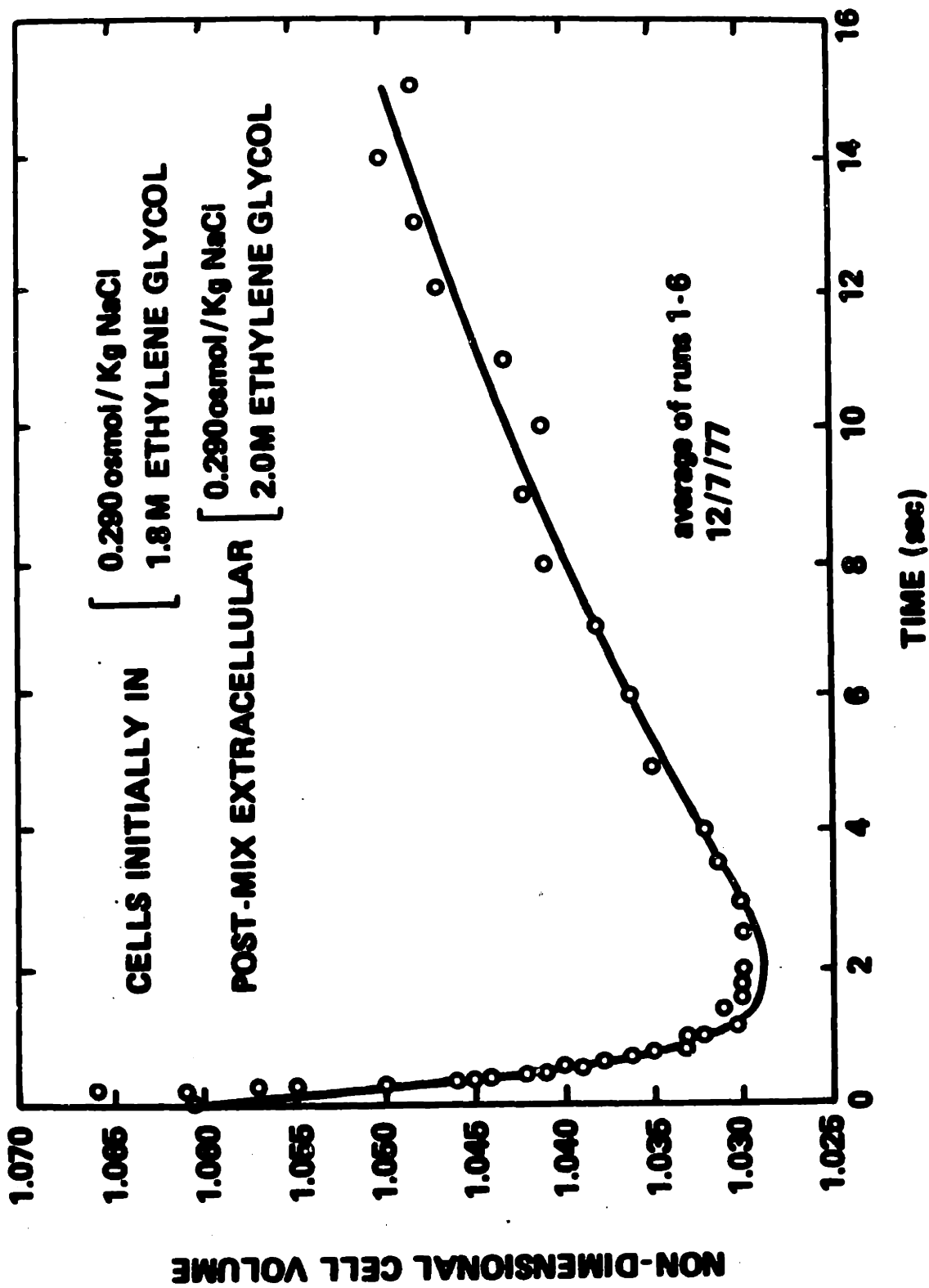


FIGURE 40 Data points and best fit line, typical permeable solute "shrink-swell" experiment

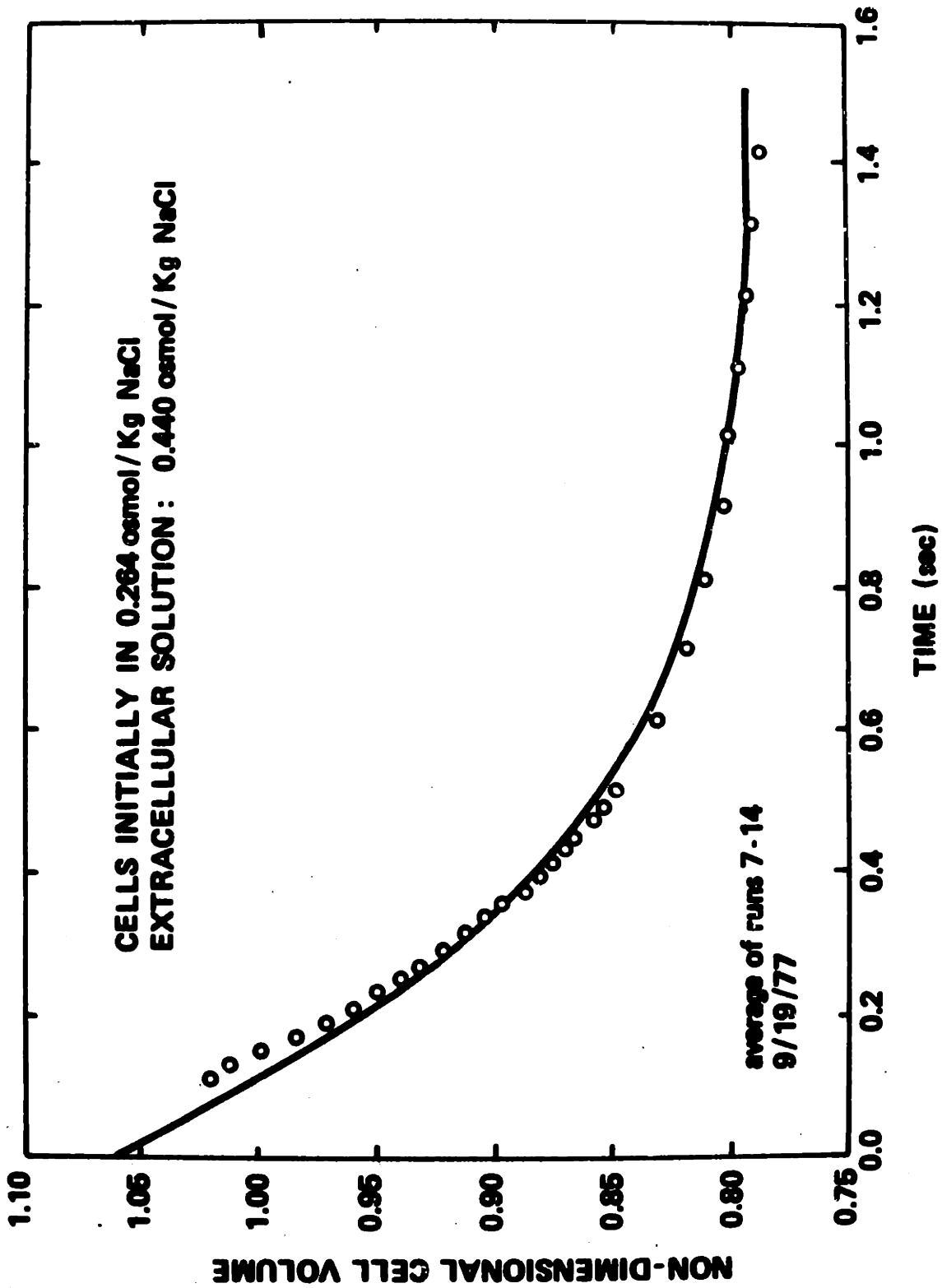


FIGURE 41 Data points and computer best fit, typical "hypertonic shrink" experiment

then passed to VOLFUN to generate a new fitting function. If the  $\chi^2$  based on this temporary fitting function exceeds the previous  $\chi^2$ , the interpolation variable  $\lambda$  is increased by a factor of ten and a new  $\bar{\alpha}$  matrix, now weighted more toward the gradient method, is computed. If the  $\chi^2$  has diminished,  $\lambda$  is divided by ten, the previous parameters are replaced by the new values in vector  $b_j$  and the program returns to MAIN.

The value of  $\chi^2$  for given data  $V(I)$  and theoretical values  $VFIT(I)$  is computed by function subprogram FCHISQ. Notice that FCHISQ actually returns the reduced chi-square statistic

$$\chi_R^2 = \frac{1}{N_F} \sum_i \left( \frac{y_i - y(x_i)}{\sigma_i} \right)^2$$

where the number of degrees of freedom  $N_F$  is equal to the number of data points minus the number of adjustable parameters. If the standard deviations  $\sigma_i$  were known,  $\chi_R^2$  would approach unity for a perfect fit, but in the present case  $\chi_R^2$  and  $\chi^2$  are arbitrarily scaled.

The theoretical cell volume history  $VFIT$  is produced by sub-routines VOLFUN, RKI, MODEL, and several auxiliary FIT functions. Given the time index  $I$  and the current parameter vector  $A$ , VOLFUN returns the non-dimensional cell volume at the time  $T(I)$ . The values of the independent variable contained in the data vector  $T$  may be arbitrarily spaced, but for a given set of parameter values, successive calls to VOLFUN must increment  $I$  by 1, beginning with  $I = 1$ . The

data time vector is passed from MAIN to VOLFUN via a labelled COMMON block. On the first call to VOLFUN with new parameter values the subroutine computes parameter non-dimensional groups and returns a cell volume based on the pseudo-binary model and the initial values of free water and permeable solute content NWFN and NSPN passed to it from MAIN. Subsequent cell volumes are generated by numerically integrating the rate equations for water and permeable solute and applying the pseudo-binary volume model.

The numerical integration from  $T(I-1)$  to  $T(I)$  is performed by subroutine RKI, using a fourth order Runge Kutta technique. RKI is derived from the similarly named SSP program, but has been rewritten for maximum computational speed in the special case of two simultaneous first order differential equations. In any numerical integration scheme, one would like to use a small time step when the variables are changing rapidly and a longer interval as the system approaches equilibrium. In the present experiments, cell volume data are typically recorded at variable time intervals such that the volume changes about 1% between data points. The integration step  $DT = 5$  msec and the limits on the number of steps between  $T(I-1)$  and  $T(I)$  specified in RKI have been selected to take advantage of these variable intervals. Continued program operation has demonstrated that these choices yield stable and accurate numerical solutions with a minimum of computation time.

The transport equations to be integrated by RKI are contained in subroutine MODEL. Given values for free water and permeable solute content, denoted Y1 and Y2 in RKI and NWF and NSP in MODEL, MODEL first computes the pseudo-solute molality MPB, and, using a polynomial curve fit, the pseudo-solute osmotic coefficient PHIPB. The permeable solute molality MSP is easily calculated from the non-dimensional water and solute content, and the arithmetic mean concentration CSPM is then obtained with the aid of the curve fit for solute molar concentration contained in function FIT2. The transmembrane difference in water activity DLNAW is calculated from the relation between osmolality and activity, the curve fit for permeable solute osmolality, and the extracellular condition LNAWO. The permeable solute driving force follows directly from the curve fit for  $\ln a_{sp}$  as a function of  $m_{sp}$  and the extracellular constant  $\ln a_{sp}^0$ . Finally, the non-dimensional rate equations yield the time derivatives  $\frac{dn_w^f}{d\hat{t}}$  (DNWFDT) and  $\frac{d\hat{n}_{sp}}{d\hat{t}}$  to be returned to RKI.

Subprograms MODEL, RKI, and VOLFUN, have been carefully written to minimize, as far as is possible, their execution time. In a typical data reduction run, there will be thirty or more data points and CURFIT will converge after four iterations. The program flow chart in Figure 38 reveals that for such a case VOLFUN and RKI will each be called 960 times, and depending on the data time intervals MODEL will be called between 7,680 and 768,000 times. For the same reason, the polynomial curve fits for pseudo-binary and permeable solute non-

ideality contained in functions FIT1 through FIT5 have been written in factored form. When run on an Interdata Model 80 computer, program execution requires between 30 and 110 seconds, depending primarily on the experimental final time.

### 8.3 Program Tests

The computer data reduction scheme was tested under controlled conditions to evaluate the numerical accuracy of the algorithm itself, and the effect of various experimental errors on the computed membrane parameters.

RBCPERM, the program used for these tests, contained the simplest possible cell and solution models but was otherwise identical to the programs actually used for data reduction. The transport equations used in RBCPERM were the Kedem-Katchalsky set, with concentration driving forces, equations 2.27 and 2.28. The cell volume model was the commonly used "osmotic dead volume" approach, roughly equivalent to a linearization of the pseudo-binary model.

In order to establish a well defined reference, subroutines VOLFUN, RKI and MODEL, identical to those in RBCPERM, were linked with a mainline program VOLSIM and used to numerically generate theoretical cell volume histories. (A similar simulation program derived from PERM2, VOLSIM2, was extensively used as an aid in experiment design.) For these program tests, two typical experiments were simulated: one in which cells initially suspended in isotonic

saline are exposed to .65 osmol/Kg NaCl, here denoted "hypertonic shrink", a second labelled "glycerol", in which cells in isotonic saline are immersed in a solution of isotonic saline and .25 M glycerol. The generating parameter values used in these simulations were taken from the literature and were: water permeability  $L_p = 1.230 \times 10^{-11}$  cm<sup>3</sup>/dyne sec; solute permeability  $\omega = 2.140 \times 10^{-16}$  mol/dyne sec; reflection coefficient  $\sigma = .880$ . The simulation routine produced values for non-dimensional cell volume at about a hundred equally spaced discrete times. From these, about thirty-five "data points" were selected at unequal time intervals, as in the actual experimental data recording process. Input to RBCPERM consisted of these data values and the same experimental conditions specified in the simulation.

Program accuracy was tested by using the unaltered simulation results, correct to four significant digits. Given initial parameter guesses within 20% of the final value, as would normally be the case, RBCPERM converged in four or less iterations. When the user supplied guesses were an order of magnitude removed, the program required no more than nine iterations. In all cases the computed parameters were within better than .1% of the parent values.

The experimental error in the volume/voltage relation may lead to errors in the parameters; to simulate a worst case, the computer generated non-dimensional cell volumes were scaled to produce modified  $\hat{V}_c' = 1.20 \hat{V}_c - 0.20$ . Given this erroneous data, RBCPERM returned parameters which differed from the generating values by the percent amounts listed in Table 2.

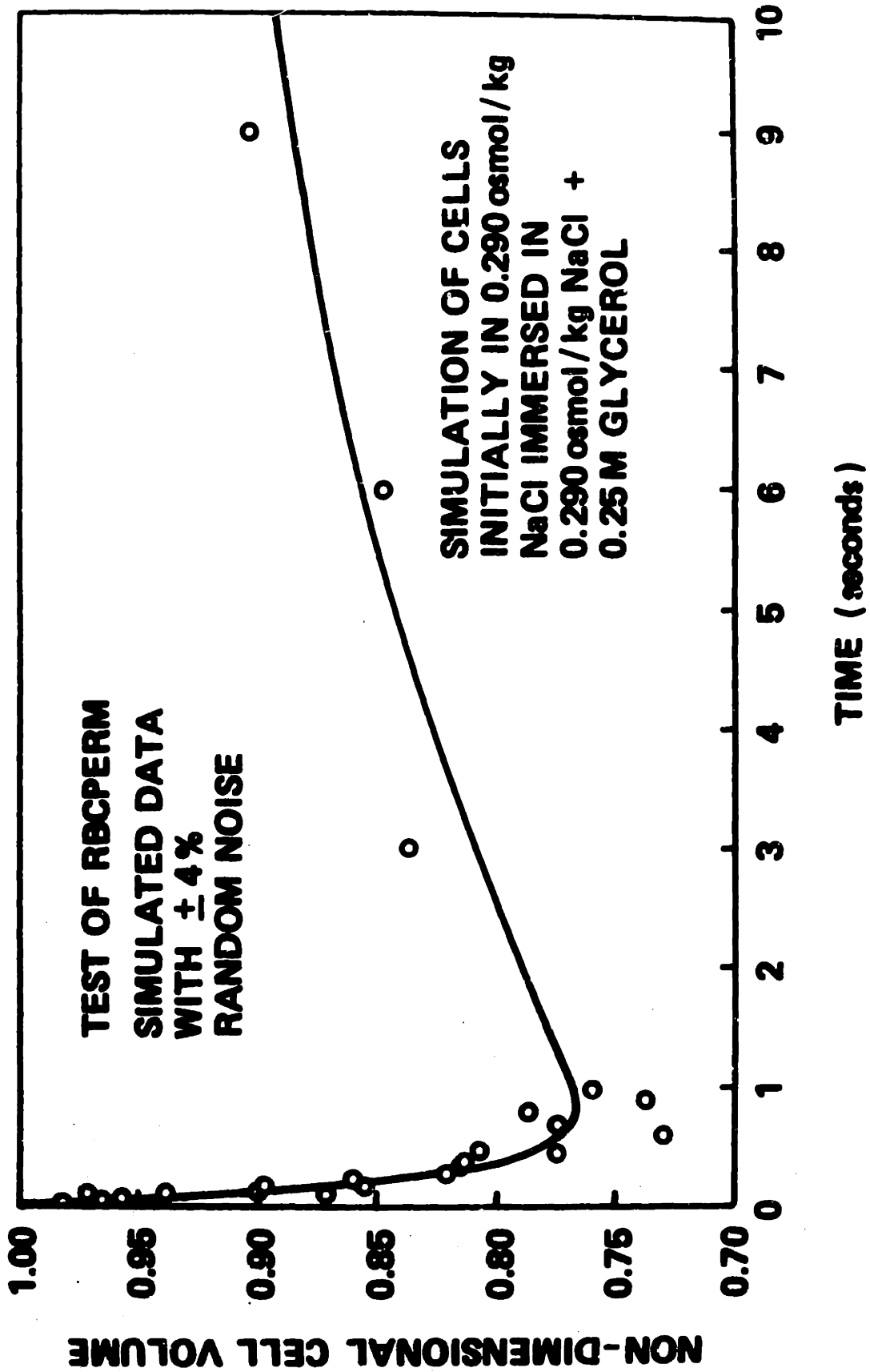


FIGURE 42 Program test - simulated noisy data



TABLE 2

## RESULTS OF DATA REDUCTION PROGRAM TESTS

Test Description	"Experiment"	Percent Error In Parameters		
		$L_p$	$\omega$	$\sigma$
unaltered data	hypertonic shrink glycerol	.00 .00	-.05	.00
20% scaling error	hypertonic shrink glycerol	26.0 -19.2	-11.4	13.6
15 msec dead time error	hypertonic shrink glycerol	11.4 13.9	-5.2	-4.7
<u>±</u> 4% random noise	hypertonic shrink glycerol	.9 9.6	-18.2	-13.3
100 msec optical transient	hypertonic shrink	-4.8		
first 100 msec data deleted	hypertonic shrink	.00		

Errors may also arise because of stop flow dead time. Although it may be measured and raw data times offset to correct for it, an uncertainty of a few msec remains. A worst case was simulated by subtracting 15 msec from the VOLSIM output times and providing RBCPERM with those modified times, but unaltered cell volumes.

Random noise in the photomultiplier signal may arise from several sources: photomultiplier shot noise; amplifier noise and cable pickup; fluctuations in light intensity due to red cell displacements and deformations. Noise was simulated by superimposing random fluctuations of between  $\pm 4\%$  on the theoretical cell volume histories. These fluctuations, which do not obey normal noise distribution statistics, were generated with a table of random numbers. This noisy data and the resulting computer best fit for the "glycerol" experiment are shown in Figure 42.

For the purpose of testing, a representative optical transient was superimposed on the simulation data, with the results shown in Figure 43. It is interesting to note that the theoretical modelling equations are sufficiently constrained that if one completely deletes the distorted first 100 msec no error in parameter computation results.

In conclusion, the computer algorithm itself contributes virtually no error to the data reduction process, and even in the worst case none of the identifiable experimental errors causes unreasonable uncertainty in the computed parameters.

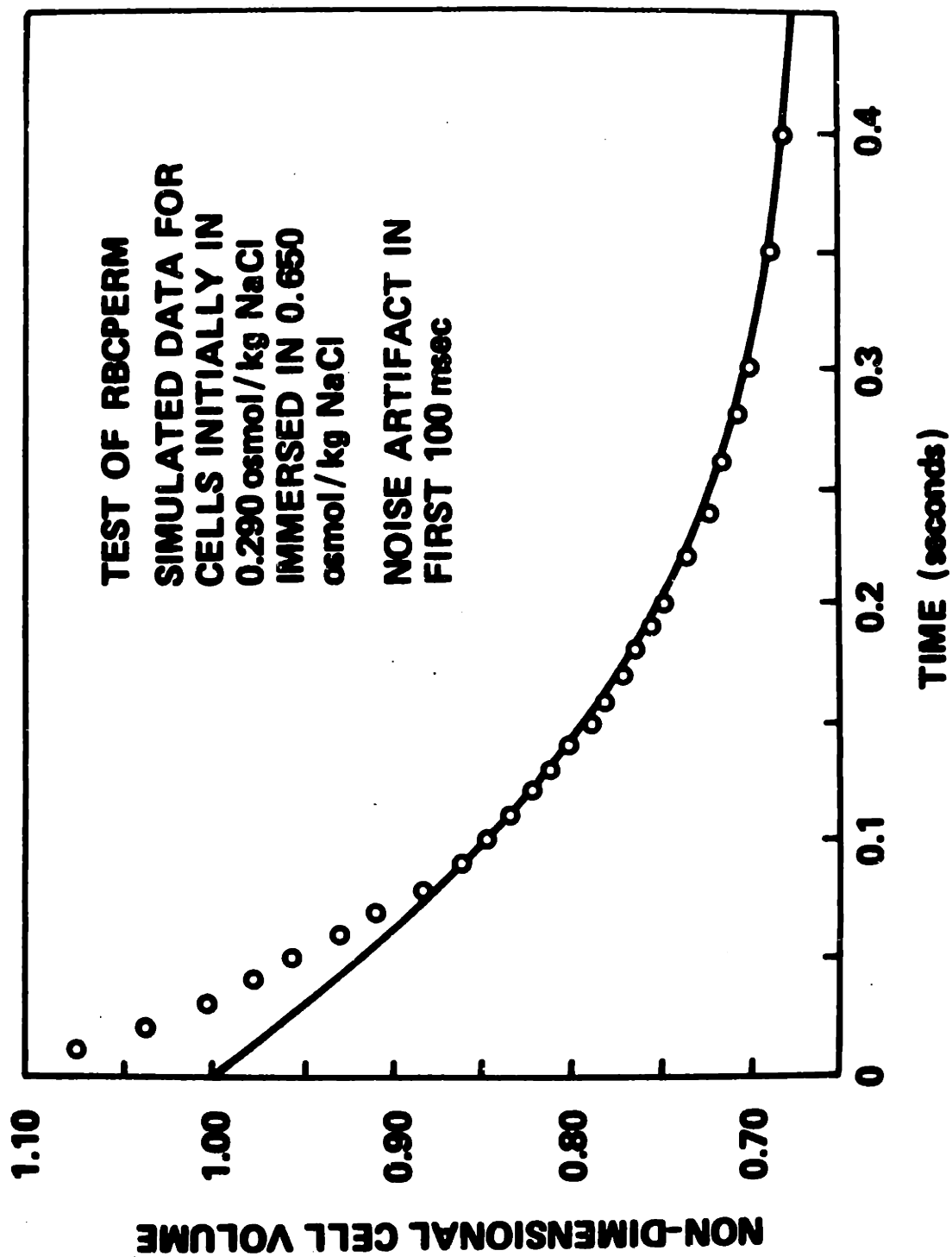


FIGURE 43 Program test - simulated optical transient

**CHAPTER 9**  
**RESULTS AND DISCUSSION**

The original intent of this research was to measure the erythrocyte water permeability as a function of temperature. However, in order to perform the experiments at sub-zero temperatures, it was necessary to add high concentrations of permeable solute anti-freeze to the solutions. It quickly became apparent that the membrane transport parameters depended not only on temperature but also on the composition of the media surrounding the cell. We then proceeded to measure these effects independently, and obtained the variation of membrane permeability with temperature at two different concentration levels, and the variation with solution concentration at constant temperature.

Experiments were performed under a wide variety of concentration conditions, listed in Table 3. In the experiments coded S, cells were exposed only to aqueous sodium chloride solutions; in those coded EG or G the solutions also contained ethylene glycol or glycerol. Solute concentrations in the pre-mix cell suspension, given in the columns labelled "cells initially in", set the initial conditions - water and permeable solute activity and cell volume. The cell suspension was then mixed in the stop flow device with the "added solution" to produce a step change to the "post-mix extracellular" condition. The latter was computed on the basis of equal syringe delivery rates and was corrected for the volume displaced by cells. The total mean concentration  $\bar{C}$  in the last column is the arithmetic average of intracellular and extracellular solution osmolalities (total) at time  $t = 0$ . Since

TABLE 3  
EXPERIMENTAL CONDITIONS - SOLUTION COMPOSITION

Experiment Code	NaCl Concentrations (osmol/Kg)			Permeable Solute Concentrations (molar)			Total Mean Concentration (osmol/Kg) $\bar{C}$
	Cells Initially In	Added Solution	Post-Mix Extracellular	Cells Initially In	Added Solution	Post-Mix Extracellular	
S 1	.265	.600	.440				.350
S 3	.290	1.000	.660				.475
S 4	.290	1.305	.815				.555
S 2	.265	1.405	.855				.560
S 5	.500	1.405	.970				.735
EG 11	.290	.290	.290	.00	.40	.21	.390
EG 2	.290	.290	.290	.20	.40	.30	.540
EG 1	.290	.745	.525	.20	.40	.30	.660
EG 4	.290	.290	.290	.40	.60	.50	.755
EG 3	.290	.900	.605	.40	.60	.50	.915
EG 6	.290	.290	.290	.90	1.10	1.00	1.315
EG 5	.290	1.000	.660	.90	1.10	1.00	1.500
EG 8	.290	.290	.290	1.80	2.20	2.01	2.440
EG 7	.290	1.000	.660	1.80	2.20	2.01	2.625
EG 10	.290	.290	.290	3.50	4.50	4.02	5.390
EG 9	.290	.995	.655	3.50	4.50	4.02	5.575
G 3	.290	.290	.290	.00	.50	.26	.415
G 2	.290	.290	.290	.20	.40	.30	.540
G 1	.290	.745	.525	.20	.40	.30	.660

osmolality is proportional to  $\ln a_w$ ,  $\bar{C}$  represents a characteristic water activity for the experiment. Although the experimental types are here arranged within each group in order of ascending  $\bar{C}$  they were not performed in any set order. Repeats of a given experiment were usually separated by days, or even months. Experiments at different temperatures were also performed at random.

The variation of water permeability  $L_p$  with temperature was measured between 25°C and 0°C in a series of S 3 experiments (the upper line in Figure 44) and from 25°C to -10°C under EG 9 conditions (the lower line). Each data point represents a mean of two to seven experiments, performed on different days with different bloods. Also, remember that each "experiment" is actually a microprocessor average of two to ten repeat stop flow runs. Both sets of data were fit with an Arrhenius expression

$$L_p = L_{p_0} e^{-\frac{E_a}{R} \left( \frac{1}{T} - \frac{1}{T_0} \right)}$$

where the reference state is at  $T_0 = 25^\circ\text{C}$ . The apparent activation energy  $E_a$  increases slightly, from 3.38 to 4.74 Kcal/mol as  $\bar{C}$  is increased, but this is within experimental uncertainty. To a first approximation then, the effects of temperature and concentration are uncoupled.

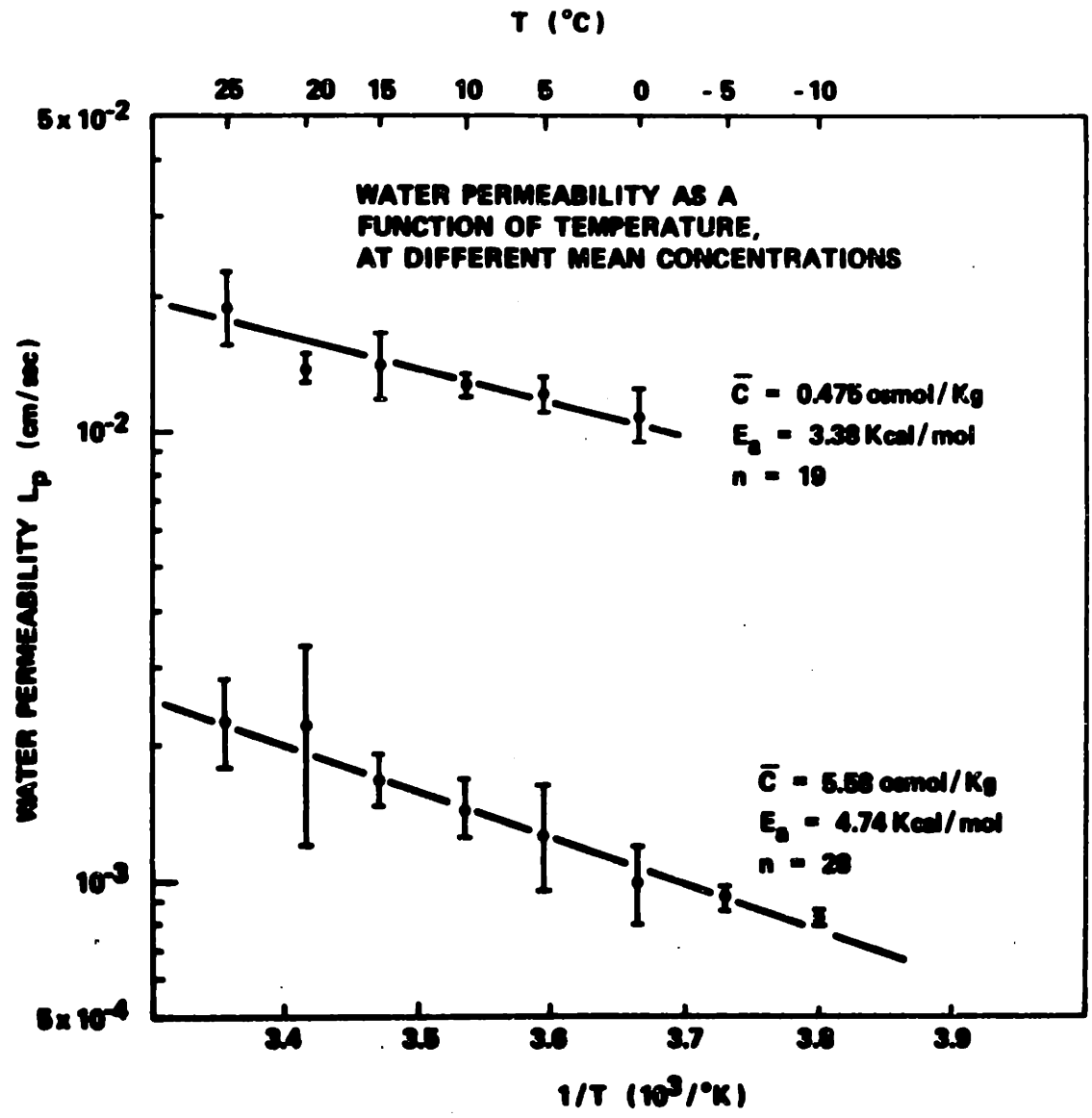


**FIGURE 44** Water permeability  $L_p$  as a function of temperature, for mean concentrations .475 Osm (S 3 conditions) and 5.58 Osm (EG 9 conditions)



Viera et al [9] measured  $L_p$  for cells in saline solutions of unspecified concentration, in the temperature range  $37^\circ$  to  $7^\circ$ , and computed an activation energy of 3.3 Kcal/mol. Their data were presented in terms of  $L_p$  ( $\text{cm}^3/\text{dyne sec}$ ), and from equation 5.24 we find that in order to compare their results with ours their  $E_a$  must be corrected by an amount  $R \frac{\ln(T/T_0)}{1/T - 1/T_0}$ . In the temperature range  $40^\circ$  to  $-20^\circ\text{C}$  this term is essentially constant and equal to about .6 Kcal/mol. Thus corrected, their value becomes  $E_a = 3.9$  Kcal/mol, in good agreement with our results.

Comparisons between the activation energy for water permeability and, for instance, water viscosity, should utilize an  $E_a$  derived from  $L_p$  data in the base units cm/sec rather than in the derived units  $\text{cm}^3/\text{dyne sec}$ . Also notice that the membrane diffusivity will be given by  $D_m$  ( $\text{cm}^2/\text{sec}$ )  $\sim L_p$  (cm/sec)  $\times 100 \times 10^{-8}$  cm.

The ethylene glycol permeability  $\omega$  as a function of temperature under EG 9 experimental conditions was also obtained and is shown in Figure 45. At  $0^\circ\text{C}$  and below, ethylene glycol transport is so slow that it can not reliably be measured. The reflection coefficient  $\sigma$  does not vary significantly with temperature, as shown in Table 5. As one would expect, the temperature dependence of each linear parameter  $L_{11}$ ,  $L_{12}$  or  $L_{22}$  is equal to that of the corresponding K-K parameter  $L_p$ ,  $\sigma$  or  $\omega$ .

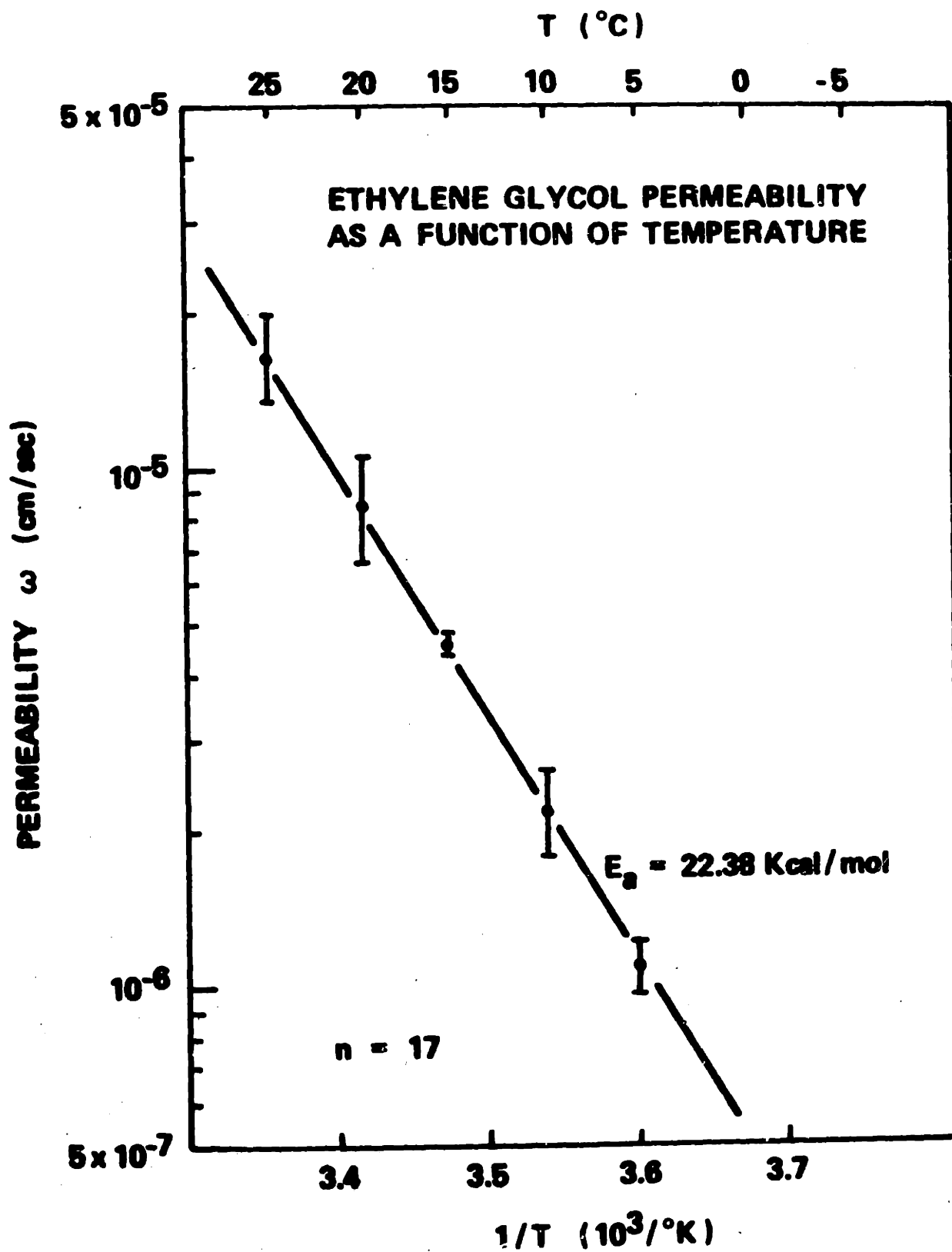


**FIGURE 45** Ethylene glycol permeability  $\omega$  as a function of temperature, under EG 9 conditions (see Table 3 for details of experimental conditions)

The effect of concentration  $\bar{C}$  on the water permeability  $L_p$ , at 25°C, is shown in Figures 46 and 47. (There is no theoretical reason for the logarithmic and inverse transforms in Figure 47 - they are used only for purposes of scale expansion.) The experimental conditions for each data point may be obtained from Table 3 by noting that within each group experiments are listed in order of ascending  $\bar{C}$ , or decreasing  $1/\bar{C}$ . Again, each point represents the mean of two to seven experiments and the error bars indicate  $\pm$  one standard deviation. The trend line in Figure 47 is not a least squares fit but is the function which, in our opinion, best represents the data, taking into account the various experimental and theoretical uncertainties. The equation of this line is

$$L_p(\bar{C}, 25^\circ\text{C}) = 1.75 \times 10^{-3} e^{1.137(1/\bar{C})}$$

where  $\bar{C}$  is in osmol/Kg and  $L_p$  is cm/sec. There is no theoretical basis for this correlation, which is presented here only for use in future cell freezing simulations. The experimental results are also presented in Tables 6 and 7, both in terms of the conventional Kedem-Katchalsky parameters and the linear set. In certain cases, indicated by a "?" in the table entry, experiment to experiment variations were so great as to make an average value meaningless. Also note there are no S type entries in Table 7, since in the absence of permeable solute  $L_{11}$  is identically equal to  $L_p$ .

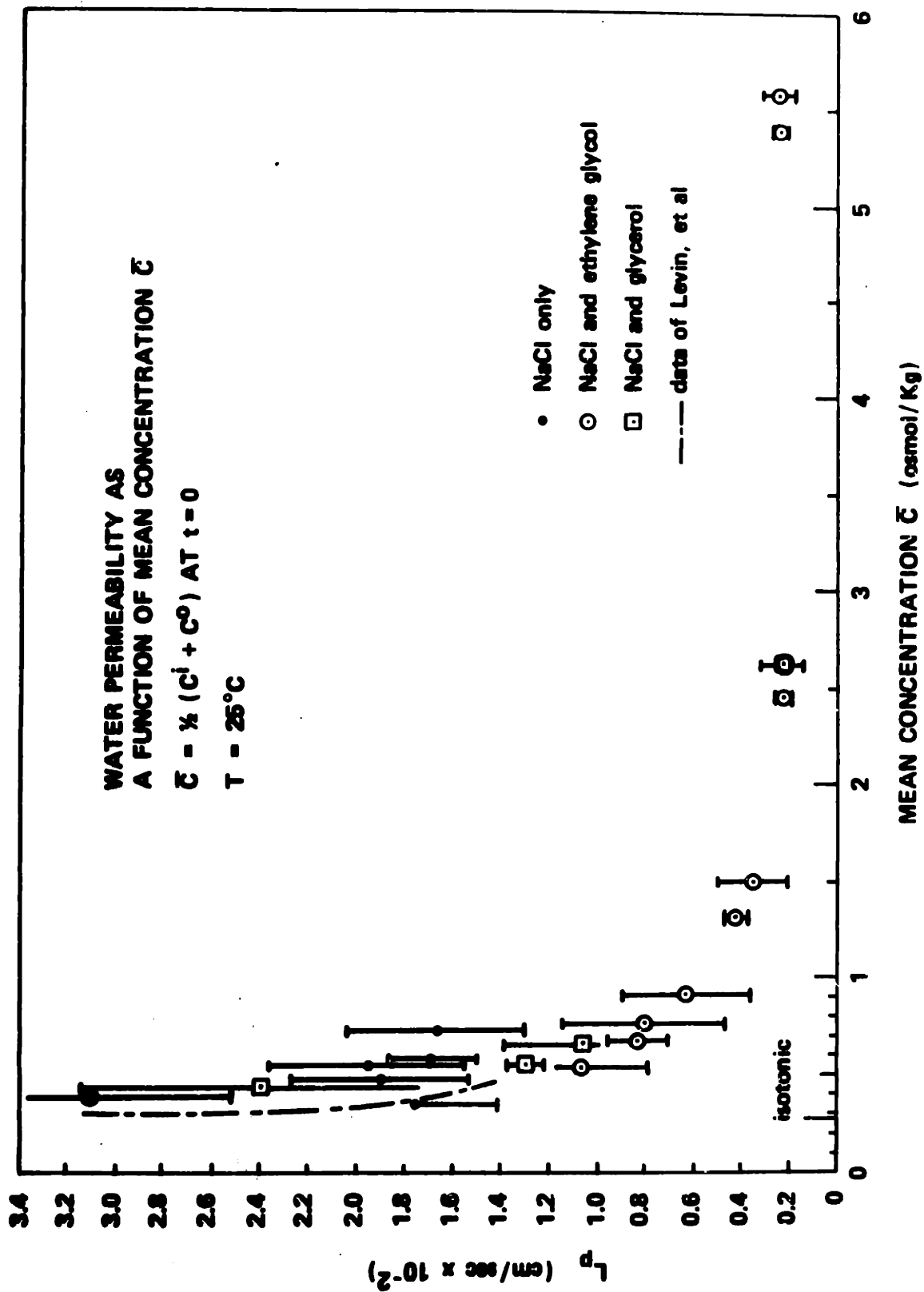
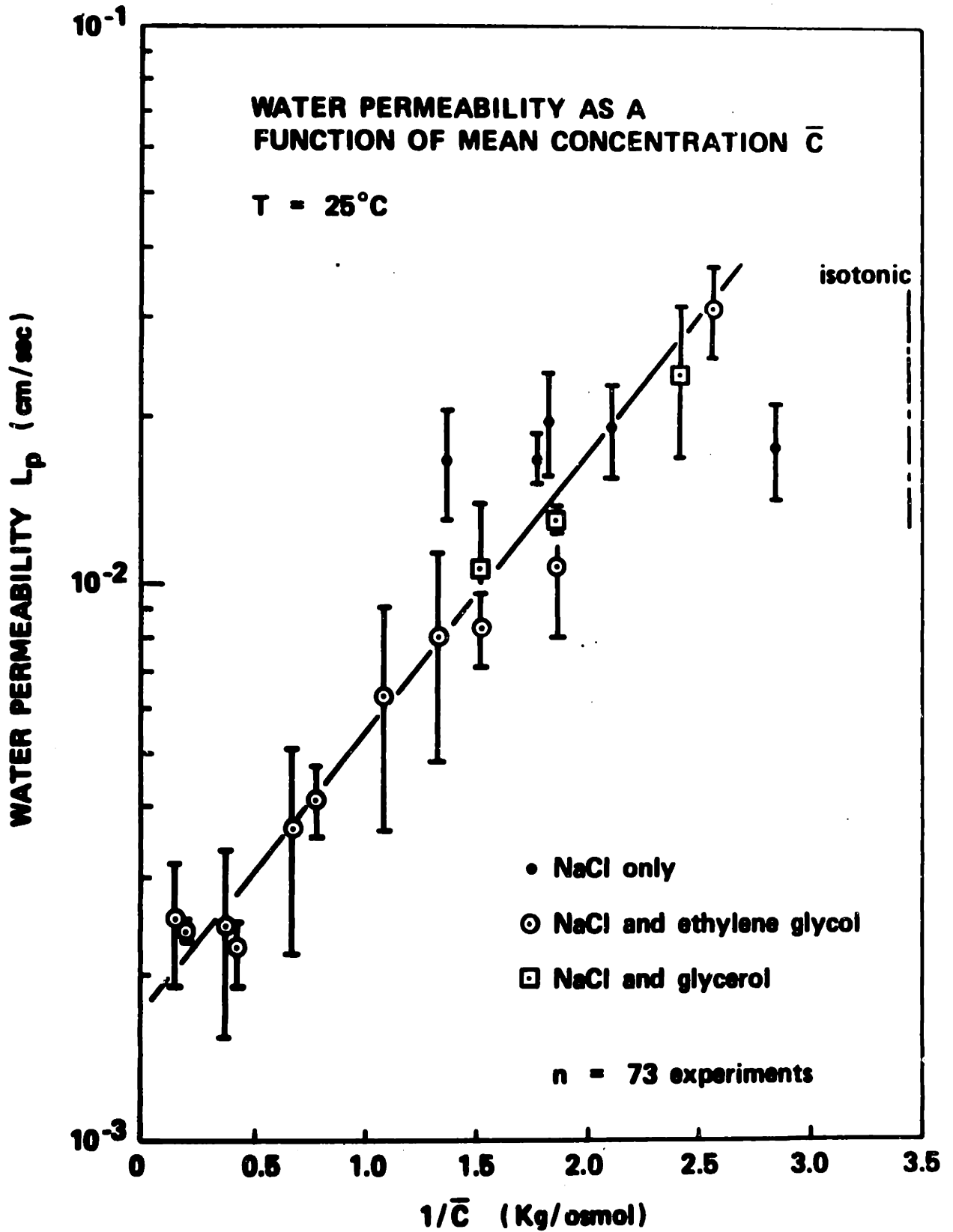


FIGURE 46 Water permeability as a function of mean concentration  $\bar{C}$  at  $25^\circ\text{C}$



**FIGURE 47** Water permeability as a function of mean concentration at 25°C, expanded scale

Previously published values for the water permeability  $L_p$  at ambient temperature and in dilute, but usually unspecified, saline solutions range from  $1.2 \times 10^{-2}$  to  $1.7 \times 10^{-2}$  cm/sec. Now, regardless of the details of the model, all permeability measurements are derived from expressions of the form

$$(V_c)_{iso} \frac{d\hat{V}_c}{dt} \sim L_p A_c \Delta C$$

Thus, in order to properly compare values of  $L_p$  from different sources, it is essential to know what values of isotonic cell volume  $(V_c)_{iso}$  and surface area  $A_c$  were used in the computation. If we recompute the data of Sha'afi [17] and Viera [9] to account for differences in cell physical parameter values, we find that their values for water permeabilities become  $1.70 \times 10^{-2}$  and  $2.13 \times 10^{-2}$  cm/sec, comparable to our results for S type experiments.

As can be seen by comparing the data in Tables 6 and 7, the measured variation in water permeability is independent of the transport model employed. A minor point here is that while the transport models assume constant parameters, the permeability is a function of extra-membrane conditions. The change in  $\bar{C}$  during a given experiment is small, however, and the use of constant parameter models is not unreasonable.

Based on the analysis of section 2.2 and Appendix A we may reject the possibility that the apparent shift in water permeability is due to concentration polarization. In fact, as permeable solute concentration is increased, the intracellular volume diffusivity  $D^V$  increases. Extra-

cellular diffusivities are an order of magnitude greater, so diffusion in the extracellular solution is certainly not the rate limiting step.

Some authors have suggested that cell volume is a determinant of permeability. With the exception of experiments S 1, S 2, and S 5, our initial cell volumes only vary from isotonic to 1.1 x isotonic, and final cell volumes do not correlate with the observed shift in  $L_p$ .

We have also been careful to design these experiments such that the maximum water flux does not change significantly from experiment to experiment. With the exception of S 4, the computed water fluxes at time  $t = 0$  lie between  $1.8 \times 10^{-6}$  and  $6.6 \times 10^{-6}$  mol/cm<sup>2</sup>-sec and do not correlate with changes in permeability.

In all of these experiments, the initial rapid water flux is outward and the cells initially shrink. We are therefore not concerned with the still unresolved question of membrane directional properties.

Is the average osmolality  $\bar{C}$  a reasonable choice of independent variable? Some researchers feel that only the extracellular concentration affects the water permeability. However, this necessarily implies a microscopic model in which the outer membrane surface is the rate limiting barrier, so we have chosen not to use this approach. The experiments themselves do not provide the information needed to choose between extracellular or mean concentration as the significant variable.

A far more important question is whether the water permeability is a function only of solution osmolality (i.e. water activity) or whether there are additional species specific effects. First, there does

not seem to be any difference in the effects of the two similar organic solutes, ethylene glycol and glycerol. Comparison between the experiments involving permeable solutes and those in saline only is somewhat ambiguous, however. Three of the data points, experiments S 3, S 4, and S 2 are consistent with the trend of the permeable solute experiments, while all of the saline-only experiments taken together exhibit essentially no concentration dependence. Levin et al [64] measured  $L_p$  in a series of experiments in which cells initially suspended in isotonic saline were exposed to various hypertonic NaCl solutions. Those results, shown in Figure 46, agree well with our data for the permeable solute experiments. There is further evidence that  $L_p$  depends only on the water activity. In three paired sets of experimental conditions - EG 2 and EG 1, EG 4 and EG 3, and EG 6 and EG 5 - the ethylene glycol concentration is the same in each member of the pair but the salt concentration is significantly higher in the second experiment. In each case, the experiment with higher NaCl concentration shows a substantially reduced  $L_p$ . To a first approximation, then, it appears that the water permeability is primarily a function of the water activity of the surrounding media, and further experimental work will be necessary to explore the question of solute specific effects.



The marked concentration dependence of water transport has several important implications for cryobiology. First, any modelling of freezing protocols must take this effect into account - at  $-10^{\circ}\text{C}$  one would predict only a twofold decrease in  $L_p$  based on the measured temperature dependence, whereas the solution equilibrium concentration of  $5.6 \text{ osmol/Kg}$  would cause more than a tenfold reduction in water permeability. These results also suggest that the cryoprotection afforded by solutes such as glycerol may be due in part to a decrease in water conductivity and thus a lessening of damage caused by cell dehydration.

Data for ethylene glycol and glycerol transport parameters were also obtained from our experiments and are presented in Tables 6 and 7. Naccache [65] measured ethylene glycol and glycerol permeability in solutions containing  $.3 \text{ M}$  solute, corresponding to our EG 2 and G 2 conditions. His values of  $\omega$ , not corrected for cell volume and area, are  $3.38 \times 10^{-5} \text{ cm/sec}$  for ethylene glycol and  $.58 \times 10^{-5} \text{ cm/sec}$  for glycerol, in excellent agreement with our results.

Using a somewhat different experimental technique, Goldstein and Solomon [27] obtained values of  $.63$  and  $.88$  for the reflection coefficients  $\sigma$  of ethylene glycol and glycerol. Given the scatter in our data, any comparison would be meaningless. Accurate measurements of the coupling coefficients  $\sigma$  or  $L_{12}$  are difficult because cell volume time histories are relatively insensitive to the magnitude of

these parameters. Fortunately, this also means that we need not be overly concerned with the value of  $\sigma$  or  $L_{12}$  used in cell freezing simulations. We should also note that many experiments could not be fit adequately with the Kedem-Katchalsky equations, while excellent fits were obtained with the linear transport model. This is a direct consequence of the restricted range of  $\sigma$ ,  $0 \rightarrow 1$ , which is intuitively correct but does not follow from the thermodynamic constraints, equations 2.8.

It is the author's conviction that future research in red cell membrane transport must address two difficult questions. First, the stop flow optical transients must be fully characterized. Until the signals produced by cell deformations or orientation changes can be properly uncoupled from signals caused by cell volume changes, we can only assume that we are measuring volume time histories. Alternatively, we must develop new experimental methodologies which do not involve cell motion. (Fortunately, the equilibrium models for chemical potential driving forces and cell volume work very well.)

Second, we must ask ourselves whether the observed variations in the solute permeability parameters represent real changes in membrane state from which we may deduce the physics of transport, or whether they are only an apparent result of untenable models which require increasingly complex corrections to accommodate the data.

TABLE 4

$L_p$  TEMPERATURE DEPENDENCE AT  $\bar{C} = .475$  osmol/Kg (S 3 CONDITIONS)

T(°C)	$L_p$ (cm/sec x $10^{-2}$ )		n
	Mean	$\pm$ SD	
25	1.910	.372	7
20	1.388	.093	3
15	1.424	.249	2
10	1.268	.059	2
5	1.215	.098	3
0	1.096	.143	2

$$L_p = L_{p_0} e^{-\frac{E_a}{R} \left( \frac{1}{T} - \frac{1}{T_0} \right)}$$

$$L_{p_0} = 1.77 \times 10^{-2} \text{ cm/sec} \quad (T_0 = 25^\circ\text{C})$$

$$E_a = 3.38 \text{ Kcal/mol}$$

TABLE 5  
 PERMEABILITY TEMPERATURE DEPENDENCE AT  
 $\bar{C} = 5.58 \text{ osmol/Kg}$  (EG 9 CONDITIONS)

T(°C)	$(L_p \text{ (cm/sec} \times 10^{-2}))$		$\omega \text{ (cm/sec} \times 10^{-5})$		$\sigma$		n
	Mean	$\pm$ SD	Mean	$\pm$ SD	Mean	$\pm$ SD	
25	.251	.067	1.621	.291	.785	.059	5
20	.227	.103	.859	.206	.788	.125	5
15	.170	.022	.457	.024	.776	.006	2
10	.148	.022	.218	.041	.752	.046	4
5	.128	.033	.109	.013	.743	.074	3
0	.100	.021	.084	.026	.776	.047	3
-5	.092	.005	?		?		4
-10	.084	.002	?		?		2

water permeability

$$L_{p_0} = .224 \times 10^{-2} \text{ cm/sec}$$

$$E_a = 4.74 \text{ Kcal/mol}$$

ethylene glycol permeability

$$\omega_0 = 1.622 \times 10^{-5} \text{ cm/sec}$$

$$E_a = 22.38 \text{ Kcal/mol}$$

( $T_0 = 25^\circ\text{C}$ )

TABLE 6

KEDEM-KATCHALSKY MEMBRANE PARAMETERS AS A  
FUNCTION OF CONCENTRATION AT 25°C

Experiment Code	Water Permeability $L_p$ (cm/sec x $10^{-2}$ )		Solute Permeability $\omega$ (cm/sec x $10^{-5}$ )		Reflection Coefficient $\sigma$		n
	Mean	$\pm$ SD	Mean	$\pm$ SD	Mean	$\pm$ SD	
S 1	1.759	.350					6
S 3	1.910	.372					7
S 4	1.958	.412					4
S 2	1.688	.182					3
S 5	1.673	.374					4
EG 11	3.105	.592	8.41	2.20	.489	.035	4
EG 2	1.074	.285	6.33	.86	.400	.054	2
EG 1	.835	.128	?		?		3
EG 4	.809	.337	4.57	1.10	.466	.127	5
EG 3	.631	.274	3.85	2.24	.969	.059	5
EG 6	.427	.050	4.20	1.27	.809	.069	3
EG 5	.363	.146	6.07	.55	.925	.089	5
EG 8	.226	.030	3.90	.55	.914	.045	2
EG 7	.244	.091	2.61	.62	.990	.019	4
EG 10	.245	.002	1.81	.10	.762	.033	2
EG 9	.251	.067	1.62	.29	.785	.059	5
G 3	2.398	.740	.661	.140	.841	.147	4
G 2	1.299	.078	.564	.118	.522	.048	2
G 1	1.063	.330	?		?		3

TABLE 7

LINEAR MEMBRANE PARAMETERS AS A FUNCTION OF CONCENTRATION AT 25°C

Experiment Code	Water Permeability $L_{11}$ (cm/sec $\times 10^{-2}$ )		Solute Permeability $L_{22}$ (cm/sec $\times 10^{-7}$ )		Coupling Coefficient $L_{12}$ (cm/sec $\times 10^{-5}$ )	
	Mean	$\pm$ SD	Mean	$\pm$ SD	Mean	$\pm$ SD
EG 11	2.851	.533	3.45	.85	2.95	.62
EG 2	.873	.068	4.39	.86	1.62	.73
EG 1	.772	.052	1.70	.63	-2.05	.63
EG 4	.745	.285	5.28	1.01	2.25	.71
EG 3	.639	.255	3.11	1.36	?	
EG 6	.410	.114	7.27	.29	?	
EG 5	.358	.138	11.74	1.85	?	
EG 8	.229	.030	14.08	1.65	?	
EG 7	.254	.084	12.45	2.36	-1.47	.43
EG 10	.285	.059	19.52	3.10	4.81	1.61
EG 9	.229	.091	18.10	5.48	4.92	1.70
G 3	2.040	.788	.413	.206	?	
G 2	?		1.427	.194	-1.308	.168
G 1	1.065	.292	1.200	.002	-1.003	.262

APPENDICES

## APPENDIX A

## MUTUAL DIFFUSION COEFFICIENT OF A PSEUDO-BINARY SOLUTION

In Chapter 2, we defined the dimensionless group  $\alpha$  as the ratio of bulk flow to diffusion flow,

$$\alpha = \frac{J_{W,W}^U \ell_c}{D^V}$$

The mutual diffusion coefficient  $D^V$  of a non-dilute solution may be computed from the diffusion coefficient of dilute solute in water  $D_{s/w}$  and the self diffusion coefficient of water  $D_{w/w}$  as follows [21]

$$D^V = \frac{\partial \ln a_s}{\partial \ln x_s} \frac{\eta_w}{\eta} [x_w D_{s/w} + x_s D_{w/w}] \quad (\text{A.1})$$

where  $\eta/\eta_w$  is the solution viscosity relative to water. In a dilute solution  $\frac{\partial \ln a_s}{\partial \ln x_s} \rightarrow 1$ ,  $\frac{\eta_w}{\eta} \rightarrow 1$ ,  $x_w \rightarrow 1$ ,  $x_s \rightarrow 0$  and the volume diffusivity simply equals the solute diffusivity  $D_{s/w}$ .

Now consider the following situation: a cell in isotonic saline is pre-loaded with 4 M ethylene glycol and then a water flux is induced by a step change in extracellular concentrations. If we examine only short time events, glycol does not cross the membrane and the counter diffusing species may be taken to be water and a composite solute  $s$  composed of all the cell proteins and salts (the pseudo-binary solute pb of Chapter 4) and ethylene glycol sp. As suggested by Levin [4] we form the total solute diffusivity  $D_{s/w}$  as a volume weighted average given by



$$\frac{\theta_s}{D_{s/w}} = \frac{\theta_{pb}}{D_{pb/w}} + \frac{\theta_{sp}}{D_{sp/w}} \quad (\text{A.2})$$

The volume fraction  $\theta_i$  is here defined in terms of mol fraction  $x_i$ , partial molar volume  $v_i$ , and total concentration  $C = \frac{1}{\sum v_i x_i}$  as

$$\theta_i = x_i v_i C \quad (\text{A.3})$$

Since we are considering a diffusion process, the independent entities are taken to be the hydrated pseudo-solute, the permeable solute, and the cell's free (unbound) water. For this case of a cell in equilibrium with isotonic saline and 4 M ethylene glycol, the mole fractions of free water, pseudo-solute and permeable solute are

$$x_w^f = .896$$

$$x_{pb}^h = 5.79 \times 10^{-3}$$

$$x_{sp}^h = 9.87 \times 10^{-2}$$

where we use superscript h to emphasize that these are hydrated properties. The volume fractions are then

$$\theta_w^f = .535$$

$$\theta_{pb}^h = .327$$

$$\theta_{sp}^h = .139$$

where we have used  $v_{sp} = 42.3$ , from section 4.2.

Using a similar procedure, Levin used data for hemoglobin and KCl diffusivities to compute the pseudo-solute diffusion coefficient  $D_{pb/w} = 7.00 \times 10^{-7} \text{ cm}^2/\text{sec}$ . In the absence of exact data for ethylene glycol, we use a value typical for most non-electrolyte solutes  $D_{sp/w} = 7.0 \times 10^{-6} \text{ cm}^2/\text{sec}$ . From equation A.2 the total solute diffusivity is then  $D_{s/w} = 9.57 \times 10^{-7} \text{ cm}^2/\text{sec}$ . We neglect solution non-ideality and set  $\gamma_s = 1$ , therefore  $\frac{\partial \ln a_s}{\partial \ln x_s} = 1$ . A value for the viscosity ratio may be obtained either from data for aqueous ethylene glycol solutions, or a correlation between intracellular solute volume fraction and solution viscosity [4], and in either case we find  $\eta_w/\eta \approx 0.5$ . With the above data, equation A.1 now provides a value for the mutual diffusion coefficient  $D^V = 1.9 \times 10^{-6} \text{ cm}^2/\text{sec}$ . In comparison, the computed value for the intracellular solution without glycol is  $2.6 \times 10^{-7} \text{ cm}^2/\text{sec}$ . Notice that, contrary to intuition, the addition of ethylene glycol has increased the diffusivity. This is because we are examining a volume exchange process, in which the diffusion of water in one direction must be balanced by diffusion of an equal volume of solute in the other direction. As we add a solute such as ethylene glycol which diffuses more readily than the intracellular proteins, the overall diffusion process becomes more rapid. The real situation is much more complicated, of course, and the solutes will separate as they move at different rates through the solution, but for our purposes this binary model with an effective overall diffusion coefficient is adequate.

APPENDIX B  
COUPLED HEAT AND MASS TRANSFER

The phenomenological equations for coupled flows of heat  $q$  and mass  $w$  across an ideal semi-permeable membrane are given by Katchalsky and Curran [12]

$$J_w = L_{ww} \Delta\mu_w + L_{wq} \Delta T \quad (\text{B.1})$$

$$J_q = L_{wq} T \Delta\mu_w + L_{qq} T \Delta T + J_w \Delta\mu_w \quad (\text{B.2})$$

The explicit dependence on temperature and the additional term  $J_w \Delta\mu_w$  in equation B.2 arise because the dissipation function is originally written for an entropy flux. It is highly unlikely that the heat-mass coupling will ever be measured in the red cell membrane, but it is still possible to make estimates of the magnitude of the effect.

We have available to us values of the water permeability coefficient  $L_{ww}$  in the (assumed) absence of heat flow and we can estimate the membrane thermal conduction coefficient  $L_{qq}$ . We may also compute the water flux  $J_w$  and driving force  $\Delta\mu_w$  for a typical experiment. The permeability coefficient is

$$L_{ww} = \frac{L_p}{v_w RT} = 4.5 \times 10^{-7} \text{ mol}^2/\text{joule cm}^2 \text{ sec} \quad (\text{B.3})$$

when  $L_p$  has the nominal value  $2.0 \times 10^{-2}$  cm/sec and  $T = 25^\circ\text{C}$ . The

thermal coefficient is taken to be a function of the membrane thermal conductivity  $K_m$  and thickness  $\ell_m$

$$L_{qq} = \frac{K_m}{T \ell_m} \quad (\text{B.4})$$

The red cell membrane is essentially a liquid phase composed chiefly of lipids, so we assign a value of  $K_m = 2.0 \times 10^{-4}$  joule/cm sec °K, typical of an organic liquid, and  $L_{qq} = 6.4 \times 10^{-1}$  joule/cm<sup>2</sup> sec °K<sup>2</sup>. The maximum value of the coupling coefficient  $L_{wq}$  is constrained by the second law of thermodynamics

$$L_{wq} \leq \sqrt{L_{ww} L_{qq}} \quad (\text{B.5})$$

$$\leq 5.4 \times 10^{-4} \text{ mol/cm}^2 \text{ sec } ^\circ\text{K}$$

In the chosen experiment, cells initially in .26 osmol/Kg NaCl are suddenly exposed to .44 osmol/Kg NaCl solution. Immediately after the step change in concentration, the driving force is  $\Delta\mu_w = 7.81$  joule/mol and the computed flux is  $J_w = 3.8 \times 10^{-6}$  mol/cm<sup>2</sup> sec.

Rather than solve the coupled rate equations for cell water content and temperature, let us make some qualitative arguments about short time events. In the imagined experiment, the cell is initially in thermal and chemical equilibrium with its environment. The extracellular water chemical potential is then suddenly changed and the driving force  $\Delta\mu_w$  induces both a mass flow  $J_w$  and a heat flux  $J_q$ . In that first instant before the cell temperature changes, the magnitude of

$J_q$  is 1.26 joule/cm<sup>2</sup> sec. If there were no conduction across the membrane, this heat flux would cause a rapid change in cell temperature; however, the thermal conductivity of the membrane is extremely high and the temperature change never appears. Even for a  $\Delta T$  of only .01 °K, the conduction heat flow  $L_{qq} \Delta T$  exceeds our maximum estimate of induced flux  $L_{wq} T \Delta \mu_w + J_w \Delta \mu_w$ . Thus, the maximum expected change in cell temperature is .01°K.

## APPENDIX C

## THE VAN LAAR COMPUTATIONAL SCHEME

1. Vary the cell water content through the range in which solution data exists, and for a given value of water content  $n_w$  compute

a) Pseudo-solute molality

$$m_{pb} = \frac{n_{pb}}{n_w} \times \frac{1000 \text{ gm/Kg}}{18.015 \text{ gm/mol}}$$

b) Pseudo-solute hydrated mole function (The independent species in the solution are the hydrated pseudo-solute and the free water.)

$$x_{pb}^h = \frac{n_{pb}}{n_{pb} + n_w^f} = \frac{n_{pb}}{n_{pb}(1 - h_{pb}) + n_w}$$

where  $h_{pb}$  is the pseudo-solute hydration number.

c) The free water mole fraction

$$x_w^f = 1 - x_{pb}^h$$

d) Water activity, using the previously derived curve fit for osmotic coefficient  $\phi_{pb}(m_{pb})$  and the expression

$$\ln a_w^f = \ln a_w = \frac{-18.015}{1000} \phi_{pb} m_{pb}$$

e) Water activity coefficient

$$\ln \gamma_w^f = \ln a_w^f - \ln x_w^f$$

- 2) Plot  $[\ln \gamma_w^f]^{1/2}$  as a function of  $\frac{x_w^f}{x_{pb}^f}$  and find the least squares best fit line.
- 3) Use this best fit line to extrapolate to more concentrated solutions and back calculate to obtain  $\phi_{pb}(m_{pb})$  in the regimes where data is not available (dotted line in Figure C1).

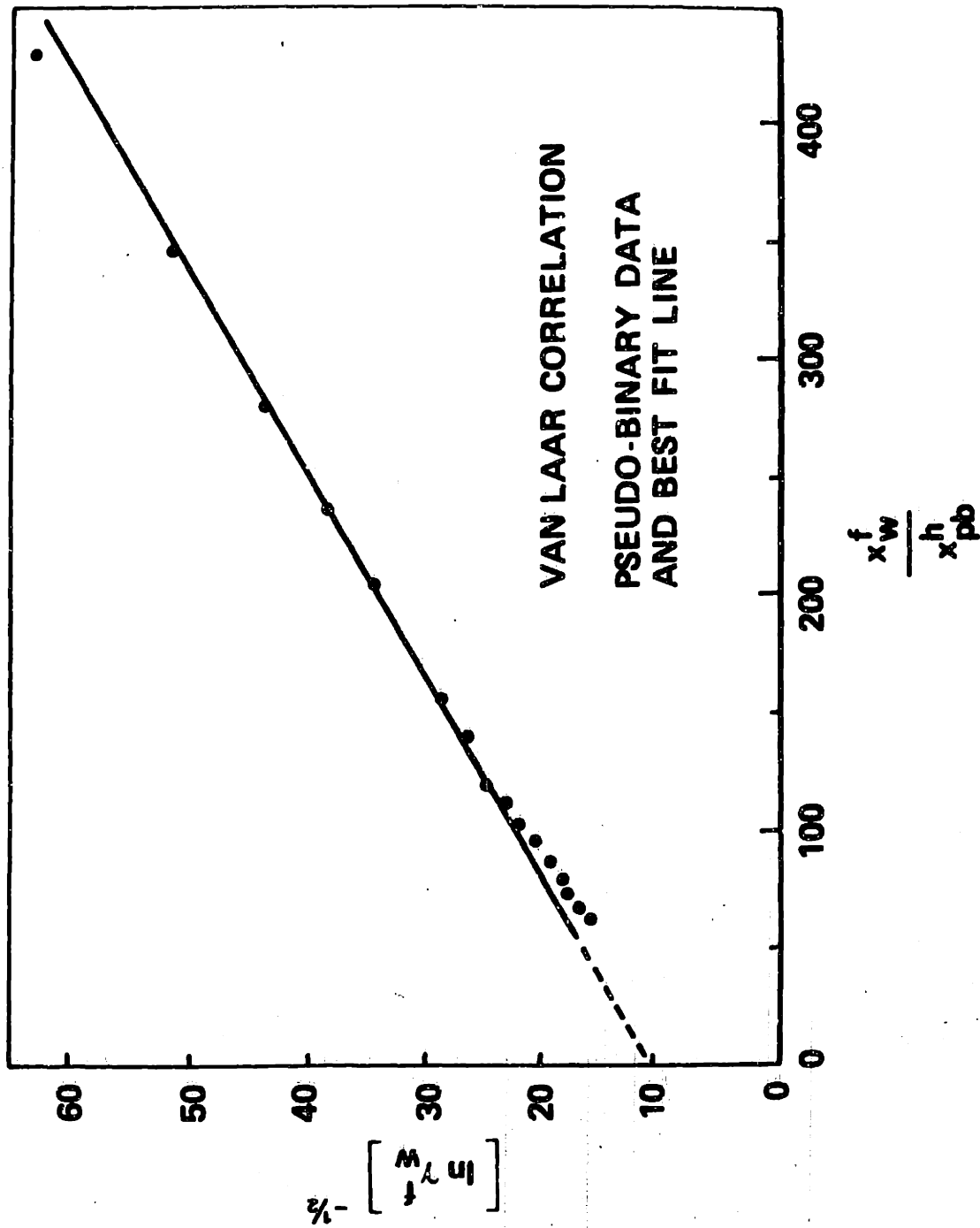


FIGURE C1 Pseudo-binary data and van Laar correlation best fit line



APPENDIX D  
PERM2 PROGRAM LISTING

The data reduction program PERM2 occupies 22K bytes and is written in ANS FORTRAN, with the exception of the plotting routines, which are local to the MIT Mechanical/Civil Engineering Computer Facility.

An explanation of the input coding follows the program listing.

If the permeable solute is other than ethylene glycol the user must supply the proper curve fits in subprograms FIT1 through FIT4.



```

5      CC=CSP0
      GO TO 16
10     CC=CSP1
C      IF NO PERMEABLE SOLUTE, USE WATER CONCENTRATION
16     IF(CSP1 .LT. 1.E-10 .AND. CSP2 .LT. 1.E-10) CC=55.5093
C      VSP IS THE SOLUTE PARTIAL MOLAR VOLUME (CUBIC CM/MOL)
C      VFC IS THE CHARACTERISTIC VOLUME FRACTION.
      VFC=CC*.001*VSP

C
C      L1 IS THE WATER PERMEABILITY (CUBIC CM/DYNE-SEC)
C      W (OMEGA) IS THE SOLUTE PERMEABILITY (MOL/DYNE-SEC)
C      SIG (SIGMA) IS THE SOLUTE REFLECTION COEFFICIENT
      A(1)=L1*RT
      A(2)=W*RT
      A(3)=SIG

C
C      COMPUTE INITIAL CONDITIONS AND FILL IN MISSING DATA POINT
C      FREE WATER (NON-DIMENSIONAL)
      NWFN=(.3590/FIT5(CSI1)) - .1997
      IF (CSI1 .GT. 0.289 .AND. CSI1 .LT. 0.291) NWFN=1.000
C      PERMEABLE SOLUTE (NON-DIMENSIONAL)
      NSPN=(NWFN + .1997)*FIT1(CSP1)/CC
      V(1)=VOLFUN(1,A)
      T(1)=0.0

C
C
C      FILL TIME VECTOR, INCLUDING STOP FLOW DEAD TIME CORRECTION
      NPTS=NDATA+1
      DO 20 I=2,NPTS
      T(I)=TIME(I-1) + TDEAD
C      NON-DIMENSIONAL CELL VOLUME DATA
      V(I)=VIN(I-1)
20    CONTINUE

C
C      SET CURFIT NUMERICAL PARAMETERS AND MAKE FIRST CALL TO TO CURF
      SIGMAV=0.05
      HALT=.01
      LAMDA=.001
      DT=.05
      KOUNT=0
      WRITE (5,120) HALT,SIGMAV,DT
      WRITE (6,127)
      CALL CURFIT (V,SIGMAV,NPTS,A,SIGMAA,LAMDA,VFIT,CHISQR,KOUNT)
      WRITE (5,121) CHISQR
      CHISAV=CHISQR

C
C      ENTER MAIN CURFIT LOOP
8     KOUNT=KOUNT+1
      CALL CURFIT (V,SIGMAV,NPTS,A,SIGMAA,LAMDA,VFIT,CHISQR,KOUNT)
      TEST=(CHISQR-CHISAV)/CHISQR
      L1=A(1)/RT
      W=A(2)/RT
      SIG=A(3)
      WRITE (5,122) KOUNT,LAMDA,CHISQR,TEST,L1,W,SIG

```

```

WRITE (6,122) KOUNT,LAMDA,CHISQR,TEST,L1,W,SIG
IF(ABS(TEST).LE.HALT) GO TO 9
CHISAV=CHISQR
GO TO 8

```

```

C
C AFTER CONVERGENCE CRITERIA IS SATISFIED, OUTPUT RESULTS
C

```

```

9 DO 14 K=1,3
ERR(K)=SIGMAA(K)
14 IF(A(K) .NE. 0.0) ERR(K)=SIGMAA(K)*100./A(K)
WRITE (5,123) (ERR(I),I=1,3)
WRITE (5,126)
WRITE (5,124)

```

```

C
C MISSING ZERO TIME DATA WILL BE DENOTED ***** ON PRINTER
V1SAV=V(1)
V(1)=111.0

```

```

C
C CALL VOLFUN USING FINAL PARAMETER VALUES TO OBTAIN BEST
C FIT CELL VOLUME AND COMPUTE INTRACELLULAR CONCENTRATIONS
DO 15 I=1,NPTS
VFIT(I)=VOLFUN(I,A)

```

```

C INTRACELLULAR CONCENTRATIONS - PSEUDO -BINARY OSMOLALITY
C AND PERMEABLE SOLUTE MOLARITY
MPB=0.3590/(NWFSAV + 0.1997)

```

```

C POLYNOMIAL FIT FOR PSEUDO-BINARY OSMOTIC COEFFICIENT
PHIPB=((1.4431*MPB-1.05013)*MPB+0.706384)*MPB+0.820722
OSMPB=PHIPB*MPB
MSP=CC*NSPSAV/(NWFSAV + 0.1997)
CSP=FIT2(MSP)
WRITE (5,125) T(I),V(I),VFIT(I),OSMPB,CSP
PLOT(1,I)=VFIT(I)
PLOT(2,I)=V(I)
PLOT(3,I)=T(I)

```

```

15 CONTINUE
PLOT(2,1)=V1SAV
C PLOTTING ROUTINES ARE LOCAL TO MIT ME COMPUTER FACILITY
CALL QPICTR(PLOT,3,NPTS,QNX(3),QLABEL(-2004),QXLAB(XLAB3))

```

```

C THEORETICAL FINAL VOLUME
NWFSAV=(.3590/FIT5(CSIO)) - .1997
IF (CSIO .GT. 0.289 .AND. CSIO .LT. 0.291) NWFSAV=1.0
NSPSAV=(NWFSAV + .1997)*FIT1(CSPO)/CC
VFINAL=.6006*(NWFSAV + VFC*NSPSAV) + .3994
WRITE (5,128) VFINAL
90 CONTINUE

```

```

C
51 FORMAT (8F10.2/2F10.2/8F10.3/2F10.3/8F10.4/2F10.4)
52 FORMAT (F10.2)
85 FORMAT ('1',30X,5A4/' TEMPERATURE= ',F5.1,' DEG C'/
1' PERMEABLE SOLUTE IS ',5A4/' WITH MOLAR VOLUME VSP= ',F6.2
2' CUBIC CM/MOL')
86 FORMAT ('0', ' BLOOD SUSPENSION (HCT',F6.2,' PERCENT)'/10X,F6.
1' OSMOLAL SALINE'/10X,F6.3,' MOLAR ',5A4)

```

```

87  FORMAT ('0', ' ADDED SOLUTION'/10X, F6.3, ' OSMOLAL SALINE'/10X,
1F6.3, ' MOLAR ', 5A4)
88  FORMAT ('0', ' EXTRACELLULAR SOLUTION AFTER MIXING'/10X, F6.3,
1' OSMOLAL SALINE'/10X, F6.3, ' MOLAR ', 5A4)
89  FORMAT('1', 'INITIAL PARAMETER GUESSES'/5X, 'L1=' , 4X, E11.4,
1' CUBIC CM/DYNE SEC'/5X, 'W=' , 5X, E11.4, ' MOL/DYNE SEC'/5X,
2'SIGMA= ', F6.3)
101  FORMAT (5A4, F10.2)
102  FORMAT (4F10.3)
103  FORMAT (2E10.2, F10.2)
104  FORMAT (F10.4)
105  FORMAT (I2)
106  FORMAT (F10.3, F10.4)
107  FORMAT (5A4)
110  FORMAT('0', ' STOP FLOW DEAD TIME = ', F6.3, ' SECONDS')
120  FORMAT('0', 'CURFIT NUMERICAL PARAMETERS'/5X,
1 'CONVERGENCE CRITERION HALT= ', F6.3/5X,
2 'ERROR ESTIMATE SIGMAV= ', 2PF6.3, ' PERCENT'/5X,
3 'INTEGRATION INTERVAL DT= ', 0PF6.3, ' SECONDS')
121  FORMAT('0', 'CHISQUARE FOR INITIAL PARAMETER GUESS = ', E11.4)
122  FORMAT('0', 'AFTER ', I2, ' ITERATIONS'/'          LAMDA= ', F7.1/
1'          CHISQUARE= ', E11.4/'          TEST= ', E10.3/'          L1= ',
2E11.4, ' CUBIC CM/DYNE-SEC'/'          W= ', E11.4,
3' MOL/DYNE-SEC'/'          SIGMA= ', F6.3)
123  FORMAT('0', 'THE FINAL PARAMETER UNCERTAINTIES ARE'/6X, 'L1', 6X,
1F7.2, ' PERCENT'/6X, 'W', 7X, F7.2, ' PERCENT'/6X, 'SIGMA ', F7.2,
2' PERCENT')
124  FORMAT('0', 5X, 'TIME', 7X, 'VC (DATA)', 5X, 'VC (FIT)', 6X,
1 'OSMPB', 9X, 'CSP'/)
125  FORMAT (' ', 5X, F6.3, 5X, F6.4, 8X, F6.4, 2(7X, F7.4))
126  FORMAT('1', 'TIME (SECONDS) INCLUDES DEAD TIME CORRECTION'/
1' VC NORMALIZED TO ISOTONIC CELL VOLUME (100 CUBIC MICRONS)'/
2' OSMPB IS PSEUDO-BINARY OSMOLALITY, CSP IS SOLUTE MOLARITY')
127  FORMAT (' FIRST CALL TO CURFIT')
128  FORMAT ('0', 'THEORETICAL FINAL CELL VOLUME=', F7.4)
END

```

SUBROUTINE CURFIT (V,SIGMAV,NPTS,A,SIGMAA,LAMDA,VFIT,CHISQR,  
1KOUNT)

```

C
C SEARCHES FOR THE PARAMETER VALUES WHICH MINIMIZE THE CHISQUARE
C FOR THE DATA AND THEORETICAL FITTING FUNCTION
C
DIMENSION BETA(3),ALPHA(3,3),A(3),R(3),ARRAY(3,3),S(3,3)
DIMENSION SIGMAA(3), V(50),VFIT(50), DERIV(3,50)
REAL LAMDA
C
IF(KOUNT .EQ. 1) GO TO 64
C
C FILL ALPHA AND BETA WITH ZEROES
DO 34 K=1,3
BETA(K)=0.
DO 34 J=1,K
34 ALPHA(J,K)=0.
C
IF(KOUNT.GT.0) GO TO 41
C
C GENERATE THE ELEMENTS OF ALPHA AND BETA
DO 40 I=1,NPTS
VFIT(I)=VOLFUN(I,A)
40
41 DO 44 K=1,3
CALL FDERIV (A,K,NPTS,DERIV)
DO 42 I=1,NPTS
42 BETA(K)=BETA(K)+((V(I)-VFIT(I))*DERIV(K,I)/(SIGMAV*SIGMAV))
DO 43 J=1,K
DO 43 L=1,NPTS
ALPHA(J,K)=ALPHA(J,K)+(DERIV(J,L)*DERIV(K,L)/(SIGMAV*SIGMAV))
43 CONTINUE
44 CONTINUE
DO 45 K=1,3
DO 45 J=1,K
45 ALPHA(K,J)=ALPHA(J,K)
DO 46 J=1,3
DO 46 K=1,3
S(J,K)=SQRT(ALPHA(J,J)*ALPHA(K,K))
IF (S(J,K) .EQ. 0.0) S(J,K)=1.0
46 CONTINUE
C
IF (KOUNT.GT.0) GO TO 64
C
CHISQR=FCHISQ(V,SIGMAV,NPTS,VFIT)
RETURN
64 CHISQ1=CHISQR
C
C INNER LOOP - ONLY LAMDA, ARRAY, AND B(J) ARE CHANGED
71 DO 74 J=1,3
DO 73 K=1,3
C ARRAY IS THE MODIFIED ALPHA MATRIX, NORMALIZED TO ITS
C DIAGONAL ELEMENTS WITH MATRIX S(J,K)
73 ARRAY(J,K)=ALPHA(J,K)/S(J,K)

```

```

74  ARRAY(J,J)=1.+LAMDA
C
C  SOLVE FOR THE NEW PARAMETERS
CALL MINV(ARRAY)
DO 84 J=1,3
B(J)=A(J)
DO 84 K=1,3
84  B(J)=B(J)+BETA(K)*ARRAY(J,K)/S(J,K)
C
C  CONSTRAIN ALL PARAMETERS POSITIVE AND SIGMA LESS THAN 1
DO 85 J=1,3
85  B(J)=ABS(B(J))
IF (B(3) .GT. 1.0) B(3)=ABS(2.-B(3))
C
C  COMPUTE CHISQUARE WITH NEW PARAMETERS
DO 92 I=1,NPTS
92  VFIT(I)=VOLFUN(I,B)
CHISQR=FCHTSQ(V,SIGMAV,NPTS,VFIT)
IF(CHISQ1-CHISQR) 95,101,101
C
C  IF CHISQUARE INCREASED, INCREASE LAMDA AND TRY AGAIN
95  LAMDA=10.*LAMDA
WRITE (6,110)
GO TO 71
C
C  IF CHISQUARE DECREASED, RETURN TO MAIN
101 DO 103 J=1,3
A(J)=B(J)
C  IF ALPHA(J,J)=0.0, OR IF A(K)=0.0, PARAMETER UNCERTAINTY
C  ERR(J) WILL BE DENOTED ***** ON OUTPUT
SIGMAA(J)=1.E5
IF (ALPHA(J,J) .NE. 0.0)
1SIGMAA(J)=(SQRT(ARRAY(J,J)/ALPHA(J,J)))*SIGMAV
103  CONTINUE
LAMDA=LAMDA/10.
110  FORMAT (' CURFIT HAS INCREASED LAMDA BY 10')
RETURN
END

```

```
SUBROUTINE FDERIV (A,K,NPTS,DERIV)
```

```
COMPUTES THE DERIVATIVE OF THE FITTING FUNCTION WITH RESPECT TO  
THE PARAMETER A(K) AT THE POINT T(I)
```

```
DIMENSION A(3), DERIV(3,50), VUP(50)
```

```
IF (A(K) .EQ. 0.0) GO TO 20
```

```
AK=A(K)
```

```
A(K)=AK*1.05
```

```
DO 12 I=1,NPTS
```

```
12 VUP(I)=VOLFUN(I,A)
```

```
A(K)=AK*0.95
```

```
DO 18 I=1,NPTS
```

```
VDWN=VOLFUN(I,A)
```

```
18 DERIV(K,I)=(VUP(I)-VDWN)/(AK*0.1)
```

```
A(K)=AK
```

```
RETURN
```

```
20 DO 25 I=1,NPTS
```

```
25 DERIV(K,I)=0.0
```

```
RETURN
```

```
END
```



## SUBROUTINE MINV(ARRAY)

```

C
C   INVERTS A 3X3 SYMMETRIC MATRIX USING GAUSS-JORDAN ELIMINATION.
C   THE INPUT MATRIX IS DESTROYED IN COMPUTATION AND
C   REPLACED BY ITS INVERSE.
C
DIMENSION ARRAY(3,3), IK(3), JK(3)
DO 100 K=1,3
  AMAX=0.
21  DO 30 I=K,3
    DO 30 J=K,3
      IF(ABS(AMAX)-ABS(ARRAY(I,J)))24,24,30
24  AMAX=ARRAY(I,J)
      IK(K)=I
      JK(K)=J
30  CONTINUE
      IF(AMAX)41,140,41
41  I=IK(K)
      IF(I-K)21,51,43
43  DO 50 J=1,3
      SAVE=ARRAY(K,J)
      ARRAY(K,J)=ARRAY(I,J)
50  ARRAY(I,J)=-SAVE
51  J=JK(K)
      IF(J-K)21,61,53
53  DO 60 I=1,3
      SAVE=ARRAY(I,K)
      ARRAY(I,K)=ARRAY(I,J)
60  ARRAY(I,J)=-SAVE
61  DO 70 I=1,3
      IF(I-K)63,70,63
63  ARRAY(I,K)=-ARRAY(I,K)/AMAX
70  CONTINUE
      DO 80 I=1,3
      DO 80 J=1,3
      IF(I-K)74,80,74
74  IF(J-K)75,80,75
75  ARRAY(I,J)=ARRAY(I,J)+ARRAY(I,K)*ARRAY(K,J)
80  CONTINUE
      DO 90 J=1,3
      IF(J-K)83,90,83
83  ARRAY(K,J)=ARRAY(K,J)/AMAX
90  CONTINUE
      ARRAY(K,K)=1./AMAX
100 CONTINUE
      DO 130 L=1,3
      K=4-L
      J=IK(K)
      IF(J-K)111,111,105
105 DO 110 I=1,3
      SAVE=ARRAY(I,K)
      ARRAY(I,K)=-ARRAY(I,J)
110 ARRAY(I,J)=SAVE

```

```
111 I=JK(K)
    IF(I-K) 130,130,113
113 DO 120 J=1,3
    SAVE=ARRAY(K,J)
    ARRAY(K,J)=-ARRAY(I,J)
120 ARRAY(I,J)=SAVE
130 CONTINUE
140 RETURN
    END
```

```
FUNCTION FCHISO(V,SIGMAV,NPTS,VFIT)
```

```
C  
C COMPUTES THE REDUCED CHI-SQUARE STATISTIC,  
C (SUM((DATA-FIT)**2))/((STANDARD DEVIATION)*(DEGREES FREEDOM))  
C
```

```
DIMENSION V(50), VFIT(50)
```

```
C  
CHISO=0.
```

```
DO 30 I=1,NPTS
```

```
DELV=V(I)-VFIT(I)
```

```
30 CHISO=CHISO+(DELV*DELV)
```

```
FCHISO=CHISO/((FLOAT(NPTS-3))*SIGMAV*SIGMAV)
```

```
RETURN
```

```
END
```

FUNCTION VOLFUN(I,A)

COMPUTES THE CELL VOLUME AT TIME T(I) FOR A GIVEN SET OF  
PARAMETERS A(K) AND INITIAL CONDITIONS

DIMENSION T(50), A(3)  
REAL NWFSAV, NSPSAV, NWFN, NSPN  
COMMON/BLK1/NWFN, NSPN, CC, VSP, VFC, DT  
COMMON/BLK3/WB, SIG  
COMMON/BLK4/ T  
COMMON/BLK5/NWFSAV, NSPSAV

IF(I.NE.1) GO TO 10  
TIME CONSTANT TAU AND NON-DIMENSIONAL SOLUTE PERMEABILITY WB  
TAU=4.449E-2/(A(1)\*CC)  
WB=A(2)/(A(1)\*CC\*.001)  
SIG=A(3)  
NWFSAV=NWFN  
NSPSAV=NSPN  
GO TO 50  
NON-DIMENSIONAL TIMES  
10 TOB=T(I-1)/TAU  
TFB=T(I)/TAU  
DTB=DT/TAU  
CALL RKI(NWFSAV, NSPSAV, TOB, TFB, DTB)  
PSEUDO-BINARY VOLUME MODEL  
50 VOLFUN=.6006\*(NWFSAV+VFC\*NSPSAV)+0.3994  
RETURN  
END

FUNCTION FIT1 (CSP)

C  
C  
C  
C

MOLALITY AS A FUNCTION OF MOLARITY  
ETHYLENE GLYCOL CURVE FIT OF 4/21/77

FIT1=CSP

IF(CSP .GT. .35) FIT1=(.0882619\*CSP+.927122)\*CSP+.0302677

RETURN

END

1950-1951

10  
11  
12

1950-1951

1950-1951

1950-1951

1950-1951

1950-1951









PROGRAM FOR THE SOLUTION OF THE

STIFFNESS MATRIX EQUATIONS BY THE NEWTON-RAPHSON METHOD. THE PROGRAM IS  
DESIGNED TO SOLVE THE EQUATIONS OF MOTION FOR A STRUCTURE WITH  
NON-LINEAR ELASTIC BEHAVIOR. THE EQUATIONS ARE SOLVED BY THE

NEWTON-RAPHSON METHOD.  
THE PROGRAM IS  
DESIGNED TO SOLVE THE

EQUATIONS OF MOTION FOR A STRUCTURE WITH  
NON-LINEAR ELASTIC BEHAVIOR. THE EQUATIONS ARE SOLVED BY THE  
NEWTON-RAPHSON METHOD. THE PROGRAM IS  
DESIGNED TO SOLVE THE EQUATIONS OF MOTION FOR A STRUCTURE WITH  
NON-LINEAR ELASTIC BEHAVIOR. THE EQUATIONS ARE SOLVED BY THE  
NEWTON-RAPHSON METHOD.

DO 10 I=1,NSTEP  
T=T+DELTA  
Y1=YSAV  
Y2=YSAV  
CALL MODEL(Y1,Y2,DY1DT,DY2DT)  
RK10=H\*DY1DT  
RK20=H\*DY2DT  
Y1=Y1SAV+RK10\*0.5  
Y2=Y2SAV+RK20\*0.5  
CALL MODEL(Y1,Y2,DY1DT,DY2DT)  
RK11=H\*DY1DT  
RK21=H\*DY2DT  
Y1=Y1SAV+RK11\*0.5  
Y2=Y2SAV+RK21\*0.5  
CALL MODEL(Y1,Y2,DY1DT,DY2DT)  
RK12=H\*DY1DT  
RK22=H\*DY2DT  
Y1=Y1SAV+RK12  
Y2=Y2SAV+RK22  
CALL MODEL(Y1,Y2,DY1DT,DY2DT)  
RK13=H\*DY1DT  
RK23=H\*DY2DT  
Y1SAV=Y1SAV+(RK10+RK13+2.\*(RK11+RK12))\*SIXTH  
Y2SAV=Y2SAV+(RK20+RK23+2.\*(RK21+RK22))\*SIXTH  
CONTINUE

30  
C

Y1CALL=Y1SAV  
Y2CALL=Y2SAV

C

RETURN  
END

SECRET - SECURITY INFORMATION

DO NOT CHANGE THE VALUE OF ANY OF THE PARAMETERS LISTED  
HEREIN UNLESS YOU ARE SURE YOU KNOW WHAT YOU ARE DOING. THE  
PERMEATION COEFFICIENTS LISTED HEREIN ARE APPROXIMATE  
VALUES FOR POLYETHYLENE AND POLYPROPYLENE FILMS.

PARAMETERS: LNASPO  
LNASPO=1.0E-10, VFC=1.0E-10, CSPH=1.0E-10, VFC=1.0E-10  
LNASPO=1.0E-10, VFC=1.0E-10, CSPH=1.0E-10, VFC=1.0E-10  
LNASPO=1.0E-10, VFC=1.0E-10, CSPH=1.0E-10, VFC=1.0E-10  
LNASPO=1.0E-10, VFC=1.0E-10, CSPH=1.0E-10, VFC=1.0E-10

PERMEATION COEFFICIENTS  
LNASPO=1.0E-10, VFC=1.0E-10, CSPH=1.0E-10, VFC=1.0E-10  
LNASPO=1.0E-10, VFC=1.0E-10, CSPH=1.0E-10, VFC=1.0E-10  
LNASPO=1.0E-10, VFC=1.0E-10, CSPH=1.0E-10, VFC=1.0E-10  
LNASPO=1.0E-10, VFC=1.0E-10, CSPH=1.0E-10, VFC=1.0E-10

PERMEABLE SOLUTE MOLALITY AND MEAN CONCENTRATION (MOLAL)  
LNASPO=1.0E-10, VFC=1.0E-10, CSPH=1.0E-10, VFC=1.0E-10  
LNASPO=1.0E-10, VFC=1.0E-10, CSPH=1.0E-10, VFC=1.0E-10  
LNASPO=1.0E-10, VFC=1.0E-10, CSPH=1.0E-10, VFC=1.0E-10  
LNASPO=1.0E-10, VFC=1.0E-10, CSPH=1.0E-10, VFC=1.0E-10

DRIVING FORCES  
LN(WATER ACTIVITY) = -18.015E-3 \* (TOTAL OSMOLALITY)  
DLNAW = -18.015E-3 \* (PHIPB \* MPB + FIT3(MSP)) - LNAW0  
DLNASP = FIT4(MSP) - LNASPO

RATE EQUATIONS FOR FREE WATER AND PERMEABLE SOLUTE  
DNWFDT = -(1.0 + VFC \* VFC \* CSPH \* WB) \* DLNAW / (CC \* 18.015E-3)  
1 - ((1.0 - SIG) - VFC \* WB) \* CSPH \* DLNASP  
DNSPDT = -((1.0 - SIG) \* CSPH - VFC \* CSPH \* WB) \* DLNAW / (CC \* 18.015E-3)  
1 - (((1.0 - SIG) \* (1.0 - SIG)) \* CSPH \* WB) \* CSPH \* DLNASP  
RETURN  
END

11 182 4  
101 11 1180  
111 10 1111  
111 10 1111  
111 10 1111  
111 10 1111  
111 10 1111

## PERM2 INPUT CODING

Card	Col:	Variable Name	Format	Example	
1	1-2	NRUNS	I2	03	number of runs stacked in data deck
2	1-20	IDRUN	5A4	Run 8 7/11/77	run label, up to 20 characters
3	1-10	HCTNOM	F10.2	7.3	hematocrit of suspension (ml cell/100 ml)
4	1-10	TEMP	F10.2	-5.0	temperature (°C)
5	1-20	SOLUTE	5A4	GLYCEROL	solute name, up to 20 characters
	21-30	VSP	F10.2	42.33	solute partial molar volume (cm <sup>3</sup> /mol)
6	1-10	CSI1	F10.3	.290	cell suspension } impermeable solute
	11-20	CSI2	F10.3	1.0	added solution } (osm/Kg)
	21-30	CSP1	F10.3	0.	cell suspension } permeable solute
	31-40	CSP2	F10.3	4.5	added solution } (molar)
7	1-10	L1	E10.2	1.E-11	water permeability L <sub>p</sub> (cm <sup>3</sup> /dyne sec) } initial
	11-20	N	E10.2	2.6E-15	solute permeability ω (mol/dyne sec) } guesses
	21-30	SIG	F10.2	0.88	reflection coefficient σ
8	1-10	TDEAD	F10.4	.008	stop flow dead time (seconds)
9	1-2	NDATA	I2	37	number of data points following (<50)
10 →	1-10	TIME	F10.3	1.205	data time (seconds)
10+ NDATA	11-20	VIN(I)	F10.4	.986	corresponding cell volume data (non-dimensional)

For NRUNS &gt; 1, repeat cards

2 → 10 + NDATA

SAMPLE PERM2 OUTPUT

AVG 1-5 12/5/77 B

TEMPERATURE= 25.0 DEG C  
PERMEABLE SOLUTE IS ETHYLENE GLYCOL  
WITH MOLAR VOLUME VSP= 42.33 CUBIC CM/MOL

STOP FLOW DEAD TIME = 0.007 SECONDS

BLOOD SUSPENSION (HCT 8.00 PERCENT)  
0.290 OSMOLAL SALINE  
0.900 MOLAR ETHYLENE GLYCOL

ADDED SOLUTION  
0.290 OSMOLAL SALINE  
1.100 MOLAR ETHYLENE GLYCOL

EXTRACELLULAR SOLUTION AFTER MIXING  
0.290 OSMOLAL SALINE  
1.004 MOLAR ETHYLENE GLYCOL

## INITIAL PARAMETER GUESSES

L1= 0.4400E-11 CUBIC CM/DYNE SEC  
 W= 0.1600E-14 MOL/DYNE SEC  
 SIGMA= 0.900

## CURFIT NUMERICAL PARAMETERS

CONVERGENCE CRITERION HALT= 0.010  
 ERROR ESTIMATE SIGMAV= 5.000 PERCENT  
 INTEGRATION INTERVAL DT= 0.050 SECONDS

CHISQUARE FOR INITIAL PARAMETER GUESS = 0.2048E-01

## AFTER 1 ITERATIONS

LANDA= 0.1E-03  
 CHISQUARE= 0.5434E-02  
 TEST= -0.277E 01  
 L1= 0.3520E-11 CUBIC CM/DYNE-SEC  
 W= 0.1778E-14 MOL/DYNE-SEC  
 SIGMA= 0.812

## AFTER 2 ITERATIONS

LANDA= 0.1E-04  
 CHISQUARE= 0.5412E-02  
 TEST= -0.400E-02  
 L1= 0.3278E-11 CUBIC CM/DYNE-SEC  
 W= 0.1888E-14 MOL/DYNE-SEC  
 SIGMA= 0.854

## THE FINAL PARAMETER UNCERTAINTIES ARE

L1 14.66 PERCENT  
 W 5.59 PERCENT  
 SIGMA 5.58 PERCENT

TIME (SECONDS) INCLUDES DEAD TIME CORRECTION  
 VC NORMALIZED TO ISOTONIC CELL VOLUME (100 CUBIC MICRONS)  
 CSMPB IS PSEUDO-BINARY OSMOLALITY, CSP IS SOLUTE MOLARITY

TIME	VC (DATA)	VC (FIT)	OSMPB	CSP
0.000	*****	1.0286	0.2923	0.88
0.207	1.0270	1.0159	0.2987	0.92
0.217	1.0240	1.0156	0.2988	0.92
0.227	1.0240	1.0152	0.2990	0.92
0.237	1.0220	1.0149	0.2992	0.92
0.247	1.0200	1.0146	0.2994	0.92
0.257	1.0180	1.0143	0.2995	0.92
0.267	1.0180	1.0140	0.2997	0.93
0.277	1.0160	1.0137	0.2998	0.93
0.287	1.0140	1.0135	0.3000	0.93
0.307	1.0130	1.0130	0.3002	0.93
0.327	1.0100	1.0126	0.3005	0.93
0.347	1.0090	1.0118	0.3008	0.94
0.367	1.0090	1.0111	0.3012	0.94
0.387	1.0080	1.0104	0.3016	0.94
0.407	1.0060	1.0097	0.3019	0.94
0.457	1.0050	1.0082	0.3027	0.94
0.507	1.0030	1.0069	0.3033	0.94
0.557	1.0030	1.0057	0.3039	0.95
0.607	1.0000	1.0047	0.3045	0.95
0.657	1.0000	1.0038	0.3049	0.95
0.707	1.0010	1.0031	0.3053	0.95
0.807	0.9980	1.0018	0.3059	0.95
0.907	0.9980	1.0010	0.3064	0.95
1.007	1.0000	1.0004	0.3067	0.95
1.507	1.0000	0.9998	0.3071	0.95
2.007	1.0030	1.0011	0.3065	0.95
2.507	1.0040	1.0028	0.3057	0.95
3.007	1.0030	1.0047	0.3048	0.95
3.507	1.0040	1.0064	0.3039	0.95
4.007	1.0080	1.0081	0.3031	0.95
4.507	1.0090	1.0097	0.3024	0.95
5.007	1.0090	1.0112	0.3017	0.95
6.007	1.0140	1.0140	0.3004	0.95
7.007	1.0180	1.0165	0.2992	0.95
8.007	1.0190	1.0187	0.2982	0.95
9.007	1.0210	1.0206	0.2973	0.95
10.007	1.0200	1.0224	0.2965	0.95
11.007	1.0250	1.0240	0.2958	0.95
12.007	1.0250	1.0254	0.2952	0.95
13.007	1.0260	1.0266	0.2947	0.95
14.007	1.0280	1.0277	0.2942	0.95
15.007	1.0290	1.0287	0.2937	0.95
16.007	1.0310	1.0296	0.2933	0.95

THEORETICAL FINAL CELL VOLUME= 1.0320



APPENDIX E  
DEAD TIME EXPERIMENT

Stop flow dead time may be directly measured by monitoring a reaction of the type



If we denote concentrations  $a$ ,  $b$ ,  $c$  respectively, the overall rate of formation of product  $C$  is given by

$$\frac{dc}{dt} = k_1 ab - k_2 c \quad (E.2)$$

This rate law takes the approximate form

$$\frac{dc}{dt} \cong k_1 a_0 b_0 - (k_1 b_0 + k_2) c \quad (E.3)$$

if initial conditions  $a_0$ ,  $b_0$  and  $c_0$  are set such that

$$\begin{aligned} c_0 &= 0 \\ b_0 &\gg a_0 \end{aligned} \quad (E.4)$$

The time dependence of this pseudo first order reaction may conveniently be written in terms of the equilibrium concentration of product  $c_f$  and the reaction time constant  $\tau$

$$c = c_f \{ 1 - e^{-t/\tau} \} \quad (E.5)$$

Photometric measurements of reaction progress are described by the Beer-Lambert law, which states that if a liquid of thickness  $d$  is illuminated with light of intensity  $I_0$ , the exiting light intensity  $I$  is given by

$$\frac{I}{I_0} = e^{-cad} \quad (\text{E.6})$$

where  $\alpha$  is the molar absorptivity and  $c$  the concentration of the light absorbing component. Although strictly true only for discrete wavelengths, the result is qualitatively the same for broad band radiation. To simplify equation E.5 one may define the solution absorbance  $A$  by

$$A = -\ln\left(\frac{I}{I_0}\right) = cad \quad (\text{E.7})$$

If the pseudo first order reaction described above has also been chosen to form a strongly absorbing product, measurements of solution absorbance will yield the time dependence

$$A = A_f \left[ 1 - e^{-t/\tau} \right] \quad (\text{E.8})$$

where  $A_f$  is the equilibrium absorbance and  $t$  is the time from initiation of the reaction. This real reaction time  $t$  is related to the stop flow experimental time  $t_s$ , measured from the instant flow stops, by

$$t = t_s + t_D \quad (\text{E.9})$$

where  $t_D$  is the system dead time.

Dead times were measured experimentally with the reaction



The reactant solutions were made up as .01 M ferric nitrate  $\text{Fe}(\text{NO}_3)_3$  in .1 N sulphuric acid  $\text{H}_2\text{SO}_4$ , and .01 M potassium thiocyanate KCNS [45]. This reaction forms a deep orange product which is easily detected with a monochromatic or broad band optical system. The reactant solutions were mixed in the stop flow apparatus and the subsequent measured intensities  $I(t_s)$  normalized to the value  $I_0$  recorded with a water filled optical chamber. The results of five repeat runs were averaged and are plotted semi-logarithmically as  $1 - \frac{A}{A_f}$  vs time  $t_s$  in Figure E1. Since the reactant solutions did not absorb measurably, a least squares fit could be used to extrapolate the data back to  $A/A_f = 0$  and so obtain the dead time from equation E.8 with  $t_s = -t_D$ .

The experiment was repeated for three different stop flow ram velocities, and a strong correlation was found between the experimentally measured dead times and the computed mixer to observation point transit times. This suggests that mixing is essentially complete immediately downstream of the mixer junction, and system dead time is due primarily to the finite time required for fluid to flow from the mixer to the optical chamber.

For a given ram velocity  $V_{\text{ram}}$  (cm/sec) the transit time  $t_T$  (sec) may be easily calculated from known fluid system cross sectional areas as

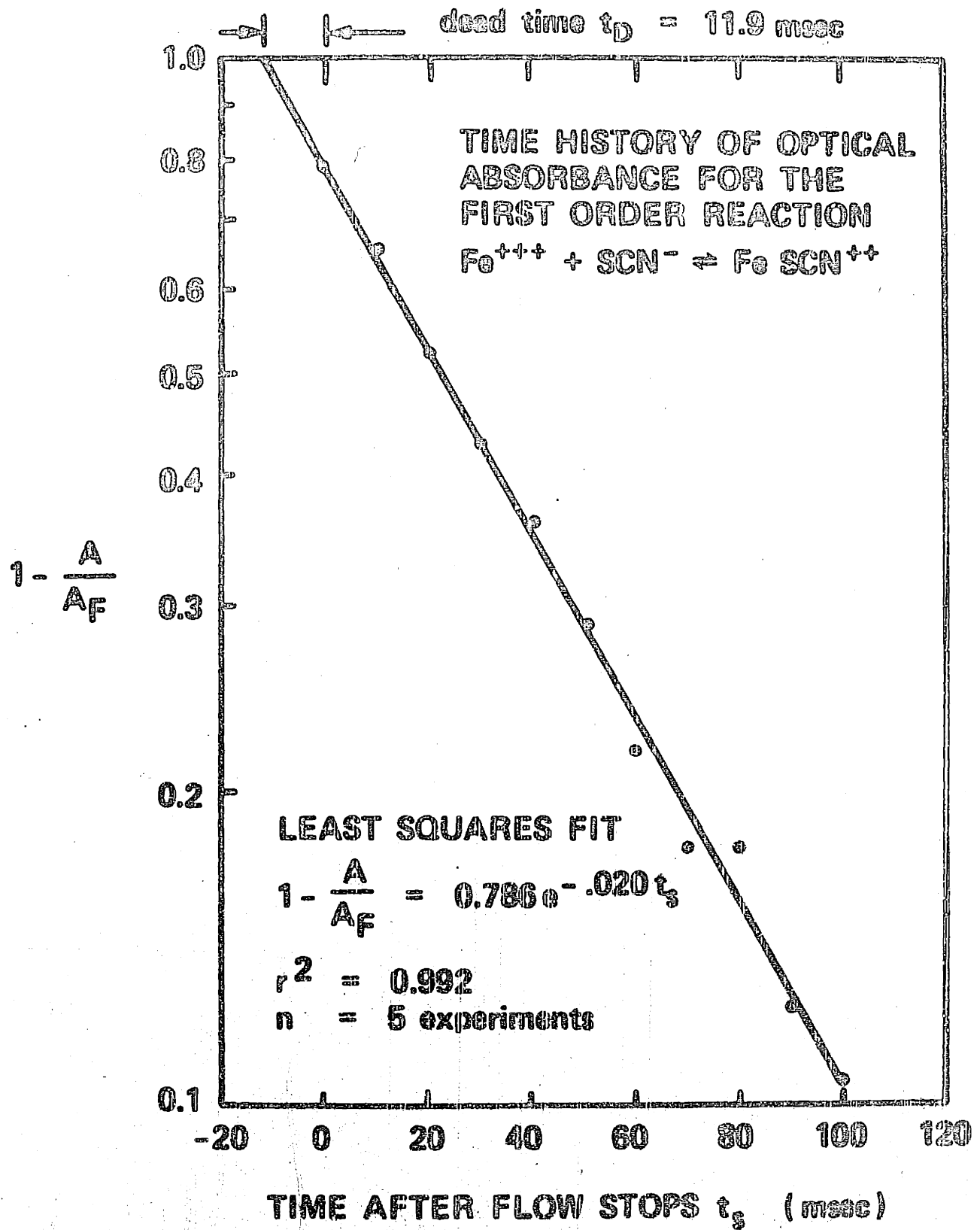


FIGURE E1 Experimental determination of stop flow dead time

$$t_T = \frac{1.31 \times 10^{-2}}{V_{ram}} \quad (E.11)$$

In subsequent permeability experiments, the recorded stop flow time  $t_s$  was corrected by an amount  $t_D = t_T$  to obtain actual reaction time  $t$ . For most experiments the dead time was 6 - 10 msec.

## APPENDIX F

## POLYNOMIAL CURVE FITS

All are of the form  $y = a_0 + a_1x + a_2x^2 \dots a_nx^n$

## 1) Pseudo-solute osmotic coefficient

computed from hemoglobin and KCl data and van Laar extrapolation

$$x = m_{pb} \quad (\text{mol/Kg}) \quad 0.18 \rightarrow 1.32$$

$$y = \phi_{pb}$$

$$a_0 = .82072$$

$$a_2 = -1.0501$$

$$a_1 = .70638$$

$$a_3 = 1.4443$$

## 2) Hemoglobin osmotic coefficient

data used in computing pseudo-solute non-ideality

$$x = m_{Hb} \quad (\text{millimol/Kg}) \quad 0.0 \rightarrow 17.0$$

$$y = \phi_{Hb}$$

$$a_0 = .98910$$

$$a_3 = .28056 \times 10^{-1}$$

$$a_1 = .30709$$

$$a_4 = .19622 \times 10^{-2}$$

$$a_2 = -.11877$$

$$a_5 = .48010 \times 10^{-4}$$

## 3) Potassium chloride osmotic coefficient

data used in computing pseudo-solute non-ideality

$$x = m_{\text{KCl}} \quad (\text{mol/Kg}) \quad 0.0 \rightarrow 0.7$$

$$y = \phi_{\text{KCl}}$$

$$a_0 = .98730 \qquad a_3 = -19.189$$

$$a_1 = -1.1435 \qquad a_4 = 25.286$$

$$a_2 = .6.7502 \qquad a_5 = -12.420$$

## 4) Pseudo-solute molality (inverse of fit 1)

used to compute equilibrium condition from extracellular concentration

$$x = \phi_{\text{pb}} m_{\text{pb}} \quad (\text{osmol/Kg}) \quad 0.17 \rightarrow 1.05$$

$$y = m_{\text{pb}} \quad (\text{mol/Kg})$$

$$a_0 = -.026855 \qquad a_2 = -.76346$$

$$a_1 = 1.3313 \qquad a_3 = .18796$$

## 5) Ethylene glycol molality

$$x = C_{\text{sp}} \quad (\text{mol/liter solution}) \quad 0.35 \rightarrow 5.40$$

$$y = m_{\text{sp}} \quad (\text{mol/Kg H}_2\text{O})$$

$$a_0 = .030268$$

$$a_1 = .92712 \qquad \text{for } x < 0.35 \text{ use } m_{\text{sp}} = C_{\text{sp}}$$

$$a_2 = .088262$$

## 6) Ethylene glycol molarity (inverse of fit 5)

$$x = m_{sp} \quad (\text{mol/Kg}) \quad 0.35 \rightarrow 7.60$$

$$y = C_{sp} \quad (\text{mol/liter})$$

$$a_0 = .023398$$

$$a_1 = .94747 \quad \text{for } x < 0.35 \text{ use } C_{sp} = m_{sp}$$

$$a_2 = -.032451$$

## 7) Ethylene glycol osmolality

$$x = m_{sp} \quad (\text{mol/Kg}) \quad 1.0 \rightarrow 7.6$$

$$y = \phi_{sp} m_{sp} \quad (\text{osmol/Kg})$$

$$a_0 = .015245$$

$$a_1 = .95255 \quad \text{for } m_{sp} < 1.0 \text{ use } \phi_{sp} m_{sp} = m_{sp}$$

$$a_2 = .026515$$

## 8) Ethylene glycol activity

$$x = m_{sp} \quad 1.0 \rightarrow 7.5$$

$$y = -\lambda n a_{sp}$$

$$a_0 = -4.5080$$

$$a_1 = .62880 \quad \text{for } m_{sp} < 1.0$$

$$a_2 = -.038168 \quad \text{use } \lambda n a_{sp} = -\lambda n(m_{sp} \times 18.015 \times 10^{-3})$$



- 9) Ethylene glycol osmotic coefficient  
used in computing solute activity

$$x = m_{sp} \quad (\text{mol/Kg}) \quad 1.0 \rightarrow 7.6$$

$$y = \phi_{sp}$$

$$a_0 = .99584$$

$$a_2 = .55234 \times 10^{-2}$$

$$a_1 = -.26981 \times 10^{-3}$$

$$a_3 = -.35792 \times 10^{-3}$$

- 10) Glycerol molality

$$x = C_{sp} \quad (\text{mol/liter solution}) \quad 0.0 \rightarrow 4.3$$

$$y = m_{sp} \quad (\text{mol/Kg})$$

$$a_0 = .027837$$

$$a_1 = .89819$$

$$a_2 = .11152$$

- 11) Glycerol molarity

$$x = m_{sp} \quad (\text{mol/Kg}) \quad 0.0 \rightarrow 5.9$$

$$y = C_{sp} \quad (\text{mol/liter})$$

$$a_0 = .016477$$

$$a_1 = .97538$$

$$a_2 = -.044557$$

## 12) Glycerol osmotic coefficient

$$x = m_{sp} \quad (\text{mol/Kg}) \quad 0.0 \rightarrow 5.9$$

$$y = \phi_{sp}$$

$$a_0 = 1.0133$$

$$a_2 = -.84974 \times 10^{-2}$$

$$a_1 = .059127$$

$$a_3 = .57365 \times 10^{-3}$$

## 13) Glycerol activity

$$x = m_{sp} \quad (\text{mol/Kg}) \quad 0.0 \rightarrow 4.0$$

$$y = -\ln(a_{sp})$$

$$a_0 = 5.2692$$

$$a_1 = -1.4540$$

$$a_2 = .18859$$

APPENDIX G

CELL VOLUME SIMULATION PROGRAM VOLSIM2



PERMEABLE SOLUTE, THE WATER CONCENTRATION (MOL/CM<sup>3</sup>)  
IS  $1.0 \times 10^{-10}$  AND CSP2 IS  $1.0 \times 10^{-10}$  CC=55.5088  
MOLAR VOLUME FRACTION  
MSPH=1.000

INITIAL (P=10) CONDITION  
NON-DEFORMABLE, FREE WATER  
MSPH=1.000/RTS(CSI1)-0.1997  
IF CS11 IS 0.289 AND CS12 IS 0.291 MSPH=1.000  
PERMEABLE SOLUTE  
MSPH=(MSPH + .1997)\*RTS(CSI1)/CC

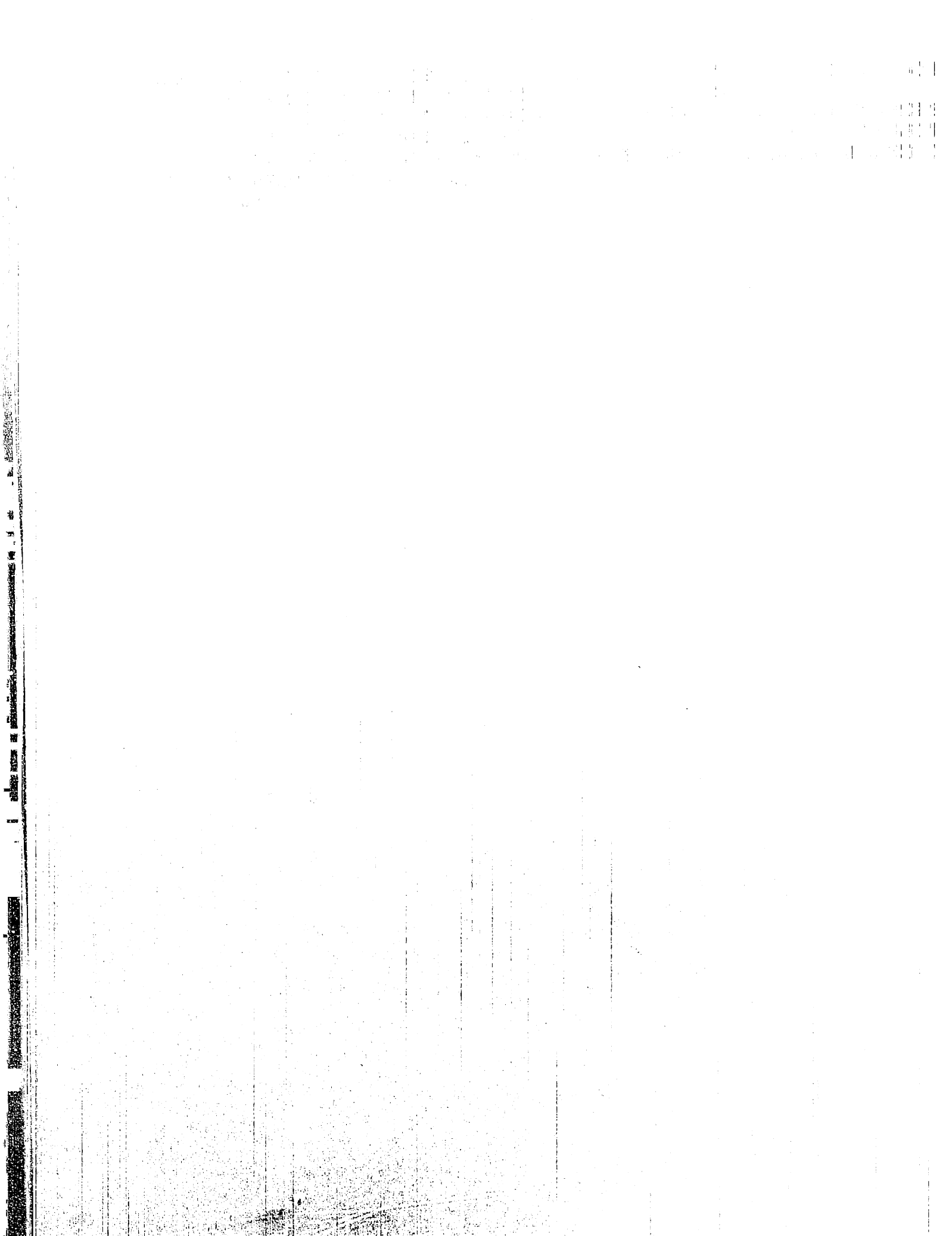
WRITE EXPERIMENTAL CONDITIONS FOR THIS RUN  
WRITE (5,85) IDRUN,TEMP,SOLUTE,ISP  
WRITE (5,86) NCFLOW,CS11,CSP1,SOLUTE  
WRITE (5,87) CS12,CSP2,SOLUTE  
WRITE (5,88) CS10,CSP0,SOLUTE  
WRITE (5,89) L1,H,SIG  
WRITE (5,91) TF,DT,NPRINT

L1 IS THE WATER PERMEABILITY (CM<sup>3</sup> CM/DYNE-SEC)  
H (OMEGA) IS THE SOLUTE PERMEABILITY (MOL/DYNE-SEC)  
SIG (SIGMA) IS THE SOLUTE REFLECTION COEFFICIENT  
A(1)=L1\*RT  
A(2)=H\*RT  
A(3)=SIG

FILL TIME VECTOR  
NPRINT1=NPRINT+1  
TPRNT=TF/FLOAT(NPRINT)  
DO 17 I=1,NPRINT1  
T(I)=TPRNT\*FLOAT(I-1)  
PLOT (1,I)=T(I)  
PLOT2(1,I)=T(I)  
PLOT3(1,I)=T(I)  
CONTINUE

WRITE (5,127) IDRUN









The above VOLSIM2 mainline is followed by subprograms VOLFUN, RKI, FIT1, FIT2, FIT3, FIT4, and FIT5 identical to those in PERM2.

Subroutine MODEL is changed only by the addition of these statements.

```
COMMON/BLK6/RATE1,RATE2
```

```
RATE1 = DNWPD
```

```
RATE2 = DNSPD
```

and the labelled common blocks are slightly altered

```
// XEQ 6
*LC 18 BLK1
*LC  C BLK2
*LC 194 BLK3
*LC  8 BLK4
*LC  8 BLK5
*LC  8 BLK6
```

Input to VOLSIM2 follows NAMELIST format.

The first list contains:

NSIM	number of simulations to be overlaid on plots
TF	final time (seconds)
DT	integration time step (seconds)
NPRNT	number of point/plot points

The second list is as follows:

IDRUN	a label, up to 20 characters enclosed in quotes
HCTNOM	hematocrit of cell suspension (ml cell/100 ml)
TEMP	temperature (°C)
SOLUTE	permeable solute name, up to 20 characters in quotes
VSP	solute partial molar volume (cm <sup>3</sup> /mol)
CSI1	cell suspension } impermeable solute
CSI2	added solution } (osm/Kg)
CSP1	cell suspension } permeable solute
CSP2	added solution } (molar)
L1	water permeability $L_p$ (cm <sup>3</sup> /dyne sec)
W	solute permeability $\omega$ (mol/dyne sec)
SIG	reflection coefficient $\sigma$

If NSIM > 1, simply repeat the second list

Below is a sample of actual input. Notice the VARIABLE NAME = VALUE format, the comma between each item, and the ampersand (&) closing each list. Also, upon repeats of a list, you only need to input those variables you wish to change.

```
NSIM=2, TF=20.0, DT=.010, NPRNT=50 &  
IDRUN=' 10/6/77 ', HCTNOM=8.0, TEMP=25.0, SOLUTE='ETHYLENE GLYCOL',  
VSP=42.33, CSI1=.265, CSI2=.265, CSP1=0.0, CSP2=0.2,  
L1=1.3E-11, W=20.0E-16, SIG=0.8 &  
CSI2=.600 &
```

APPENDIX H  
RED CELL AND BLOOD PHYSICAL PROPERTIES

TABLE H1

PROPERTIES OF NORMAL HUMAN WHOLE BLOOD

red cell count	5.2 $\pm$ .8	$10^6$ cells/mm <sup>3</sup>	[46]
white cell count	7.2 $\pm$ 1.8	$10^3$ cells/mm <sup>3</sup>	[46]
hematocrit	46 $\pm$ 5	ml cells/100 ml blood	[47]
blood pH	7.3 - 7.5		[48]
plasma osmolality	.288 - .292	osmol/Kg	[48]*

\*and measurements in this  
laboratory

TABLE H2

## HUMAN ERYTHROCYTE DIMENSIONS

Volume ( $10^{-12} \text{ cm}^3$ )	Surface Area ( $10^{-8} \text{ cm}^2$ )	Major Diameter ( $10^{-4} \text{ cm}$ )	
$97 \pm 14$	$135 \pm 16$	$7.82 \pm .62$	[49]
$107.5 \pm 16.8$	$138.1 \pm 17.4$	$8.07 \pm .43$	[50]
$87 \pm 5$		$6.5 - 9.3$	[47]
	103	8.6	[51]
100	135		as used in this thesis

TABLE H3

## WATER CONTENT OF HUMAN RED CELLS, AS MEASURED BY DRYING

.70	gm/ml	[26]
$.742 \pm .015$	gm/ml	[52]
$.661 \pm .014$	gm/ml	[52] citing McLeod
$.717 \pm .005$	ml/ml	[53]
$.685 \pm .005$	gm/gm	[54]

TABLE H4

## PRINCIPAL CONTENTS OF THE NORMAL HUMAN ERYTHROCYTE

Component	m mol/ Kg	osmotic coef- ficient $\phi$	charge/ mol	total charge	m osmol/Kg	Note
$K^+$	141	.91	+1	141	128.3	
$Na^+$	18	.93	+1	18	16.7	
$Mg^{++}$	3.5	.93	+2	7	3.3	
$Ca^{++}$	1.4	.86	+2	2.8	1.2	
$Cl^-$	78	.93	-1	-78	72.5	
Hemoglobin	7.2	3.2	-4.7	-34.3	23.0	1
Total Phosphate	17.7	.91	-2	-35.4	16.1	2
Glucose	5.5	.95	0	0	5.2	3
$HCO_3^-$	20	.93	-1	-20	18.6	3,4
				+1.1	284.9	5

Note:

These values were compiled from [48] [47] [46] [55] [56] [57] [58] [59] [50] and each represents an average of at least two reported values. Literature values which varied significantly from the commonly reported value were given less weight.

1. Hemoglobin charge at the given concentration from [61].
2. Total phosphate is the sum of all phosphate radicals and the valence of -2 represents a rough average.

3. Glucose and bicarbonate osmotic coefficient from [62], all other  $\phi$  from [21].
4. Bicarbonate concentration computed using the Donnan equilibrium

$$\frac{[\text{Cl}^-]_{\text{in}}}{[\text{Cl}^-]_{\text{out}}} = \frac{[\text{HCO}_3^-]_{\text{in}}}{[\text{HCO}_3^-]_{\text{out}}}$$

5. These totals only serve as a check. Net charge should be zero and total osmolality should be equal to that of plasma, .290 Osm.

APPENDIX I

## CONCENTRATION CONVERSIONS (AQUEOUS SOLUTIONS)

## 1. Weight percent to molality

$$m_s = \frac{1000 A\%}{18.015 (100 - A\%)}$$

## 2. Molality to mole fraction

$$x_s = \frac{v_s m_s}{v_s m_s + \frac{1000}{18.015}}$$

## 3. Weight percent to mole fraction

$$x_s = \frac{v_s A\%}{v_s A\% + (100 - A\%) \frac{MW_s}{18.015}}$$

## 4. Molality to molarity

A closed form expression is not possible, but data such as in Figure I-1 may be found in the Handbook of Chemistry and Physics [20] for many aqueous solutions.

A useful approximate expression is

$$M_s = \frac{m_s}{\frac{v_s m_s}{1000} + 1}$$

Nomenclature

$M_s$	molarity	mol solute/liter solution
$v_s$	specific volume of pure solute	$\text{cm}^3/\text{mol}$
$m_s$	molality	mol solute/Kg $\text{H}_2\text{O}$
A%	weight percent	gm solute/100 gm solution
$x_s$	mole fraction	mol solute/mol solution
$\nu_s$	dissociation number	ions/molecule
$MW_s$	molecular weight	gm/mol



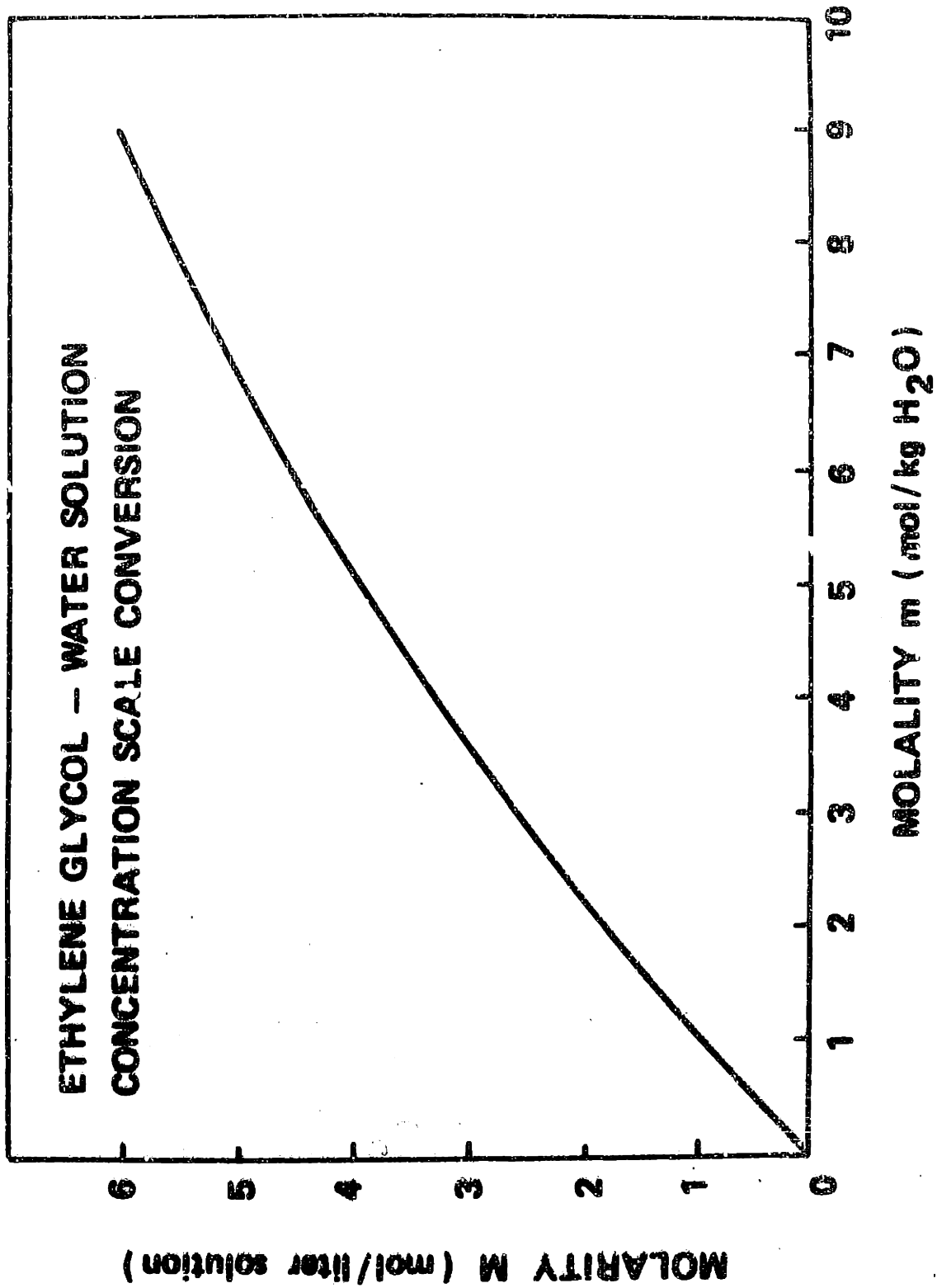


FIGURE I1 Ethylene glycol molar - molal conversion

## APPENDIX J

## CONFIDENCE LIMITS OF VOLUME/VOLTAGE CALIBRATION DATA

The data of Figure 21 was fit with a least squares line

$$y = ae^{bx}$$

or

$$y' = a' + bx$$

where

$$y = \text{volt/volt}^*$$

$$x = \text{Hct/Hct}^*$$

$$y' = \ln(y)$$

$$a' = \ln(a) = \ln(.0945) = -2.359$$

$$b = 2.353$$

Given the data and the regression line, the probability is  $1 - \alpha$  that a future observation  $x$  corresponding to a value  $y$  will lie in the interval [63]

$$x_{\text{fit}} \pm t_{\alpha/2, n-2} s_{xy} \sqrt{1 + \frac{1}{n} + \frac{(y' - \bar{y}')^2}{\sum_{i=1}^n (y'_i - \bar{y}')^2}}$$

where

$t_{\alpha, \nu}$  is the  $100\alpha$  percentage point of the  $t$  distribution for  $\nu$  degrees of freedom

$$s_{xy'} = \sqrt{\frac{\sum (x_i - x_{\text{fit}}(i))^2}{n-2}}$$

is an estimate of variability  
about the fit line

$n$  is the number of data points

$$\bar{y}' = \frac{1}{n} \sum y'_i \text{ the mean value}$$

for our data

$$n = 125$$

$$\bar{y}'_i = -.445$$

$$s_{xy'} = 1.825 \times 10^{-2}$$

$$t_{\alpha/2, n-2} = 1.984 \text{ for } \alpha = 0.5 \text{ (95\% confidence)}$$

we can now compute

<u>volt/volt*</u>	<u>Hct/Hct* = <math>x_{\text{fit}} \pm</math></u>
.4	.613 $\pm$ .037
.6	.786 $\pm$ .036
.8	.908 $\pm$ .036
1.0	1.000 $\pm$ .037
1.2	1.080 $\pm$ .037

APPENDIX K  
LIST OF MANUFACTURERS

- |     |  |   |
|-----|--|---|
| 1.  | Keithly Instruments<br>52 Main St.<br>Flemington, N.J.                         | high voltage supply                                   |
| 2.  | Hyperion Industries<br>134 Coolidge Ave.<br>Watertown, Mass. 02172             | lamp power supply                                     |
| 3.  | Teledyne Philbrick<br>Allied Drive<br>Dedham, Mass. 02026                      | op-amps   |
| 4.  | Analog Devices<br>Route One Industrial Park<br>Norwood, Mass. 02062            | op-amps   |
| 5.  | Carl Zeiss, Inc.<br>444 Fifth Ave.<br>New York, New York 10018                 | lamp and housing                                      |
| 6.  | Ditric Optics<br>247 Maple St.<br>Marlboro, Mass. 01752                        | optical filter  |
| 7.  | Edmund Scientific<br>800 Edscorp Bldg.<br>Barrington, N.J. 08007               | fiber optic light pipe                                |
| 8.  | Heath Schlumberger Instruments<br>Benton Harbor, Mich. 49022                   | strip chart recorder                                  |
| 9.  | R.C.A. Electronic Components<br>360 First Ave.<br>Needham Heights, Mass. 02194 | photomultiplier                                       |
| 10. | Velonex<br>560 Robert Ave.<br>Santa Clara, Cal. 95050                          | digital panel meter                                   |
| 11. | Rollins Associates<br>Concord Rd.<br>Lincoln, Mass. 01773                      | digital data acquisition<br>system and microprocessor |

12. Tektronix  
P.O. Box 500  
Beaverton, Ore. 97005  
oscilloscope
13. Advanced Instruments, Inc.  
1000 Highland Ave.  
Needham Heights, Mass. 02194  
freezing point osmometer
14. Hamilton Syringe  
P.O. Box 17500  
Reno, Nevada 98510  
miniature valves
15. AST/Servo Systems  
30 Shawsheen Ave.  
Bedford, Mass. 01730  
velocity transducer
16. Clippard Instrument Lab  
7390 Colerain Rd.  
Cincinnati, Ohio 45239  
air cylinder

APPENDIX L  
THERMOCOUPLE TABLE FOR LIQUID NITROGEN REFERENCE

	0	1	2	3	4	5	6	7	8	9	10	
-40	4.060	4.025	3.991	3.956	3.921	3.887	3.853	3.818	3.784	3.750	3.716	-40
-30	4.414	4.378	3.343	4.307	4.272	4.236	4.201	4.165	4.130	4.095	4.060	-30
-20	4.778	4.741	4.705	4.668	4.632	4.595	4.559	4.522	4.486	4.450	4.414	-20
-10	5.152	5.114	5.077	5.039	5.001	4.964	4.927	4.889	4.852	4.815	4.778	-10
- 0	5.535	5.496	5.458	5.419	5.381	5.342	5.304	5.266	5.228	5.190	5.152	- 0
0	5.535	5.574	5.613	5.662	5.691	5.730	5.769	5.808	5.847	5.886	5.926	0
10	5.926	5.965	6.005	6.045	6.084	6.124	6.164	6.204	6.244	6.284	6.324	10
20	6.324	6.365	6.405	6.446	6.486	6.527	6.567	6.608	6.649	6.693	6.731	20
30	6.731	6.772	6.814	6.855	6.896	6.938	6.979	7.021	7.063	7.104	7.146	30
40	7.146	7.188	7.230	7.273	7.315	7.357	7.400	7.442	7.485	7.527	7.570	40

- 1) copper-constantan thermocouples
- 2) this table derived by adding 5.535 to ice point table
- 3) units are millivolts and °C

## REFERENCES

1. Mazur, P., Kinetics of Water Loss From Cells at Subzero Temperatures and the Likelihood of Intracellular Freezing, 1963, *J. Gen. Phys.* 47, 347.
2. Diller, K. R., A Microscopic Investigation of Intracellular Ice Formation in Frozen Human Erythrocyte, 1972, Ph.D. Thesis, M.E. Dept., MIT.
3. Silvaes, O., A Thermodynamic Model of Water and Ion Transport Across Cell Membranes During Freezing and Thawing: The Human Erythrocyte, 1974, Ph.D. Thesis, M.E. Dept. MIT.
4. Levin, R.L., Kinetics of Water Transport in Biomaterials During Freezing, 1976, Sc.D. Thesis, M.E. Dept., MIT.
5. Sidel, V.W., Solomon, A.K., Entrance of Water into Human Red Cells Under an Osmotic Pressure Gradient, 1957, *J. Gen. Phys.*, 41, 243.
6. Rich, G.T., Sha'afi, R.I., Romualdez, A., Solomon, A.K., Effect of Osmolality on the Hydraulic Permeability Coefficient of Red Cells, 1968, *J. Gen. Phys.*, 52, 941.
7. Farmer, R.E.L., Macey, R.I., Perturbation of Red Cell Volume: Rectification of Osmotic Flow, 1970, *Biochim. Biophys. Acta.*, 196, 53.
8. Blum, R.M., Forster, R.E., The Water Permeability of Erythrocytes, 1970, *Biochim. Biophys. Acta.*, 203, 410.
9. Vieira, F.L., Sha'afi, R.I., Solomon, A.K., The State of Water in Human and Dog Red Cell Membranes, 1970, *J. Gen. Phys.*, 55, 451.
10. de Groot, S.R., Mazur, P., Non-Equilibrium Thermodynamics, 1962, Interscience Publishers, N.Y.
11. Prigogine, I., Introduction to Thermodynamics of Irreversible Processes, 1955, Interscience Publishers, N.Y.
12. Katchalsky, A., Curran, P.F., Non-Equilibrium Thermodynamics in Biophysics, 1967, Harvard University Press, Cambridge.
13. Kedem, O., Katchalsky, A., Thermodynamic Analysis of the Permeability of Biological Membranes to Non-Electrolytes, 1958, *Biochim. Biophys. Acta.*, 27, 229.
14. Rand, R.P., Burton, A.C., Mechanical Properties of the Red Cell Membrane, 1964, *Biophys. J.*, 4, 115.

15. Dick, D.A.T., The Rate of Diffusion of Water in the Protoplasm of Living Cells, 1959, *Exp. Cell Res.*, 17, 5.
16. Dainty, J., Water Relations of Plant Cells, in Advances in Botanical Research, R.D. Preston, ed., 1963, Academic Press, N.Y.
17. Sha'afi, R.I., Rich, G.T., Sidel, V.W., Bossert, W., Solomon, A.K., The Effect of the Unstirred Layer on Human Red Cell Permeability, 1967, *J. Gen. Phys.*, 50, 1377.
18. Denbigh, K., The Principles of Chemical Equilibrium, 1971, Cambridge Press, London.
19. Katchalsky, A., Alexandrowicz, A., On the Additivity of Osmotic Properties of Polyelectrolyte Salt Solutions, 1963, *J. Polymer, Sci.*, Part A, 1, 2093.
20. Handbook of Chemistry and Physics, R.C. Weast, ed., 1974, CRC Press, Cleveland, Ohio.
21. Robinson, R.A., Stokes, R.H., Electrolyte Solutions, 1955, Academic Press, N.Y.
22. Lewis, G.N., Randall, M., Thermodynamics, 1961, McGraw Hill, N.Y.
23. Kuntz, I.D., Kauzman, W., Hydration of Proteins and Polypeptides, 1974, *Adv. Protein Chem.*, 28, 239.
24. Bragg, W.L., Perutz, M.F., The External Form of the Hemoglobin Molecule, 1952, *Acta. Cryst.*, 5, 277.
25. Adair, G.S., The Thermodynamic Analysis of the Observed Osmotic Pressures of Protein Salts in Solutions of Finite Concentration, 1929, *Proc. Roy. Soc. Lon.*, 126, Series A, 16.
26. McConaghey, P.D., Maizels, M., The Osmotic Coefficient of Hemoglobin in Red Cells Under Varying Conditions, 1961, *J. Phys.*, 155, 28.
27. Goldstein, D.A., Solomon A.K., Determination of Equivalent Pore Radius for Human Red Cells by Osmotic Pressure Measurement, 1960, *J. Gen. Phys.*, 44, 1.
28. Papenek, T., An Apparatus to Measure Red Cell Permeability at Low Temperature, 1975, M.S. Thesis, M.E. Dept., MIT.
29. Anderson, N.M., Light Transmission and Scattering by Red Blood Cell Suspensions, 1966, Ph.D. Thesis, Dept. of Physiology, McGill Univ.
30. Latimer, P., Pyle, B.E., Light Scattering at Various Angles: Theoretical Predictions of the Effects of Particle Volume Changes, 1972, *Biochim. Biophys. Acta.*, 12, 764.



31. Lin, J.C., Guy, A.W., A Note on the Optical Scattering Characteristics of Whole Blood, 1974, *IEEE Trans, Biomed. Eng.*, Jan., 43.
32. Lothian, G.F., Lewis, P.C. Spectrophotometry of Granulated Materials, With Particular Reference to Blood Corpuscles, 1956, *Nature*, 178, 1342.
33. Van Assendelft, C.W., Spectrophotometry of Haemoglobin Derivatives, 1970. Charles C. Thomas, Springfield.
34. Robbin, M. Private Communication, June 1977, Cryogenic Engineering Lab., MIT.
35. Papenek, T., Robbin, M., Huggins, C.E., Cravalho, E.G., The Effects of Anticoagulants ACD and CPD on the Glycerol Permeability of the Human Erythrocyte, 1976, Society for Cryobiology, Thirteenth Annual Meeting.
36. Burton, A.C., Physiology and Biophysics of the Circulation, 1965, Year Book Medical Publishers, Chicago.
37. Lightfoot, E.N., Transport Phenomena and Living Systems, 1974, Wiley Interscience, N.Y.,
38. Frojmovic, M.M., Okagawa, A., Mason, S.G., Rheo-Optical Transients in Erythrocyte Suspensions, 1975, *Biochim, Biophys. Res. Com.* 62, 17.
39. Rich, G.T., Sha'afi, R.I., Barton, T.C., Solomon, A.K., Permeability Studies on Red Cell Membranes of Dog, Cat, and Beef, 1967, *J. Gen. Phys.*, 50, 2391.
40. Canham, P.B., Differences in Geometry of Young and Old Human Erythrocytes Explained by a Filtering Mechanism, 1969, *Circ. Res.*, 25, 39.
41. Bevington, P.R., Data Reduction and Error Analysis for the Physical Sciences, 1969, McGraw Hill, N.Y.
42. Marquardt, D.W., An Algorithm for Least-Squares Estimation of Non-linear Parameters, 1963, *J. Soc. Indust. Appl. Math.*, 11, 431.
43. Stusnick, E., Numerical Determination of Membrane Permeability Parameters, 1972, *J. Theor. Biol.*, 37, 261.
44. Rand, R.P., Mechanical Properties of the Red Cell Membrane (Viscoelastic Breakdown of the Membrane), 1964, *Biophys. J.*, 4, 303.
45. Operating Manual for Model D-110 Stopped Flow Spectrophotometer, Durrum Instrument Corp., 3950 Fabian Way, Palo Alto, Cal.

46. Williams, W.J., Beutler, E., Erslev, A.J., Rundles, R.W., Hematology, 1972, McGraw Hill, N.Y.
47. Wintrobe, M.W., Clinical Hematology, 1967, Lea and Febiger, Phila.
48. Altman, P.L., ed., Blood and Other Body Fluids, 1961, Fed. Am. Soc. Exp. Bio., Wash. D.C.
49. Evans, E., Fung, Y.C., Improved Measurements of the Erythrocyte Geometry, 1972, Microvasc. Res., 4, 335.
50. Canham, P.B., Burton, A.C., Distribution of Size and Shape in Populations of Normal Human Red Cells, 1968, Circ. Res., 22, 405.
51. Watson, W.W., Volumetric Changes in Human Erythrocytes During Freezing at Constant Cooling Velocities, 1974, S.M.M.E. Thesis, M.E. Dept., MIT.
52. Le Fevre, P.G., The Osmotically Functional Water Content of the Human Erythrocyte, 1964, J. Gen. Phys., 47, 585.
53. Savitz, D., Sidel, V.W., Solomon, A.K., Osmotic Properties of Human Red Cells, 1964, J. Gen. Phys., 48, 79.
54. Farrant, J., Woolgar, A.E., Human Red Cells Under Hypertonic Conditions - A Model System for Investigating Freezing Damage, 1972, Cryobiology, 9, 9.
55. Solomon, A.K., Red Cell Membrane Structure and Ion Transport, 1960, J. Gen. Phys., 43 (suppl), 1.
56. Kotyk, A., Janacek, K., Cell Membrane Transport, 1970, Plenum Press, N.Y.,
57. Bolis, L., Gomperts, B.D., Red Blood Cells, in Transport and Accumulation in Biological Systems, Harris, E.J., ed., 1972, University Park Press, Baltimore.
58. Bartlett, G.R., Human Red Cell Glycolytic Intermediates, 1959, J. Bio. Chem., 234, 457.
59. Bernstein, R.E., Potassium and Sodium Balance in Mammalian Red Cells, 1954, Science, 120, 459.
60. Bishop, C. Surgenor, D.M., The Red Blood Cell, 1964, Academic Press, N.Y.
61. Gary Bobo, C.M., Solomon, A.K., Hemoglobin Charge Dependence on Hemoglobin Concentration in Vitro, 1971, J. Gen. Phys., 57, 283.
62. Wolf, A.V., Aqueous Solutions and Body Fluids, 1966, Harper and Row, N.Y.

63. Bowker, A.H., Lieberman, G.J., Engineering Statistics, 1959, Prentice-Hall, N.J.
64. Levin, S.W., Levin, R.L., Solomon, A.K., Permeability of Human Red Cells and Ghosts to Water, 1978, pre-publication communication, Biophysical Laboratory, Harvard Medical School, Boston, Mass.
65. Naccache, P., Sha'afi, R.I., Patterns of Nonelectrolyte Permeability in Human Red Cell Membrane, 1973, J. Gen. Phys., 62, 714.

## BIBLIOGRAPHY OF STOP FLOW TECHNIQUES

- Berger, R.L., Balko, B., Borchardt, W., Friauf, W., High Speed Optical Stopped Flow Apparatus, 1968, Rev. Sci. Inst., 39, 486.
- Chance, B., The Accelerated Flow Method for Rapid Reactions, 1940, J. Franklin Inst., 229, 455 and 737.
- Chance, B., Eisenhardt, R.H., Gibson, Q.H., Lonberg-Holm, K.K., Rapid Mixing and Sampling Techniques in Biochemistry, 1964, Academic Press, N.Y.
- Gibson, Q.H., Milnes, L., Apparatus for Rapid and Sensitive Spectrophotometry, 1964, Biochem., 91, 161.
- Morrow, J.I., A New High Resolution Stopped Flow Apparatus, 1970, Chem. Instr., 2, 375.
- Reich, R.M., Instrumentation for the Study of Rapid Reactions in Solution, 1971, J. Anal. Chem., 43, 85A.

## BIOGRAPHY

The author was born in Boston, Massachusetts on October 18, 1948. Upon graduating from The Stockbridge School, he entered the liberal arts program at Antioch College. Co-op job experiences at Diamond Automation and IBM confirmed his decision to study engineering, and he transferred to the Mechanical Engineering Department of Columbia University, where he received the B.S. degree in 1972. After working as a motorcycle mechanic for a year, he entered the Master of Science program at MIT as a research assistant under Professor E.G. Cravalho. He received the M.S. degree in Mechanical Engineering in 1975.

The author's publications include the following:

Papanek, T., Fabry, T.L., "A High Pressure Optical Cell for Study of Biochemical Solutions", 1972, Rev. Sci. Inst., 43: 738.

Papanek, T., Robbin, M., Cravalho, E.G., Huggins, C.E., "The Effects of Anticoagulants ACD and CPD on the Glycerol Permeability of Human Erythrocytes", presented at the Thirteenth Annual Meeting of the Society for Cryobiology, Washington, D.C., August, 1976.

Papanek, T., "An Apparatus to Measure Red Cell Permeability at Low Temperature", 1975, M.S. Thesis, Department of Mechanical Engineering, MIT.